

**CONSTRUCTING A CRUSTAL-SCALE 3-D EARTH MODEL OF OFFSHORE-
TO-ONSHORE WESTERN NEWFOUNDLAND USING SEISMIC REFLECTION,
SEISMIC REFRACTION, GRAVITY AND MAGNETIC DATA**

by ©Ederson Villamizar (Thesis) submitted to the School of Graduate Studies in partial
fulfillment of the requirements for the degree of

**Master of Science: Geophysics (M.Sc.), Earth Sciences/ Department of Earth
Sciences**

Memorial University of Newfoundland

May, 2019

St. John's Newfoundland and Labrador

Abstract

Western Newfoundland is characterized as a geologically complex region for which the potential field data have not been incorporated into tectonic models. To this end, a 3D density model of Western Newfoundland was constructed by means of forward gravity modelling and gravity inversion to better understand the complexity of the Appalachian structures on which Western Newfoundland is placed. This model was constrained by seismic refraction and seismic reflection data located in the study area, and surface geology. Density values were calculated from empirical velocity-density functions and gravity forward modelling adjustments.

The 3D density model, 3D gravity inversion results, and magnetic data support the presence of a high density lower crustal body in the Grenville Province. It is possible that this particular body may extend further north and could be related to the denser body found in southeast Labrador. The high resolution magnetic map for the study area showed two WNW-ESE linear magnetic anomalies in the Gulf of St. Lawrence that lie perpendicular to the Newfoundland coast. They could be explained by the presence of ancient inherited basement involved transfer faults that resulted from offset ancient ridge axis segments during the opening of the Iapetus ocean.

Acknowledgments

I would like to start thanking the person who envisioned this project, my supervisor Kim Welford. Thank you so much for trusting me with this project. Thank you so much for accepting me as one of your students and taking me under your supervision and into your research group. You changed my life. Thank you so much for emailing me back in May, 2016.

I thank HIM for being my unconditional and unwavering support and love during these last two years. Thank you so much for taking care of me and always leading me to good people. Thank you God for being my strength and lifting me up when I thought I would give up.

Finally, thank you so much to all the people from the university that helped me academically and also gave me a hand with the use of the different software during these two years. Thank you family, church family and Elena for being my dear friends, for supporting me spiritually and morally.

I love you all.

Table of Contents

Title Page	i
Abstract	ii
Acknowledgments	iii
Table of Contents	iv
List of Tables	vii
List of Figures	viii
<u>Chapter 1: Introduction</u>	1
<u>1.1 Overview</u>	1
<u>1.2 Theoretical Framework</u>	2
<u>1.2.1 Gravity Acceleration</u>	2
<u>1.2.2 The Ellipsoid and the Geoid</u>	5
<u>1.2.3 Gravity Anomalies and Gravity Corrections</u>	5
<u>1.2.4 Magnetic Force and Magnetic Field Strength</u>	8
<u>1.3 Geological Background</u>	9
<u>1.3.1 Tectonic Evolution</u>	10
<u>1.3.2 Major Geological Subdivisions</u>	15
<u>1.4 Previous Work</u>	20
<u>1.5 Purpose</u>	23
<u>1.6 Summary</u>	23
<u>Chapter 2: Data and Methods</u>	24
<u>2.1 Datasets</u>	24
<u>2.1.1 Gravity Data</u>	24
<u>2.2.2 Topography Data</u>	26
<u>2.2.3 Magnetic Data</u>	28
<u>2.2.4 2D Seismic Reflection Data</u>	29
<u>2.2 Statistical Analysis</u>	31
<u>2.3 Separation of Regional and Residual Anomalies</u>	32
<u>2.4 Derivative-based Filters for Potential Field Data and Reduction to the Pole</u>	33
<u>2.5 Euler Deconvolution and Curvature analysis</u>	35

2.2	<u>3D Modelling</u>	38
2.2.1	<u>Initial Structure of the Model</u>	40
2.3	<u>Gravity Inversion</u>	43
2.3.1	<u>GRAV3D</u>	44
2.3.2	<u>Probabilistic Inversion Approach</u>	45
2.3.3	<u>Inversion Process</u>	46
2.4	<u>Summary</u>	47
	<u>Chapter 3: Description of the gravity and magnetic anomalies</u>	48
3.1	<u>Maps and description of anomalies</u>	48
3.2	<u>Statistical analysis</u>	54
3.3	<u>Spectral analysis and filtering</u>	55
3.4	<u>Curvature</u>	63
3.5	<u>Euler Deconvolution</u>	68
3.6	<u>Summary</u>	73
	<u>Chapter 4: Seismic Interpretation and Gravity modelling</u>	75
4.1	<u>Seismic Interpretation</u>	75
4.2	<u>Forward Modelling</u>	79
4.1.1	<u>Model precision and limitations</u>	89
4.2.2	<u>Model sections</u>	91
4.2.3	<u>Moho and Depth to the Basement Maps</u>	100
4.4.4	<u>High density lower crustal body</u>	101
4.3	<u>Summary</u>	104
	<u>Chapter 5: Gravity Inversion</u>	105
5.1	<u>3D Gravity Inversion</u>	105
5.2	<u>Summary</u>	120
	<u>Chapter 6: Discussion</u>	121
6.1	<u>Crustal Thickness and Structure</u>	121
6.2	<u>High density lower crustal body</u>	125
6.3	<u>Sedimentary basin thickness and Humber Arm Allochthon</u>	128
6.4	<u>Ophiolites and Odd Twins Anomaly</u>	129
6.5	<u>Faults</u>	130

<u>6.6 Summary</u>	131
<u>Chapter 7: Conclusions and Future work</u>	132
<u>References</u>	135
<u>Appendix A: Elements of GRAV3D 2.0 Program Library</u>	144

List of Tables

Table 2. 1: Structural Index (SI) values. Taken from Reid et al. (2014).	35
Table 4. 1: Summary of 3D gravity forward models and final model.	83
Table 5. 1: Summary of 3D gravity inversions	106
Table 5. 2: Summary of reference density contrast models in g/cm^3	107

List of Figures

Figure 1.1: Western Newfoundland topographic map (Ante and Eakins, 2009), indicating the available constraints.	4
Figure 1.2: a) The variation in angular velocity with latitude around the Earth. b) An exaggerated representation of the shape of the Earth.	6
Figure 1.3: a) Free-air correction for an observation at a height h above datum. b) The Bouguer correction.	7
Figure 2.1: Western Newfoundland gravity map.	26
Figure 2. 2: Western Newfoundland topographic map (Ante and Eakins, 2009).	27
Figure 2. 3: Western Newfoundland residual magnetic map.	29
Figure 2. 4: Map of selected seismic reflection lines.	30
Figure 2. 5: Line CAH90-01 with depth conversion.	31
Figure 2.6: Interface of EULER3D module of Oasis Montaj.	36
Figure 2. 7: Interface of the Java program Curvature (Schmidt and Götze, 2003).	38
Figure 2. 8: Map of E-W parallel initial cross-sections (thick black lines).	42
Figure 3. 1: Western Newfoundland topographic and bathymetric map	58
Figure 3. 2: Western Newfoundland gravity map.	59
Figure 3. 3: Western Newfoundland high resolution residual magnetic maps.	60
Figure 3. 4: Western Newfoundland residual magnetic maps.	61
Figure 3. 5: Western Newfoundland high resolution residual magnetic map.	62
Figure 3. 6: Histograms of a) Free Air and Bouguer anomaly data values and b) Residual Magnetic anomaly data values	65
Figure 3. 7: Power Spectra of a) Free Air and Bouguer gravity anomaly data and b) Residual Magnetic anomaly data.	66
Figure 3. 8: Power Spectra of a) Corner Brook, b) Deer Lake, c) Gros Morne, d) Indian head and e) Offshore Western Newfoundland.	67
Figure 3. 9: Reduction to the Pole of the magnetic anomaly data: a) Residual magnetic anomaly data, b) reduced to the Pole magnetic anomaly.	68

Figure 3. 10: Separation of the Regional/Residual field from the Magnetic anomaly data using the Power Spectrum: a) Magnetic anomaly data, b) Regional Magnetic anomaly data and c) Residual magnetic anomaly data.	59
Figure 3. 11: Special filters applied to the Magnetic anomaly data, a) Magnetic anomaly data, b) Analytic Signal, c) Tilt derivative (TDR) and d) Horizontal derivative of the tilt derivative (HD-TDR).	60
Figure 3. 12: Separation of the Regional/Residual fields from the Gravity anomaly map using the Power Spectrum: a) Gravity anomaly data, b) Regional Gravity anomaly data and c) Residual gravity anomaly data.	61
Figure 3. 13: Special filters applied to the Free Air offshore and Bouguer onshore Gravity anomaly data: a) Gravity anomaly data, b) Analytic Signal, c) Tilt derivative (TDR) and d) Horizontal derivative of the tilt derivative (HD-TDR).	62
Figure 3. 14: Dip Angle Curvature results for the high resolution magnetic data.	64
Figure 3. 15: Dip Angle Curvature results for the high resolution magnetic data.	65
Figure 3. 16: Map of a) dip angle and b) dip curvature of the Western Newfoundland Magnetic anomaly data.	66
Figure 3. 17: Map of a) dip angle and b) dip curvature for the Western Newfoundland combined Bouguer/ Free Air gravity map.	67
Figure 3. 18: Map of a) dip angle and b) dip curvature of the Western Newfoundland Free Air anomaly data.	68
Figure 3. 19: Maps of tests of the Euler deconvolution results for the combined Bouguer/ Free Air gravity data.	70
Figure 3. 20: Maps of Euler deconvolution for the combined Bouguer/ Free Air gravity data.	71
Figure 3. 21: Map of Euler's deconvolution for magnetic data.	72
Figure 3. 22: Map of Euler's deconvolution for Free Air anomaly and high resolution magnetic data.	73

Figure 4. 1: Uninterpreted and interpreted seismic line CAH90-01.	77
Figure 4. 2: Uninterpreted and interpreted seismic line 91-1493.	78
Figure 4. 3: Uninterpreted and interpreted seismic line CAH91-20.	80
Figure 4. 4: Western Newfoundland Residual gravity maps for the preliminary models 1 to 4.	82
Figure 4. 5: Evolution of a 2D cross-section through the preliminary models 1 to 4.	85
Figure 4. 6: Western Newfoundland Residual gravity maps of Free Air anomaly offshore and Bouguer anomaly on land for models 5 to 7 with 0 contour labelled.	86
Figure 4. 7: Western Newfoundland modelling area with Euler deconvolution points.	87
Figure 4. 8: Example sections of model 5.	88
Figure 4. 9: Section from model 5.	89
Figure 4. 10: Residual gravity field of the study area.	90
Figure 4. 11: Residual gravity field of the study area with cross-sections.	93
Figure 4. 12: E-W cross-section 1 at the southern end of the study area.	93
Figure 4. 13: Cross-section 2.	94
Figure 4. 14: Cross-sections along seismic profiles CAH90-1(a) and CAH90-2 (b)	96
Figure 4. 15: E-W Cross-section 3 near the centre of the study area.	96
Figure 4. 16: E-W Cross-section 4 at the northern end of the study area.	97
Figure 4. 17: Cross-section 88-4.	97
Figure 4. 18: Cross-section 91-3.	98
Figure 4. 19: Vertical cross-section 1 from N to S across the full study area.	99
Figure 4. 20: Vertical cross-section 2 from N to S across the full study area.	99
Figure 4. 21: a) Depth to the basement and b) Moho depths map for Western Newfoundland.	101
Figure 4. 22: a) Residual gravity field of the study area with the presence of the High density body and b) Residual gravity field for the same model with a lower crust without the High density body.	103

Figure 5. 1: First inversion using the mesh automatically created by GRAV3D.	107
Figure 5. 2: Residual gravity field of the study area with cross-sections.	108
Figure 5. 3: Evolution of 2D horizontal cross-sections in the gravity inversion process.	110
Figure 5. 4: Evolution of 2D horizontal cross-sections in the gravity inversion process.	111
Figure 5. 5: Evolution of 2D horizontal cross-sections in the gravity inversion process.	112
Figure 5. 6: Evolution of 2D horizontal cross-sections in the gravity inversion process.	113
Figure 5. 7: Comparison of the a) N-S gravity forward model cross section with the b) seventh inversion result and c) eleventh inversion result.	114
Figure 5. 8: Evolution of 2D horizontal cross-sections in the gravity inversion process.	116
Figure 5. 9: Comparison of the a) N-S gravity forward model cross section with the b) fourteenth inversion result.	117
Figure 5. 10: Comparison of Moho depths for Western Newfoundland.	119
Figure 6. 1: Western Newfoundland Bouguer anomaly map.	122
Figure 6. 2: Sediment thickness and crustal thickness map.	124
Figure 6. 3: Cross-section 88-4.	126

Chapter 1: Introduction

Western Newfoundland is a site of naturally occurring hydrocarbon seeps and it has been an exploration target for many decades. Although geophysical studies have been performed in the past (Hall et al., 1998; Michel et al., 1992; Quinlan et al., 1992; Stockmal et al., 1998; Waldron, 1994), no comprehensive attempt has been made to incorporate gravity and magnetic data from Western Newfoundland into tectonic models. Hence, the general objective of this research is to construct a 3D lithospheric model of Western Newfoundland to better understand the Appalachian structure in the region using satellite gravity data and other geophysical constraints. This chapter introduces the geology of the study area, the basic theoretical concepts necessary to understand the tools, and the physics used to develop this research project. Previous geophysical work in the study area is also presented as well as the purpose and goals of this research project.

1.1 Overview

Western Newfoundland (Fig. 1.1) is characterized as a geologically complex region, for which the surface geology is well known (Knight, 1983; Lavoie, 2008; Waldron et al., 2012; Williams, 1995). This geology records multiphase deformation of a Cambrian-Ordovician passive margin, younger Ordovician to Devonian foreland basins formed during the Taconian, Salinian and Acadian orogenic events, and Carboniferous deformation (Cooper et al., 2001). Hydrocarbon seeps in Western Newfoundland lie within an area containing three basins capable of generating oil: the Anticosti Basin, the Deer Lake Basin and the Bay St. George sub-basin. Together, these basins remain important targets for petroleum exploration (Cooper et al., 2001).

Geophysical studies in Western Newfoundland have mainly focused upon understanding the development of the Appalachian Orogen in the region (Hall et al., 1998; Michel et al., 1992; Quinlan et al., 1992; Stockmal et al., 1998; Waldron, 1994). Much of the significant seismic acquisition in this area was completed before 2000, and in many

cases the data are poor and difficult to interpret. However, potential field methods, such as gravity and magnetic methods, can be useful for studying complex regions, as they can build a bridge between sparse seismic studies. Constrained gravity and magnetic studies used in other regions have provided interpretable results down to the lithospheric scale. (e.g., Sanchez-Rojas and Palma, 2014; Sanchez et al., 2011; Tassara et al., 2006; Welford and Hall, 2013).

No comprehensive attempt has been made to incorporate gravity and magnetic data from Western Newfoundland into tectonic models. This research represents an attempt to synthesize this information to better understand the complexity of Appalachian structures and how they may have evolved.

The research area is located in eastern Canada, specifically in Western Newfoundland and its offshore continuation beneath the Gulf of St. Lawrence (Fig. 1.1). In total, this area covers about 115,608 km² and is located between 55°W and 61°W, and 47°N and 52°N.

1.2 Theoretical Framework

Gravity and magnetic methods provide the foundation for this project. In this section, basic concepts for understanding the physics behind the gravity and magnetic method are explained. Mathematical tools used during the research, such as Curvature, Euler Deconvolution and Spectral Analysis, are outlined and explained. The final section of this chapter describes the forward modelling and inverse problem.

1.2.1 Gravity Acceleration

Gravitational acceleration (g) towards a spherical Earth is given by:

$$g = \frac{GM_E}{r^2} \quad (1)$$

where M_E is the mass of the Earth, r is the radius of the Earth and G is the universal gravity constant which is an empirical physical constant. The units of gravitational acceleration are $\frac{m}{s^2}$, which are also known as Gal. However, in geophysical prospecting, it is necessary to measure very small changes in gravity accurately because they are caused by subsurface structures. Therefore, we use the mGal which is equal to 0.001 Gal.

The Earth, of course, is not a perfect sphere; it has an irregular shape and surface. Therefore, in geophysics/geodesy, it is necessary to approximate the shape of the planet in order to properly study the density contrasts within it.

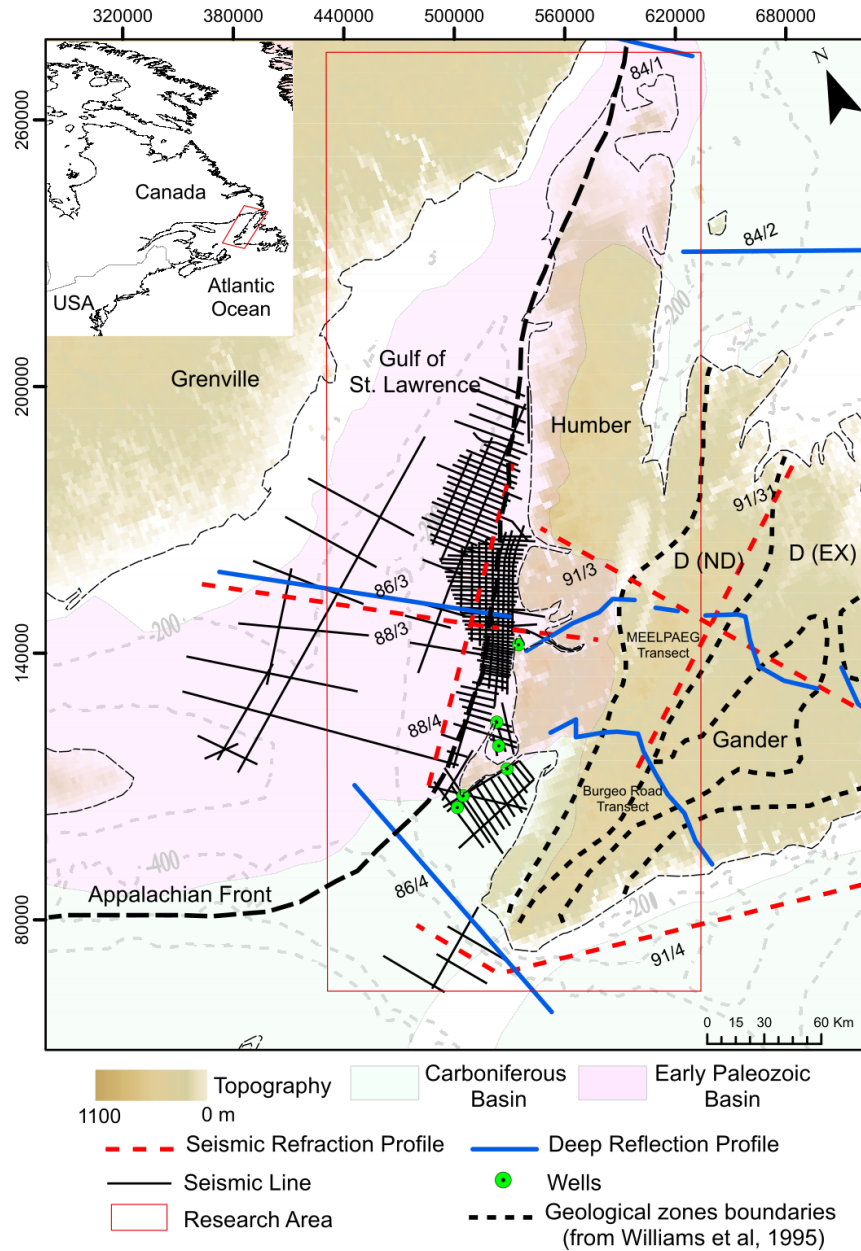


Figure 1.1: Western Newfoundland topographic map (Ante and Eakins, 2009), indicating the available constraints. Map shows surface geological zones of the Appalachian Orogen in Newfoundland (Williams, 1995), outlined by dashed black lines. Red dashed lines and blue lines indicate seismic profiles from Jackson et al. (1998), Marillier et al. (1994) and Hall et al. (1998). Black lines indicate seismic reflection profiles available from the Canada-Newfoundland Offshore Petroleum Board (C-NLOPB) and the Department of Natural Resources of the Government of Newfoundland and Labrador. Dashed grey lines offshore correspond to bathymetric contours (m). The red square outlines the model area used for this project. Abbreviations: D (Ex), Exploits subzone of the Dunnage zone; D (ND), Notre Dame subzone of the Dunnage zone.

1.2.2 The Ellipsoid and the Geoid

The Ellipsoid is an approximation of the real shape of the Earth. Its surface is taken to be the mean sea-level surface of the Earth. Although the Earth does not have an ellipsoidal shape, this approximation provides a simple, consistent, and uniform reference system for all purposes of geophysics (Li and Götze, 2001).

The physical equipotential surface of gravity is called the geoid. It reflects the true distribution of mass inside the Earth and differs from the theoretical ellipsoid by small amounts (Lowrie, 2007).

Unlike the ellipsoid, the geoid cannot be described with a simple mathematical expression due to mass variations within the continents and the transient effects of tides and winds on the oceans.

1.2.3 Gravity Anomalies and Gravity Corrections

The rotating flattened Earth generates gravity values that vary uniformly over the surface of the normal ellipsoid. The Earth's interior is not uniform, which causes localized gravity variations that are superimposed onto the global variations of the Earth's gravity (Alsadi and Baban, 2014).

In geophysical exploration, the localized variations are the targets since they correspond to the localized subsurface structure. Thus, the measured gravity must be corrected to remove the effect of the ellipsoid. Once the correction is done, the measured gravity is called the gravity anomaly and is interpreted to reflect the localized lateral changes in density.

The Free Air correction, Bouguer correction, the Free Air anomaly and the Bouguer anomaly are all presented in this thesis.

1.2.4 Latitude Correction

Gravity varies with latitude because of the non-spherical shape of the Earth (Fig. 1.2b) and because the angular velocity of a point on Earth's surface decreases from a maximum at the equator to zero at the poles (Fig. 1.2a) (Kearey et al., 2002). The latitude correction compensates for this effect by using the geodetic reference system formula of 1967 or GRS67:

$$g_n = 978.03185(1 + 0.005278895\sin^2\phi + 0.000023462\sin^4\phi) \frac{cm}{s^2} \quad (2)$$

Latitude is represented by ϕ and g_n represents the value of gravitational acceleration that we observe when measuring gravity at various positions on the Earth's surface. Equation 2 corrects for position (Burger et al., 2006).

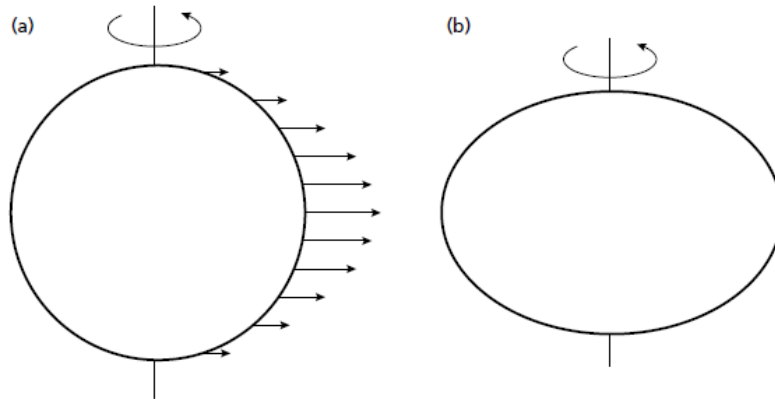


Figure 1.2: a) The variation in angular velocity with latitude around the Earth represented by vectors whose lengths are proportional to angular velocity. b) An exaggerated representation of the shape of the Earth. Taken from Kearey et al. (2002).

1.2.5 Tidal Correction

Gravity measured at a fixed location varies with time because of periodic variations in the gravitational effects of the Sun and Moon, associated with their orbital motions. Generally, the tidal correction is made during the drift instrument correction but the effects of tides can also be calculated using computer programs (Kearey et al., 2002).

1.2.6 Free Air Correction

The free air correction (Fig. 1.3a) accounts for the decrease of gravitational acceleration with distance from the center of the Earth. It is also known as the elevation effect correction and it is calculated by taking the derivative of equation 1 with respect to the radius.

$$\frac{\partial g}{\partial r} = -0.3086h \frac{mGal}{m} \quad (2)$$

1.2.7 Bouguer Correction

The Bouguer plate correction (Fig. 1.3b) compensates for the effect of a layer of rock whose thickness corresponds to the elevation difference between the measurement and the reference levels. This mass excess is computed by assuming an infinite horizontal slab of rock-material, of thickness (h), mean density (ρ), and of infinite extent.

$$g_B = 2\pi G\rho h \approx 0.04192\rho \frac{mGal}{m} \quad (3)$$

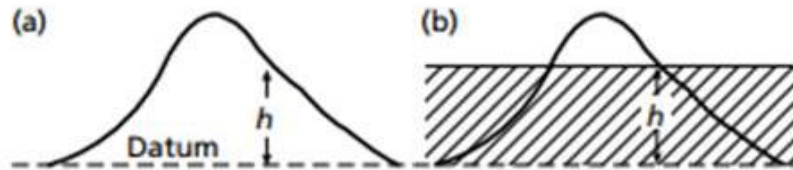


Figure 1.3: a) Free-air correction for an observation at a height h above datum. b) The Bouguer correction, the shaded region corresponds to a slab of rock of thickness h extending to infinity in both horizontal directions. Taken from and modified from Kearey et al. (2002).

1.2.8 Free Air Anomaly

The Free Air anomaly is defined by:

$$\Delta g_{FA} = g_m + (g_{FA} + g_L + g_{tide}) - g_n(4)$$

In this formula g_m and g_n are the measured and the calculated gravity values for the ellipsoid respectively. The corrections in parentheses are the free air correction (g_{FA}), latitude correction (g_L), and tidal correction (g_{tide}).

1.2.9 Bouguer Anomaly

The Bouguer anomaly is defined by:

$$\Delta g_B = g_m + (g_{FA} + g_L + g_{tide} - g_B) - g_n(5)$$

In this formula g_m and g_n are the measured and the calculated gravity values for the ellipsoid. The corrections in parentheses are the free air correction (g_{FA}), latitude correction (g_L), tidal correction (g_{tide}), and Bouguer correction (g_B).

The Free Air Anomaly takes into account the elevation of the measurement station. The Bouguer Anomaly does the same and also compensates for the attraction of the land-mass above the ellipsoid.

1.2.4 Magnetic Force and Magnetic Field Strength

The force between two magnetic poles is inversely proportional to the square of their separation. An inverse square law for the force, F , between magnetic poles with strengths p_1 and p_2 at distance r from each other can be formulated as (Lowrie, 2007):

$$F(r) = K \frac{p_1 p_2}{r^2} \quad (6)$$

The proportionality variable K is the inverse of the magnetic permeability, which is a property of the medium in which the poles are located.

The gravitational field of a given mass is defined as the force it exerts on a unit mass. However, this concept cannot be transferred to magnetism because magnetic poles do not exist. Therefore, the magnetic field B is defined as the force exerted by a pole of strength p on a unit pole at a distance r :

$$B(r) = K \frac{p}{r^2} \quad (7)$$

1.3 Geological Background

Williams (1979) divided the Canadian Appalachians into five zones based on stratigraphic and structural characteristics between Cambrian-Ordovician and older rocks. From west to east, these are the Humber, Dunnage, Gander, Avalon and Meguma Zones (Fig. 1.4). Each of these zones represents a different stage of the generation and destruction of the late Precambrian- Early Paleozoic Iapetus Ocean, embodying a distinctive tectonostratigraphic complex in the Appalachian Orogen.

Much of Western Newfoundland lies within the northeast Canadian Appalachians (Figure 4), and specifically within the Humber zone. This zone represents the deformed margin of the Laurentian continent (Williams, 1979; Williams et al., 1988) and it is divided in two parts: the internal zone, mainly characterized by metamorphic rocks affected by the Appalachian tectonism, and the external zone with weakly metamorphosed rocks (Waldron et al., 1998) (Fig. 1.5).

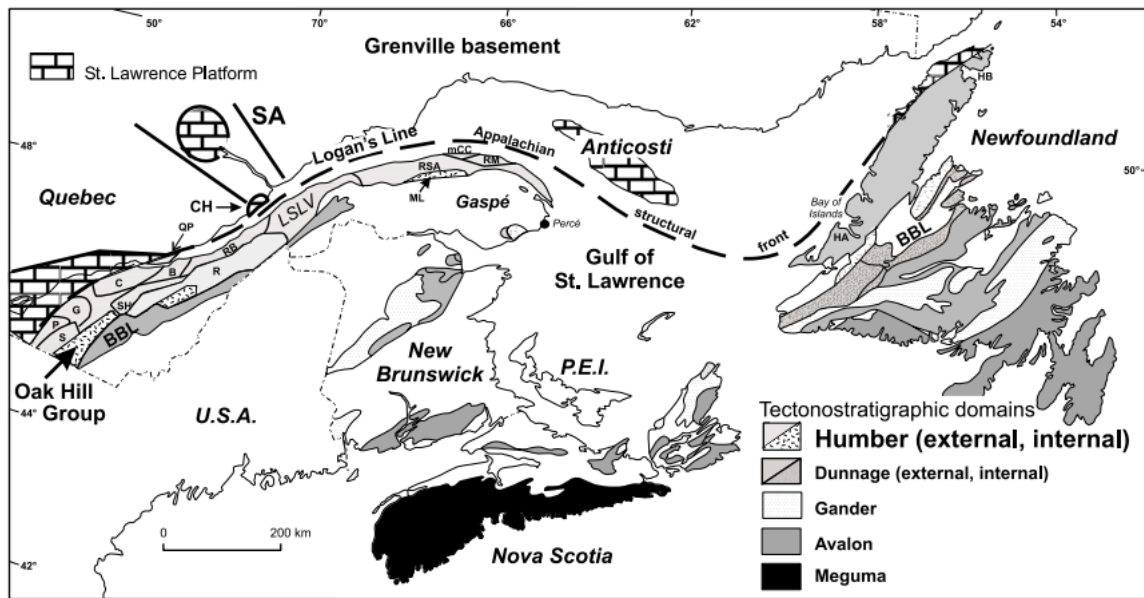
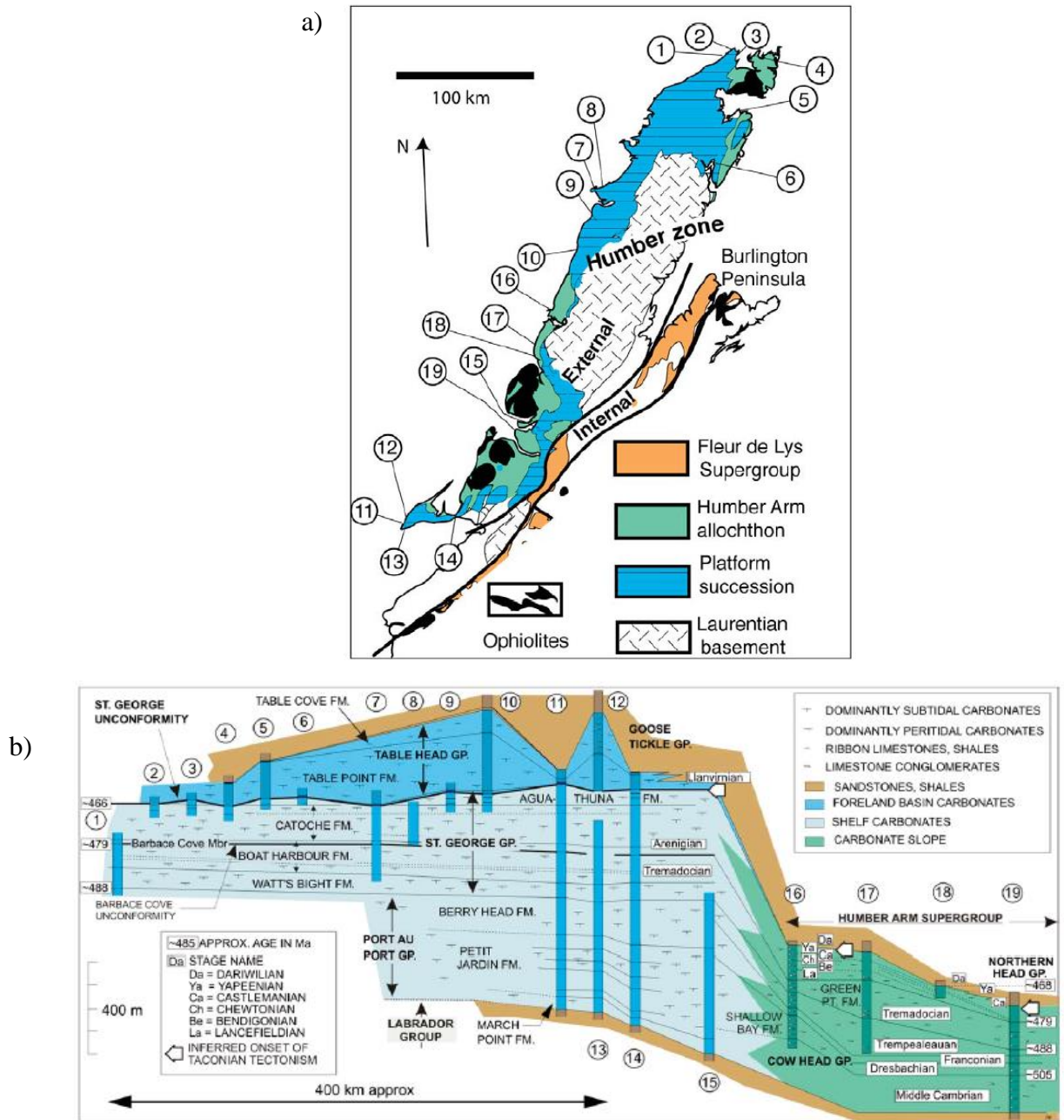


Figure 1.4: Tectonostratigraphic domains of the Canadian Appalachians. Taken from Lavoie et al. (2003), after Williams (1995).

1.3.1 Tectonic Evolution

The tectonic evolution of Western Newfoundland can be traced back to the Grenville Orogen, an event associated with the assembly of the supercontinent Rodinia. The Grenville Orogen provides the Mesoproterozoic foundation on which the Laurentian margin was built (Waldron et al., 2012). The Neoproterozoic rifting of the Supercontinent Rodinia led to the opening of the Iapetus Ocean and development of a predominantly carbonate rift-drift succession along the eastern Laurentia margin (Waldron et al., 2012).

In Western Newfoundland, the passive margin consisted of a Middle-to-Late Cambrian, narrow, high-energy platform that evolved into an early Middle Ordovician, wide, low-energy platform (James et al., 1989). The passive margin stage ended with the onset of eastward seafloor subduction and the eventual collision and suturing of the microcontinent Dashwoods and emplacement of allochthons onto the margin during the Middle Ordovician Taconic Orogen (Lavoie, 2008; Waldron et al., 2012).



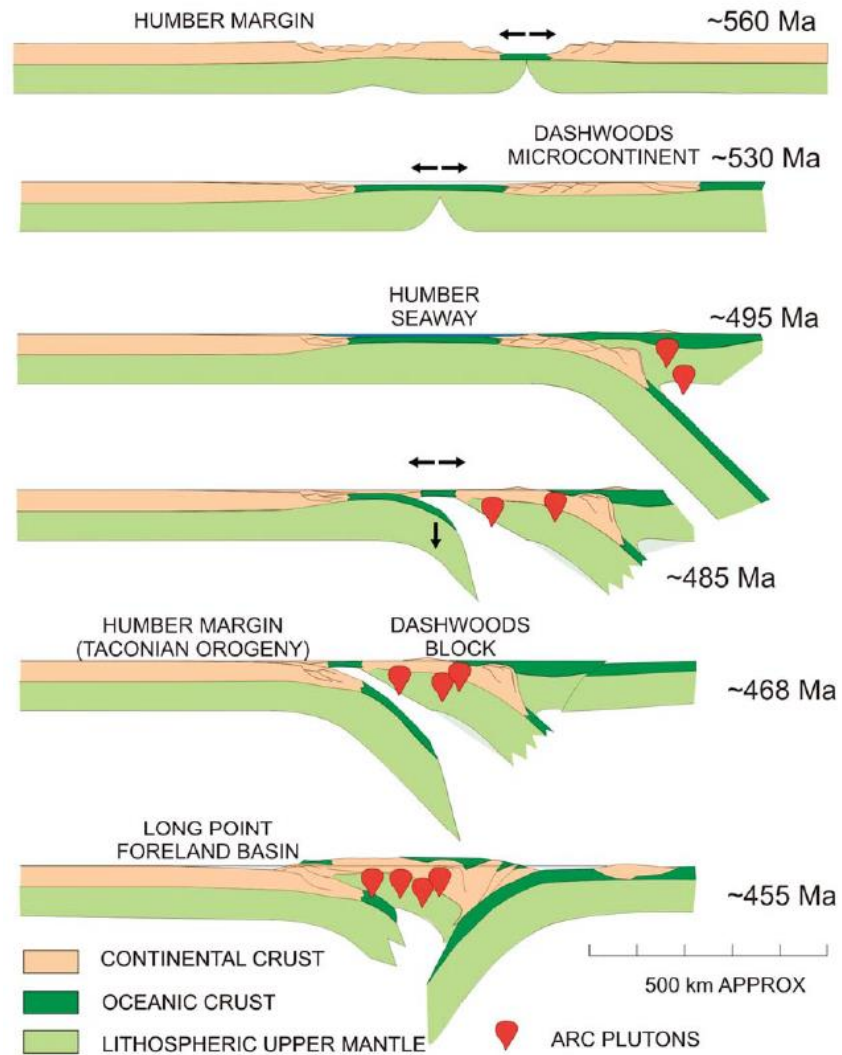


Figure 1.6: Continental collision and subduction leading to the formation of the Humber Margin during the Taconian Orogen, from Waldron et al. (2012).

The Taconic Orogen and other subsequent orogenic events (the Salinic and the Acadian orogenies) shaped Western Newfoundland (van Staal and Barr, 2012). Taconic deformation established the overall structural style of the Humber Zone (Cawood, 1993), as allochthons of the deep sea floor and continental slope were obducted and carried to their current position in Western Newfoundland (Fig. 1.6 & Fig. 1.7). The Salinic Orogen (Lower Silurian) is characterized by imbrication of the Taconic allochthon and additional displacement toward the west of this feature (Cawood et al., 1994). It is better preserved in

central Newfoundland (van Staal and Barr, 2012) but deformed shelf rocks in Western Newfoundland were also affected by this event (Hinchey et al., 2015). During the Acadian Orogen (Early Devonian), the Humber Arm Allochthon was apparently located in an elongate depression surrounded by uplifted platform carbonates and Grenville basement blocks (Cawood and Williams, 1988). The Acadian Orogen caused the inversion of pre-existing deep-seated basement-involved normal faults like the Round Head thrust, mapped as the frontal thrust responsible for the deformation observed in the region (Cawood and Williams, 1988; Hinchey et al., 2015; White and Waldron, 2018). This deformation led to the formation of an offshore tectonic wedge, or triangle zone, imaged on several seismic lines (Fig. 1.8) (Waldron et al., 2012) and caused thick-skinned compressional faulting (Cooper et al., 2001).

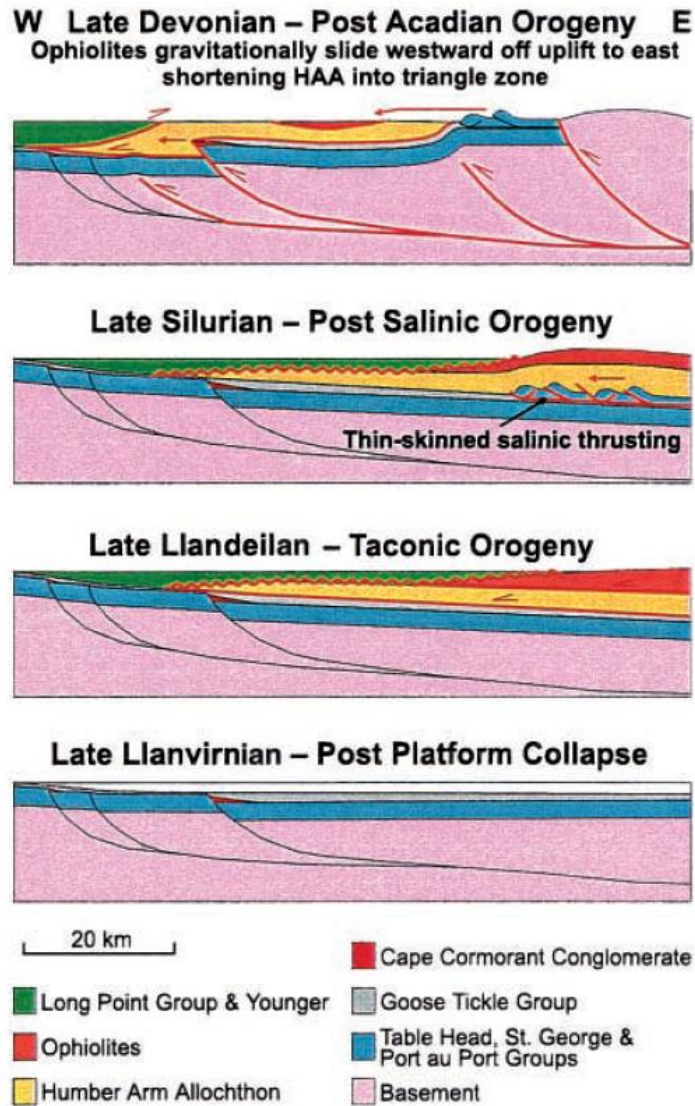


Figure 1.7: Conceptual Model of structural evolution of the Humber Zone, from Cooper et al. (2001), after Knight and Boyce (1991).

A final Carboniferous orogenic episode, the Alleghanian Orogen, had a minor effect in Western Newfoundland. Inasmuch as it involved the collision of Laurentia with the main part of Gondwana, forming the supercontinent Pangea (van Staal and Barr, 2012). The Alleghanian Orogen was a relatively mild transtensional event leading to major dextral movement on faults with Appalachian trend (Cawood, 1993; Waldron et al., 2012). This movement generated the Maritimes Basin in a transtensional environment at a releasing bend formed around a promontory along the Laurentia margin, and thinned the crust,

accounting for the major subsidence of the basin and the sedimentation along the Cabot Fault system (Waldron et al., 2015).

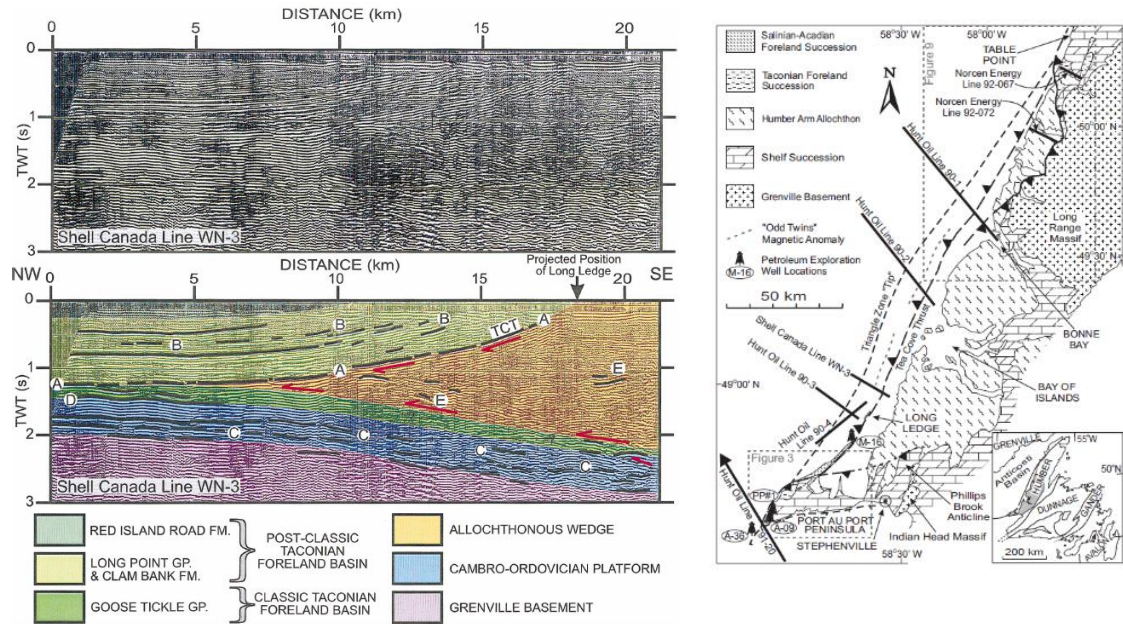


Figure 1.8: Uninterpreted and interpreted seismic data, Shell Canada Ltd. line WN-3. TCT with geometry of thrusts in Port au Port Peninsula, from Stockmal et al. (1998). TCT = Tea Cove Thrust.

1.3.2 Major Geological Subdivisions

1.3.2.1 Basement, Rift and Shelf Successions

Mesoproterozoic Grenville crystalline basement underlies Western Newfoundland (Waldron et al., 2012). It consists of igneous and metamorphic rocks that record the assembly of the earlier supercontinent Rodinia at ~ 1 Ga during the Grenville Orogen (Heaman et al., 2002; Waldron et al., 2012). Outcrops of this ancient rock can be found in the Long Range massif and the much smaller Indian Head Range to the south.

The transition to passive margin sedimentation is characterized by the Cambrian Labrador Group, and other rift-related units (Waldron, 1994). The upper part of this group consists of shale and limestone deposited in shallow-marine shelf environments. The

Curling Group is a deep-water time-correlative sequence with the Labrador Group (James et al., 1989) (Fig. 1.9).

Early Cambrian clastic rocks were flooded by a major sea level rise leading to the development of a broad carbonate-dominated passive margin. The Upper Cambrian-Lower Ordovician Port au Port Group was deposited upon a high energy carbonate platform, whereas the younger Lower Ordovician St. George Group was a low-energy carbonate platform (Fig. 1.9) (James et al., 1989). These carbonate shelf rocks can have excellent porosities which make them significant prospects for oil exploration (Baker and Knight, 1993; Cooper et al., 2001; Burden et al., 2014). At the same time and farther offshore, on the slope of the Laurentian continent, two laterally correlative successions, the Cow Head Group in the north and the Northern Head Group in the south, were deposited (James and Stevens, 1986; Lavoie, 2008; Waldron et al., 2012).

A regional paleokarst surface representing a depositional hiatus (Knight et al., 1991), known as the St. George Unconformity (Fig. 1.7), marks the boundary between the St. George Group and the overlying Table Head Group. The unconformity is thought to be generated by the passage of a lithospheric flexural bulge associated with a westward advancing arch trench system (Jacobi, 1981; Knight and Cawood, 1991).

1.3.2.2 Taconian Foreland Basin

Tectonic loading of Taconian allochthons, which were emplaced onto the Laurentian margin during the Taconian Orogen, generated a foredeep into which sediments of the Taconian foreland basin were deposited. Shallow marine carbonates of the Table Point Formation (Table Head Group) were the first units deposited into the tectonically active basin. Due to rapid subsidence, deeper water facies were soon deposited upon these rocks (e.g., Table Cove Formation) (Figure (Klappa et al., 1980; Stenzel et al., 1990). Later, extensional faulting accompanied subsidence of the foreland basin and collapse of the platform (Stockmal et al., 1998; Waldron et al., 1993). A strong reflection, observed along

offshore seismic profiles, marks the transition from platform carbonates to more muddy lithologies (Waldron et al., 2012).

Overlying the Table Head Group are clastic sediments of the Darriwillian Goose Tickle Group which were shed from the advancing orogen and were deposited in the foreland basin during the Taconian Orogen (Quinn, 1992; Stenzel et al., 1990).

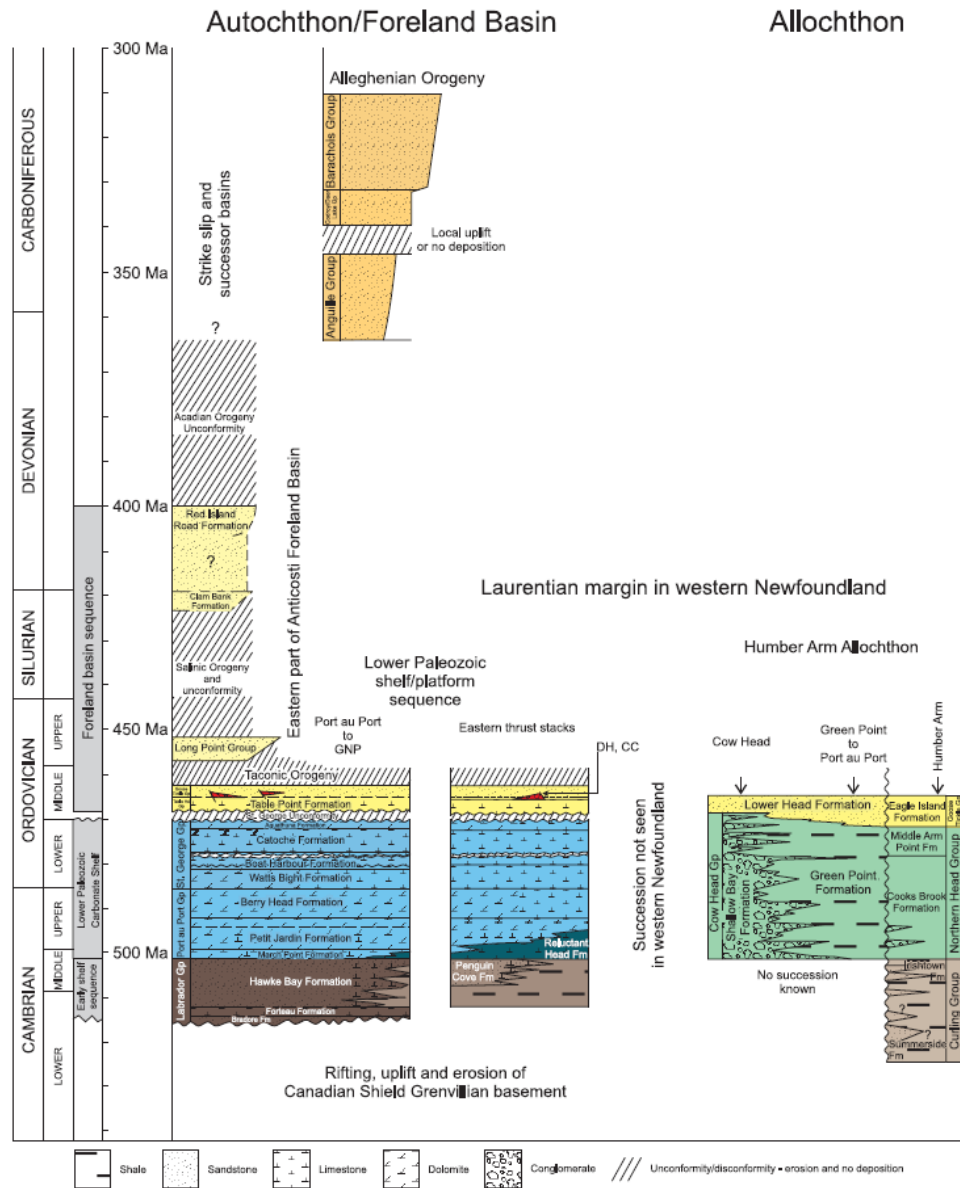


Figure 1.9: Simplified stratigraphy of Lower Paleozoic sequences in Western Newfoundland, from Hinchey et al. (2015), after Cooper et al. (2001). DH = Daniels Harbour conglomerate, CC = Cape Cormorant conglomerate.

1.3.2.3 Taconian Allochthons

Taconic thrusting detached and carried large slices of deep marine sediments and oceanic crust onto the marine carbonate platform (Burden et al., 2014). Allochthonous rocks from the Humber Arm and Hare Bay allochthons in Western Newfoundland consist of: rift-related units, continental slope and rise units, and Taconian flysch. The highest structural slices are ophiolite complexes, considered to represent suprasubduction zone ocean floor (Jenner et al., 1991).

The Taconic unconformity, an interpreted major hiatus (6-8 m.y.), defines the base of the Taconic basin and reflects the emplacement of the Taconic allochthons onto the shelf margin (Burden and Williams, 1995; Cooper et al., 2001). Even though the Humber Arm Allochthon's emplacement is generally interpreted to have occurred during Middle Ordovician Taconian orogenesis, seismic reflection data suggest final emplacement is Early Devonian (Stockmal et al., 1998). The Long Point Group is structurally at the top of a triangle zone and was thrust eastward (Tea Cove Thrust) above rocks of the Humber Arm Allochthon relative to its current position (Stockmal et al., 1998; Waldron et al., 1993).

The Humber Arm Allochthon is the proposed source for some Cambro-Ordovician petroleum systems in Western Newfoundland. Specifically, the shales of the Green Point Formation (Cow Head Group) are excellent source rocks with high TOC content derived from Type I-II organic matter (Fowler et al., 1995).

1.3.2.4 Post-Taconian Foreland Basin

After the Taconian Orogen, the margin continued to subside. Shallow marine carbonate units of the Lourdes Formation onlap the Goose Tickle Group. It has excellent porosities (10-12%) and it can be identified on seismic reflection profiles offshore as the lowest reflector of a folded package (Cooper et al., 2001; Stockmal and Waldron, 1990; Waldron et al., 2002). The Lourdes Formation is overlain by the Winterhouse Formation, deeper

water siliciclastics, and lastly by the Misty Formation, a cross bedded and parallel laminated marginal marine sandstone (Quinn et al., 1999).

A major unconformity, with a time gap of about 20 m.y., separates the Long Point Group from the Early Devonian marginal marine clastic and minor carbonate sediments of the Calm Bank Formation (Burden et al., 2002; Cooper et al., 2001). The Calm Bank Formation and the overlying Emsian Red Island Road Formation may represent foreland fill corresponding to the Salinian and Acadian orogenies (Stockmal et al., 1998; Waldron et al., 1998; Waldron, 1994).

1.3.2.5 Maritimes Basin: Carboniferous Rocks

The next overlying rock succession comprises the youngest preserved sediments in Western Newfoundland. The Carboniferous strata consist of the Anguille, Codroy and Barachois Groups found in the Deer Lake and Bay St. George basins (offshore and onshore Western Newfoundland) (Fig. 1.10).

The Anguille Group consists of sandstone and shale with rare carbonate. Sediments from this group are derived primarily from uplands to the southeast and represent early manifestations of the Long Range Fault (Knight, 1983; Miller et al., 1990). The overlying concordant and locally conformable Codroy Group is characterized by thick basal evaporites, grey shales, marine carbonates and redbeds (Knight, 1983). Strata in the lower Codroy Group record a tectonically inactive period of low subsidence rates and marine transgression, while those of the upper Codroy Group indicate renewed tectonic activity and a return to dominantly clastic sedimentation (Miller et al., 1990). The Barachois Group is the youngest unit in the St. George and Deer Lake basins. It encompasses non marine fluvial successions up to 2500 m thick in the Codroy Lowlands (Knight, 1983).

The Carboniferous sequence contains a significant thickness of mostly continental clastic rocks, making Codroy and Barachois starta target reservoirs. In addition, some coals,

lacustrine shales and limestones in the Carboniferous strata may act as source rocks for this basin and the Anticosti Basin (Burden et al., 2014; Enachescu, 2012).

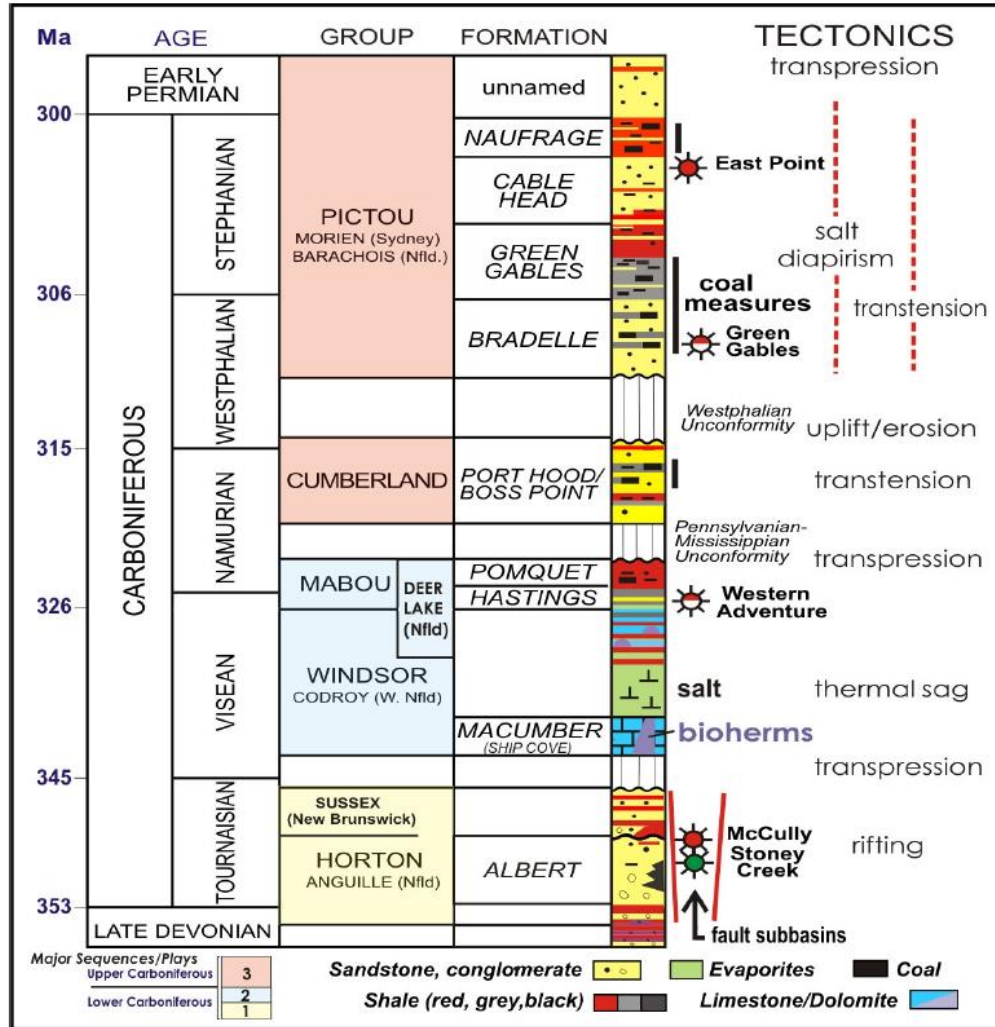


Figure 1.10: Maritimes Basin lithostratigraphic column, with major tectonic phases and unconformities, key lithologic elements, and stratigraphic position of discovered oil and gas fields, from Lavoie et al. (2009).

1.4 Previous Work

Approximately 12,000-line km of 2-D offshore seismic and 1100-line km of 2-D onshore seismic data were collected in Western Newfoundland from the 1980s to the mid-1990s (Hinchey et al., 2015) (Fig. 1.11a). These early 2-D seismic studies focused on the nature of the Appalachian structural front (Hall et al., 1998; Stockmal and Waldron, 1990) to understand the tectonic evolution of the Humber Zone, the Anticosti Basin (Waldron et al., 1998; Waldron, 1994), and the basin's potential for oil exploration (Cooper et al., 2001; Hall et al., 1992; Stockmal et al., 2004). Seismic refraction profiles have also been acquired and different authors have used them to study the deep structure of the Newfoundland Appalachians (Hughes et al., 1994; Jackson et al., 1998; Marillier et al., 1994, 1991, 1989; Michel et al., 1992) (Fig. 1.12).

Recently, aeromagnetic data were collected offshore and onshore Western Newfoundland from 2009-2012 (Fig. 1.11b) (Hinchey et al., 2015). Waldron et al. (2002) interpreted a pair of asymmetric positive magnetic anomalies (Odd-twins magnetic anomaly (Ruffman and Woodside, 1970)) located in the Gulf of St. Lawrence as magnetite rich strata within the Winterhouse and Misty Point formations. Generally, strong magnetic anomalies are interpreted as ophiolites (Hinchey et al., 2015). However, limited use of these new data has yet been made for research.

Gravity and integrated studies in Western Newfoundland are very sparse (Hayward et al., 2001; Miller, 1990). A few studies in the St. George Basin have been performed (Miller et al., 1990; Peavy, 1985) in order to determine the internal structure of this basin.

a)

b)

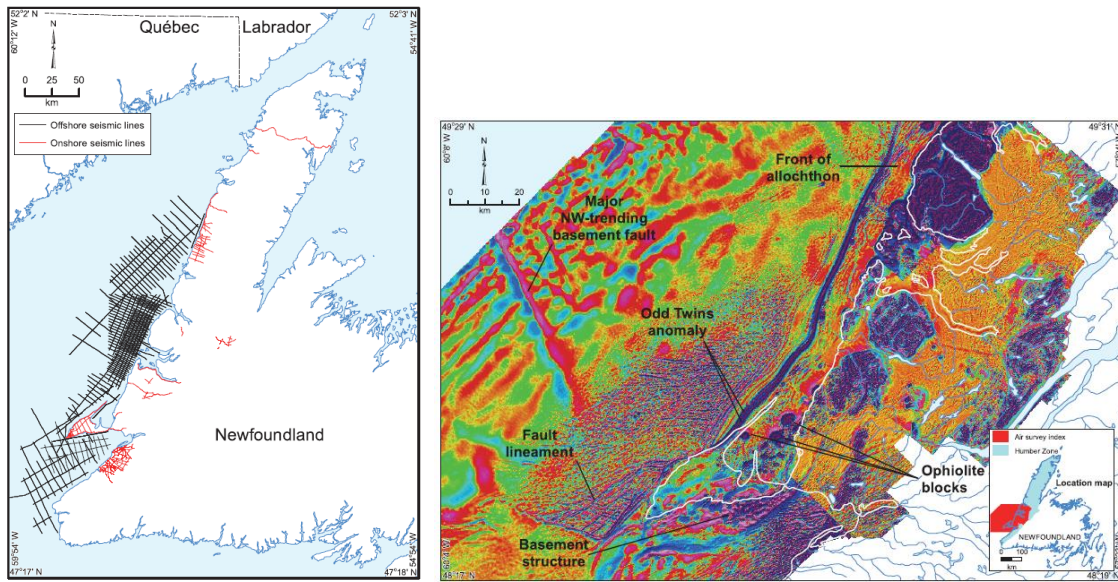


Figure 1.11: a) Distribution of seismic lines, onshore and offshore, Western Newfoundland and b) regional geophysical map of the second derivate of aeromagnetic data in Western Newfoundland flown in 2009-2012, from Hinchey et al. (2015).

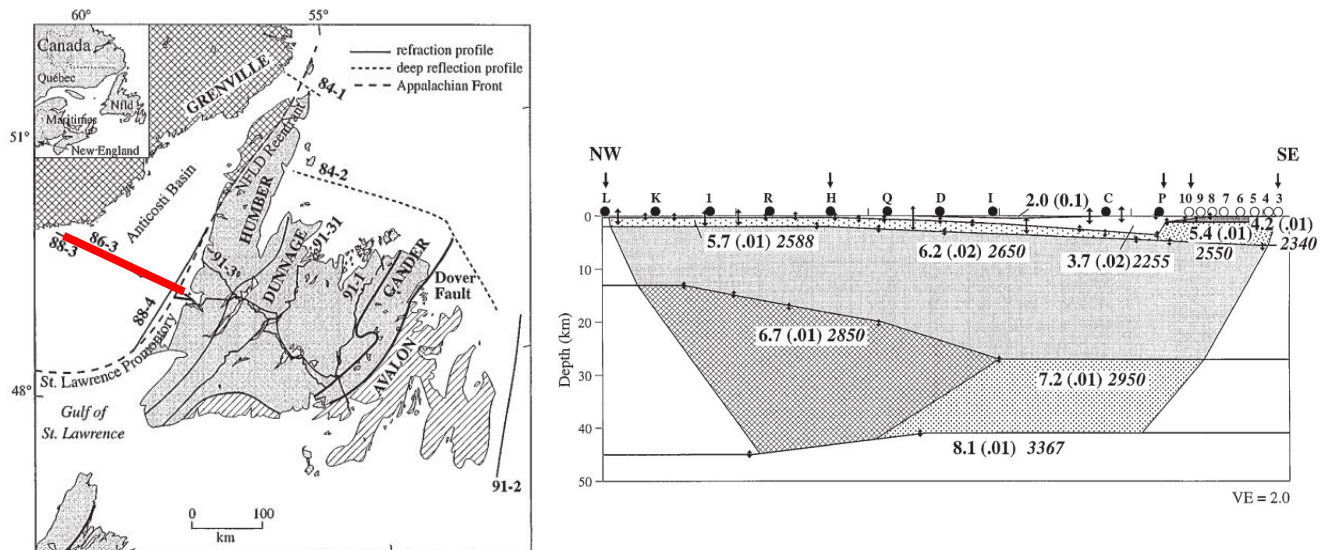


Figure 1.12: Seismic refraction line in Western Newfoundland. Red line shows the position of the profile, from Jackson et al. (1998)

1.5 Purpose

The general objective of this research is to construct a 3D lithospheric model of Western Newfoundland to better understand the Appalachian structure in the region.

This research has the following specific objectives:

- Review previous geophysical and geological studies in the study area.
- Analyse gravity and magnetic data and generate anomaly maps.
- Perform Spectral analysis of the potential field data.
- Analyse magnetic and gravity datasets using Euler deconvolution and Curvature analysis.
- Interpret a selection of offshore seismic reflection lines to obtain additional structural constraints.
- Generate a 3D density model using the potential field data and the constraints from seismic reflection and seismic refraction profiling.

1.6 Summary

Chapter II contains the methodology followed in this research project. Details of the acquisition of the potential field data, the analysis of the data, the gravity modelling and inversion, and the seismic interpretation can be found in that chapter. The results for each analysis are presented in Chapter III, Chapter IV and Chapter V. A final discussion of the results and conclusions are stated in Chapter VI and Chapter VII.

Chapter 2: Data and Methods

In this chapter, the steps undertaken for this research project are explained in detail. Specifications of the gravity, magnetic, topographic and seismic datasets are also described. The chosen parameters for each of the analyses of the gravity and magnetic datasets are stated and justified. The key software packages used, IGMAS and GRAV3D, are also described.

2.1 Datasets

2.1.1 Gravity Data

The gravity data used for this study are obtained from the World Gravity Model 2012 (WGM 2012), a high resolution satellite dataset which includes Free Air, Bouguer and Isostatic anomalies, derived from an earlier EGM2008 Geopotential model and the ETOPO1 Global Relief model (Bonvalot et al., 2012).

The EGM2008 is developed using spherical harmonics up to a degree of 2160 (with some terms up to degree and order 2190) by the National Geospatial-Intelligence Agency (NGA) (Pavlis et al., 2008). The EGM2008 includes surface gravity measurements, satellite altimetry, and satellite gravimetric measurements.

The surface free-air gravity anomaly (Fig. 2.1a) is computed at the Earth's surface using Molodensky's theory (Heiskanen and Moritz, 1967) with a 1 degree x 1 degree resolution and taking into account corrections for the mass of the atmosphere (Bonvalot et al., 2012). Molodensky's theory uses the Earth's surface as the boundary surface. The corresponding solution consists of integrals involving gravity anomalies and topographic heights (Denker and Tziavos, 1999; Molodensky et al., 1962).

The complete spherical Bouguer anomaly (Fig. 2.1b) is calculated by taking into account the continents, oceans, and the precise characteristics of major lakes, inland seas, polar ice caps, shelves and land areas below sea level, and the isostatic effects at the Earth's surface. The reference density used to calculate the Bouguer anomaly map is 2670 kg/m^3 (Bonvalot et al., 2012).

These gravity datasets (Fig. 1.1) were downloaded in April 2017, from the International Gravimetric Bureau website (<http://bgi.obs-mip.fr/>). This organization collects all measurements and pertinent information about the Earth's gravity field and makes them available for scientific purposes upon request.

The Free Air Anomaly and Bouguer Anomaly are combined to produce a 1 minute x 1 minute grid from the Free Air anomalies offshore and Bouguer anomalies on land.

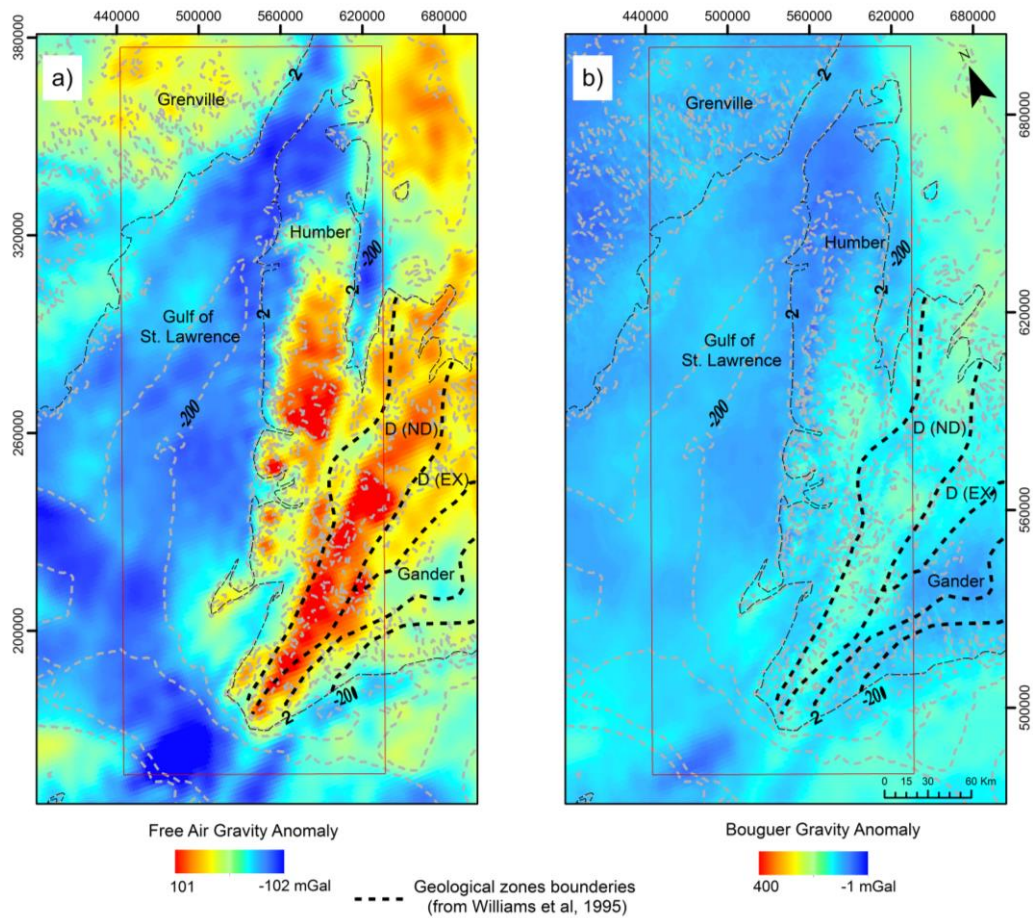


Figure 2.1: Western Newfoundland gravity map. Map shows surface geological zones of the Appalachian Orogen in Newfoundland (Williams, 1995). Dashed grey lines correspond to bathymetric and topographic contours (m). a) Free Air anomaly, b) Bouguer anomaly. Abbreviations: D (Ex), Exploits subzone of the Dunnage zone; D (ND), Notre Dame subzone of the Dunnage zone.

2.2.2 Topography Data

ETOPO1 is a 1 arc-minute relief model of Earth's surface that integrates land topography and ocean bathymetry. It was developed in 2008 by the National Geophysical Data Center (NGDC), an office of the National Oceanic and Atmospheric Administration (NOAA). ETOPO1 is generated from diverse global and regional digital datasets, which are shifted to common horizontal and vertical datums (Ante and Eakins, 2009; Bonvalot et al., 2012).

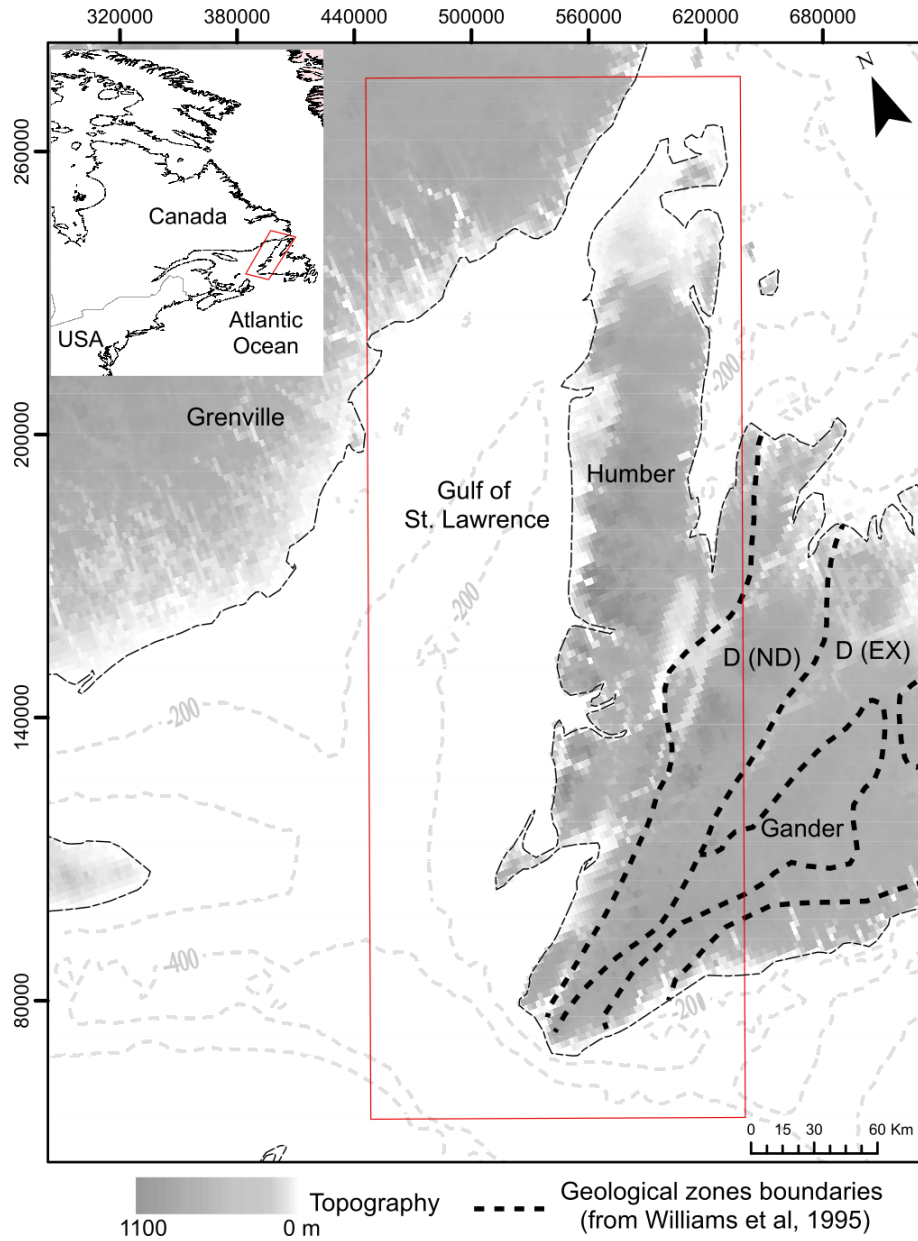


Figure 2. 2: Western Newfoundland topographic map (Ante and Eakins, 2009). Map shows surface geological zones of the Appalachian Orogen in Newfoundland (Williams, 1995), outlined by dashed black lines. Abbreviations: D (Ex), Exploits subzone of the Dunnage zone; D (ND), Notre Dame subzone of the Dunnage zone.

These topography/bathymetry data (Fig. 2.2) are included when downloading the WGM2012 model, explained in the previous section. However, they can also be downloaded from the National Oceanic and Atmospheric Administration (NOAA) website: <https://www.ngdc.noaa.gov/mgg/global/global.html>.

2.2.3 Magnetic Data

High resolution magnetic data (Fig. 2.3a) for the province of Newfoundland and Labrador were acquired by the federal and provincial governments during different surveys. These data are available from the virtual atlas website: <http://geotlas.gov.nl.ca/>.

The Corner Brook dataset is from a survey conducted by the Geological Survey of Newfoundland and Labrador between November, 2008 and March, 2009. Three Geometrics G822 split-beam cesium vapour magnetometers mounted at 14.8 m separation in aircraft wingtip pods and in a tail boom, an RMS DAARC500 automatic aeromagnetic digital compensator, and a GEM Systems GSM-19 Overhauser base station are used for the acquisition. Grid cell size is 40 m (Kilfoil, 2009; Kilfoil and Cook, 2009).

The Indian Head, Deer Lake and Gros Morne acquisitions are from a survey conducted by Nalcor Energy and the Department of Natural Resources of the Government of Newfoundland and Labrador between October, 2008 and May, 2009. Two Geometrics G822 split-beam cesium vapour magnetometers mounted at 11.0 m separation in aircraft wingtip pods, a GEM Systems GSM-19 Overhauser base station, and fluxgate magnetometers for aircraft magnetic compensation were used during the acquisition. Grid cell size is 50 m (Kilfoil, 2009; Kilfoil and Cook, 2009).

The magnetic dataset for offshore Western Newfoundland was acquired by Nalcor Energy and the Department of Natural Resources of the Government of Newfoundland and Labrador from June to October 2012. Three Geometrics G822 split-beam cesium vapour magnetometers mounted in aircraft wingtip pods and tail boom were used for this acquisition (Dumont and Jones, 2013).

A compilation of magnetic data for Canada (Miles and Oneschuk, 2016) is also downloaded from the Oasis Montaj seeker (Fig. 2.3b) . This compilation has a grid size of

2 km. This compilation is knitted with the other magnetic data sets onto a grid size of 50 m using the Oasis Montaj software and blended using the stitch method.

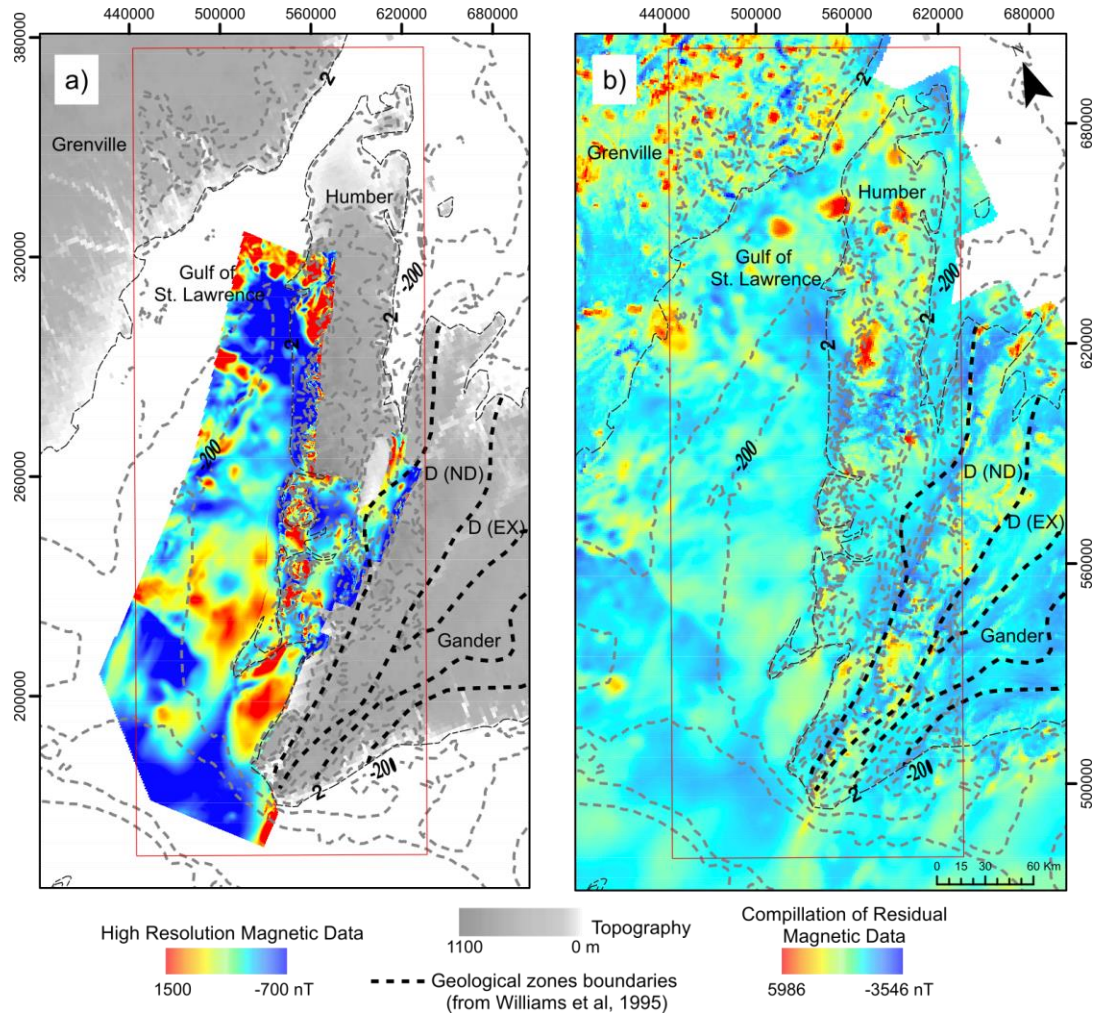


Figure 2. 3: Western Newfoundland residual magnetic map. Map shows surface geological zones of the Appalachian Orogen in Newfoundland (Williams, 1995). Dashed grey lines correspond to bathymetric and topographic contours (m). a) High resolution magnetic map, b) Compilation of residual magnetic data for Western Newfoundland. Abbreviations: D (Ex), Exploits subzone of the Dunnage zone; D (ND), Notre Dame subzone of the Dunnage zone.

2.2.4 2D Seismic Reflection Data

Twelve seismic lines are strategically chosen to interpret and constrain the sedimentary structure for the 3D density model generated for this project. The seismic lines (Fig. 2.4) are from projects CA-3000205-GOA, CA-3000701-GOA, CA-3000719-GOA and CA-

3000686-GOA, completed before 2000. These seismic lines are available as paper plots from the Provincial Department of Natural Resources and the Canada-Newfoundland Offshore Petroleum Board (CNLOPB). The seismic lines are then scanned, digitized, and interpreted with Petrel software, a seismic interpretation software package available at Memorial University.

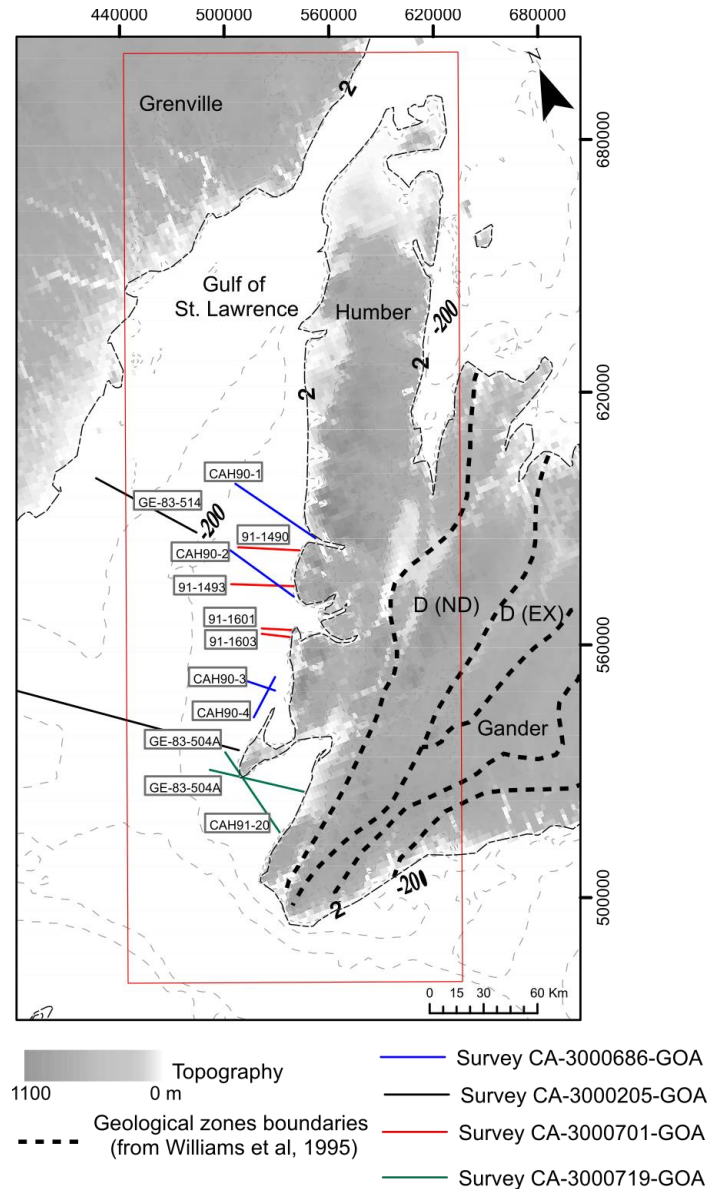


Figure 2. 4: Map of selected seismic reflection lines. Map shows surface geological zones of the Appalachian Orogen in Newfoundland (Williams, 1995). Dashed grey lines correspond to bathymetric contours (m). Abbreviations: D (Ex), Exploits subzone of the Dunnage zone; D (ND), Notre Dame subzone of the Dunnage zone.

The seismic interpretation is completed by following strong reflectors associated within the basement and platform succession. Despite the chaotic geometry of the reflectors, the allochthonous wedge can be interpreted. The foreland and HAA units are also imaged but are not discussed in detail since they are beyond the scope of this crustal-scale research.

The seismic horizons are converted to depth using a standard velocity of 4000 m/s for sediments (Fig. 2.5), and then introduced into IGMAS.

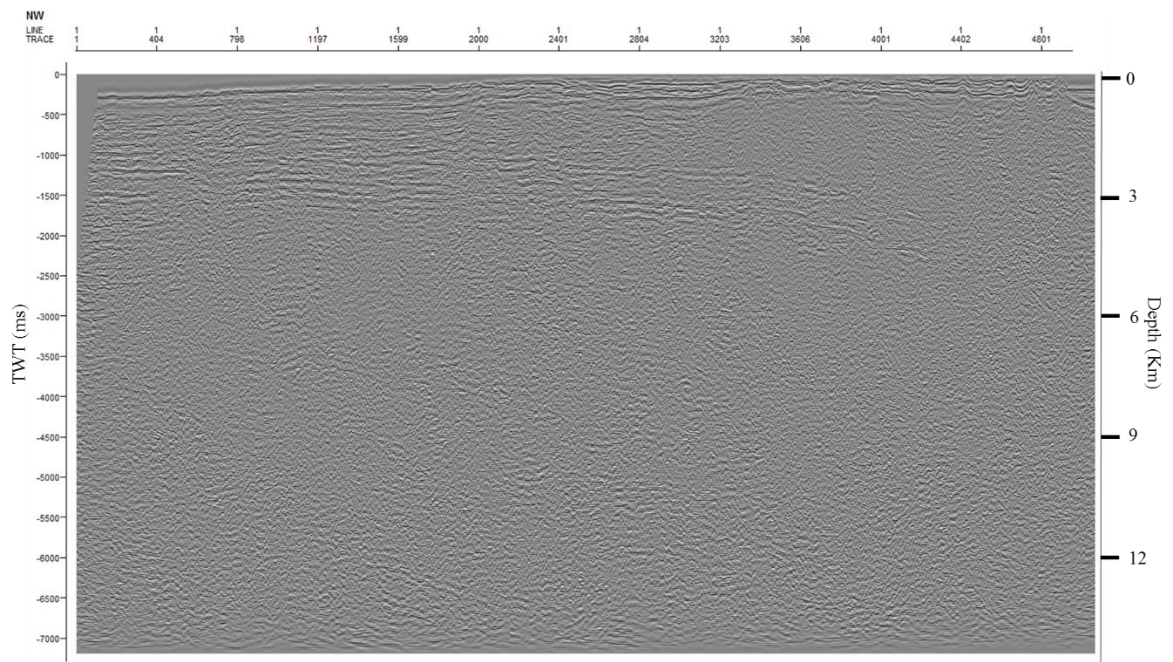


Figure 2. 5: Line CAH90-01 with depth conversion. See Fig. 1.4 for location.

2.2 Statistical Analysis

The statistical analysis of the gravity and magnetic anomalies is performed in Microsoft Excel. Dispersion trends are calculated for the different gravity and magnetic datasets. Correlation factors of observed and predicted gravity and magnetic data, along with basic statistics (means and standard deviations) were computed. The statistical analysis is useful to understand the behavior and nature of the potential field data, and to study the correlation between the observed and calculated gravity data.

2.3 Separation of Regional and Residual Anomalies

Spectral analysis is one method that can be used for the study of potential field anomalies by transforming the data from the space domain to the frequency domain and then analyzing their frequency characteristics (Dimitriadis et al., 1987; Spector and Grant, 1970). This method assumes that for large numbers of samples, the relationship between the logarithm of the power spectrum (E) of the gravity field of a monopole source versus the wave number (radial/distance) is linear. The slope of the straight line is proportional to the depth to the top of the corresponding body causing the gravity anomaly. Thus, if k denotes the wavenumber and $S(k)$ denotes the power spectrum of the gravity field, the depth (d) to the source can be estimated from the relationship $S(k) = f(k)$ by employing the formula:

$$\ln S(k) = -2 * k * d \quad (1)$$

Spectral analysis (Dimitriadis et al., 1987; Spector and Grant, 1970) is based on calculating the wavelengths of the bodies that cause the gravity or magnetic anomalies. Long wavelengths are inferred to relate to deep bodies while short wavelengths are inferred to relate to shallower bodies. The MAGMAP tool, which is part of the Oasis Montaj software, applies the Fast Fourier Transform (FFT) to the data and then plots the radially averaged power spectrum of the potential field data.

The gravity and magnetic anomaly grids are imported into Oasis in order to compute the power spectrum data. These values are exported to and plotted in Microsoft Excel, which allows for better visualization of the graph points and control over the points to calculate the slope trends.

Once the slope trends are known, the MIGMAP module of Oasis Montaj is then used. This module applies different filters, such as Gaussian, Band pass and Butterworth, to the

gravity and magnetic grids. From these, differences between the regional anomaly and the total anomaly are calculated in order to extract the residual anomaly.

2.4 Derivative-based Filters for Potential Field Data and Reduction to the Pole

Semiautomatic methods based on the use of derivatives are widely used to determine potential field source parameters such as locations boundaries and depths (Blakely, 1995; Nabighian et al., 2005; Salem et al., 2007).

The total gradient (Analytic Signal) is a popular method for locating the edges of potential field data. The Analytic signal is the square root of the sum of squares of the data derivatives in the x, y, and z directions (Nabighian, 1984, 1972):

$$\text{Analytic signal} = \sqrt{\left(\frac{\partial M}{\partial x}\right)^2 + \left(\frac{\partial M}{\partial y}\right)^2 + \left(\frac{\partial M}{\partial z}\right)^2} \quad (2)$$

where M is the observed potential field.

The tilt derivative is the generalized local phase. This method assumes that the source is a buried vertical contact model (Fairhead et al., 2008). Calculating the tilt angle of a residual magnetic field enhances weak magnetic anomalies, which would otherwise be overshadowed by stronger structures. The Tilt derivative is defined as:

$$TDR = \tan^{-1}\left(\frac{VDR}{THDR}\right) \quad (3)$$

where VDR and THDR are the first vertical and total horizontal derivatives of the total magnetic intensity, respectively. Due to the nature of the arctan trigonometric function, all amplitudes are restricted to values between $\pi/2$ and $-\pi/2$, which makes this function like an automatic gain control filter (Verduzco et al., 2004). The tilt angle has the property of

being positive over the sources, crossing through zero at or near the edge of a vertical sided source, and being negative outside the source region (Arisoy and Dikmen, 2013). The tilt angle will be relatively insensitive to the depth of the source and should resolve shallow and deep sources equally as well (Miller and Singh, 1994).

Another edge detection technique, the total horizontal derivative of the tilt angle, is outlined in Verduzco et al. (2004). It is defined as:

$$THDR_{Tilt} = \sqrt{\left(\frac{\partial tilt}{\partial x}\right)^2 + \left(\frac{\partial tilt}{\partial y}\right)^2} \quad (4)$$

The total horizontal derivative of the tilt angle is independent of the geomagnetic field and generates maximum values over the edges of the magnetized bodies (Arisoy and Dikmen, 2013).

Reduction to pole (RTP) is a standard part of magnetic data processing. This procedure can transform a magnetic anomaly caused by an arbitrary source into the anomaly that the same source would produce if it is located at the pole and magnetized by induction only (Dian and Wang, 2013). In other words, RTP uses mathematical filtering methodology to calculate the magnetic anomaly that would be observed at 90° angle.

RTP was introduced by Baranov (1957) and can be computed by twice differentiating the source function in the vertical direction. This operation is easier to perform in the wavenumber domain, which is given by (Ravat, 2007):

$$\Delta T_z(k) = |k|^2 \frac{\Delta T(k)}{B^2} \quad (5)$$

where ΔT_z is the magnetic anomaly reduced to the pole, k is the wavenumber in Cartesian coordinates, $B = 1/[ik_x \cos I \cos D + ik_y \cos I \sin D + k \sin I]$, and I and D are the main field inclination and declination.

2.5 Euler Deconvolution and Curvature analysis

This technique was first proposed by Thompson (1982). It assumes that the potential field is homogeneous and that it obeys Euler's homogeneity equation:

$$(x - x_o) \frac{dT}{dx} + (y - y_o) \frac{dT}{dy} + (z - z_o) \frac{dT}{dz} = N(B - T) \quad (5)$$

where x_o, y_o, z_o is the position of a source whose total potential field T is detected at x, y, z . The total field has a regional value of B . The degree of homogeneity, N , is interpreted as a structural index (SI), which is a measure of the rate of change with distance of a field.

Table 2.1: Structural Index (SI) values. Taken from Reid et al. (2014).

Model	Magnetic SI	Gravity SI
Point, sphere	3	2
Line, cylinder, thin bed fault	2	1
Thin sheet edge, thin sill, thin dyke	1	0
Thick sheet edge	0	-1
Contact of infinite depth extent	0	Not useful

Euler deconvolution is performed using the Euler3D module of Oasis Montaj (Fig. 2.6). This module interactively allows the user to calculate the Euler solutions. Using the anomaly grid, the program calculates the directional derivatives. Afterwards, the user can input the following parameters: window size, structural index, and the tolerance of the solutions.

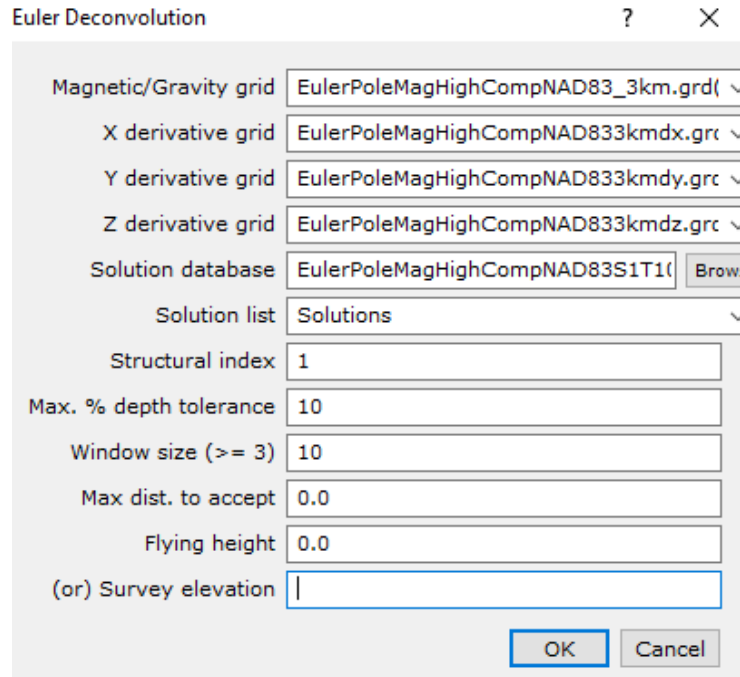


Figure 2.6: Interface of EULER3D module of Oasis Montaj.

Tests with different tolerances and window sizes are first performed to determine the range of parameters that give the best visual solutions. When establishing these parameters, the structural index (SI) is varied from 0 to 2. Solutions are plotted using the software ArcMap 10.4 to geographically compare them with the geology of the study area.

Curvature is a two dimensional property of a curve and describes how bent a line segment is at a particular point on the curve. The smaller the radius of curvature, the more bent the curve is and hence the larger the curvature (Roberts, 2001). This attribute of a surface is typically applied in seismic interpretation. However, the principal can also be applied to potential field data (Li, 2015; Madeline et al., 2013).

Curvature can be defined as the reciprocal of the radius of a circle that is tangent to the given curve at a point (Li, 2015). In terms of derivatives, curvature can be expressed as:

$$K = \frac{d^2z/dx^2}{[1 + (dz/dx)^2]^{3/2}} \quad (6)$$

where curvature, K , is closely related to the second derivative of a curve.

This two-dimensional concept can be extended to three-dimensions. A curve can be constructed by mathematically cutting a surface with a plane. The intersection that the plane makes with the surface describes a curve from which the curvature can be calculated at any point along the curve (Roberts, 2001). However, at a point (x, y) , different curvatures may exist. The most useful subsets of curvatures are those defined by planes that are orthogonal to the surface. These are called normal curvatures (Roberts, 2001).

Roberts (2001) developed 11 curvature attributes based on their applicability to seismic interpretation: mean, Gaussian (or total), maximum, minimum, most positive, most negative, dip (profile), strike (tangential), contour (plan), curvedness, and shape index. Schmidt and Götze (2003) used many of the attributes from Roberts (2001) and produced a Java Program for curvature analysis of potential field data.

For the curvature analysis (Fig. 2.7), a 5 km anomaly grid is created. Consequently, this grid is then input into the Java Program Curvature in order to detect faults and lineaments, and any other features in the potential field data that are not visible or are difficult to observe. All curvature attributes are calculated. However, dip curvature and dip angle are deemed the most meaningful.

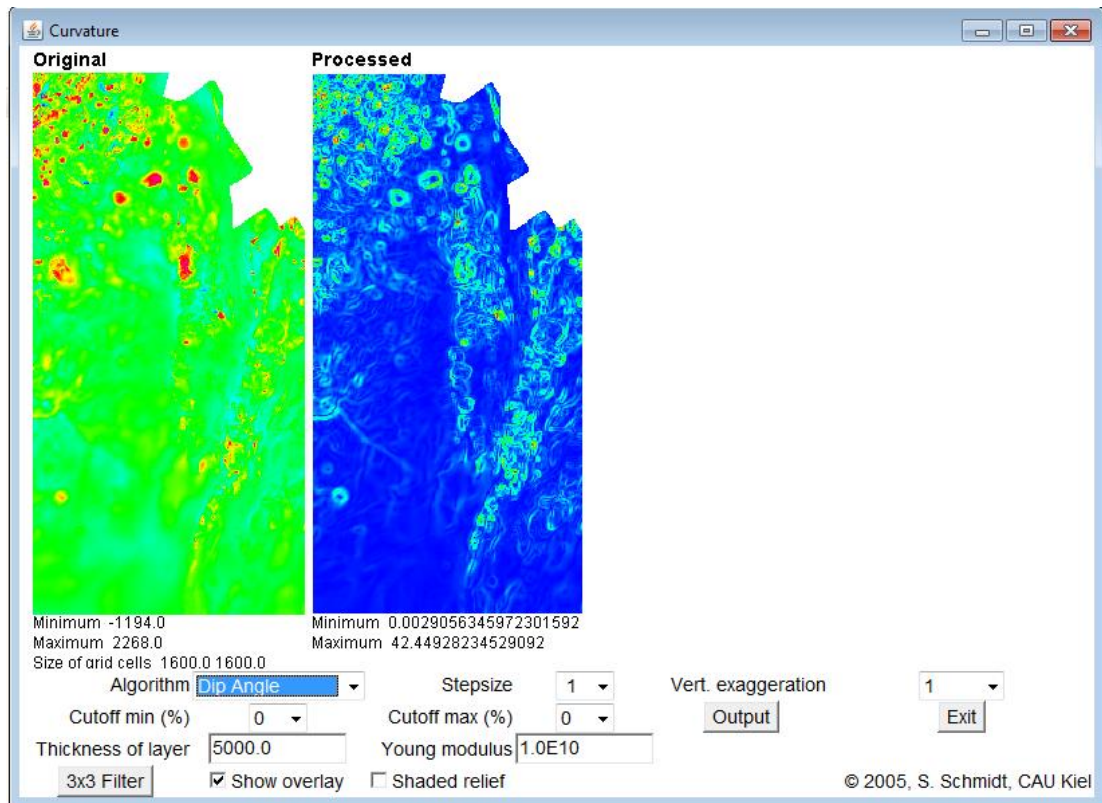


Figure 2. 7: Interface of the Java program *Curvature* (Schmidt and Götze, 2003). The *Original* grid is the Canada 200 m magnetic grid and the output grid is the result of applying the Dip Angle attribute.

2.2 3D Modelling

After processing and in some cases removal of residual effects from potential field data, the regional field data are interpreted in terms of anomalous density distributions, in the case of gravity data. Early methods of interpretation involved comparison of observed gravity anomalies with computed anomalies from simple geometric shapes, such as a sphere or a cylinder. However, this approach is simplistic and it does not adequately represent realistic subsurface structure in many cases. Modern forward modelling is based on an interactive process in which a starting Earth model with an assumed geometry and density contrast is assumed for the study area. The gravity anomaly over the model is calculated and then compared with the observed anomaly over the study area. The density contrast and geometry of subsurface dense bodies are adjusted until the calculated gravity matches the observed gravity (Lowrie, 2007).

Forward modelling can be applied in two dimensions (2D) or three dimensions (3D). The 2D forward modelling method assumes that anomalous bodies extend to infinity, perpendicular to the model. This approach tends to over or underestimate the density properties of the subsurface structures.

There are several methods available to calculate the potential field anomalies of 3D bodies. Nagy (1966) derived an equation to calculate the gravity anomalies of a tridimensional prism with a constant density contrast. Talwani and Ewing (1960) derived an equation to calculate the potential field anomalies of a horizontal layer with an irregular surface using numerical integration. Barnett (1976) and Okabe (1979) computed potential field equations for polyhedral bodies. The modern 3D potential field modelling methods are based on the construction of polyhedral bodies to approximate geological bodies with constant density.

The 3D density model created for this research project is developed using the interactive forward-modelling software Interactive Gravity and Magnetic Application System (IGMAS). The software uses polyhedrons for the approximation of geological bodies with constant density in order to compute the gravity effect of the model. The algorithm transforms the volume integral involved in the vertical attraction of a homogeneous polyhedron into a sum of line integrals by applying the Gauss theorem in 2D and 3D (Götze and Lahmeyer, 1988; Schmidt and Götze, 1998). The calculated gravity effect of the modelled structures is compared to the observed gravity. To minimize the ambiguity that results from the non-uniqueness of the derived model, the interpretation of select seismic profiles, well data, a refraction seismic profile (Jackson et al., 1998; Marillier et al., 1994), and the outputs from the various mathematical tools are used as independent constraints on the geometry of the different boundary layers. The density values used in the 3D gravity model are initially derived from the seismic velocity observations. Specifically, an empirical function from Nafe and Drake (1963) is used (Equation 7).

$$\rho \left(\frac{g}{cc} \right) = 1,6612V_p - 0,4751V_p^2 + 0,067V_p^3 - 0,0043V_p^4 + 0,000106V_p^5 \quad (7)$$

V_p in km/s

2.2.1 Initial Structure of the Model

The initial 3D model extends from 0 to 250 km in depth with 18 west-east parallel sections (Fig. 2.8) which are rotated 22 degrees with respect to the geographic north to be perpendicular to the Gulf of St. Lawrence and the Humber zone. Two of these sections are located in an area without gravity stations to control the geometry variations of the model outside the study area. The separation between sections is arbitrary and varies within the model. However, the mean separation is 20 km.

Due to the complex surface geology of Western Newfoundland, as described in Chapter I, the sedimentary cover throughout this thesis is originally modelled as an undifferentiated layer, for lack of constraints, and includes rift to passive margin sediments, foreland sediments, and sediments derived from metamorphic and igneous bodies with heterogeneous properties. For the initial model, the depth to the sediments and Moho are set to 3 and 40 km respectively, following the seismic refraction model from Jackson et al. (1998) and Marillier et al. (1994).

Since the initial model is too simplistic and geologically unreasonable, the topography and bathymetry from the ETOPO1 datasets are then included into subsequent models. The crust is also divided into upper and lower crust according to the seismic refraction profiles (Hall et al., 1998; Jackson et al., 1998) (see Fig. 1.1 of Chapter I). Additionally, results from the Euler deconvolution and spectrum analysis are also included to constrain the depth to the different model layers.

The preliminary 3D models are constructed and tested using the Free Air Gravity data. However, the final 3D models use the combined Free Air offshore and Bouguer data on

land. The surface geology and seismic line interpretations of Cooper et al. (2001) and deep seismic refraction lines (Hall et al., 1998; Jackson et al., 1998; Marillier et al., 1989; Quinlan et al., 1992) allow the subdivision of the sediments into blocks that better represent the density structures beneath the study area.

Three different models are constructed to test for the possible existence of a high density body in the lower crust beneath the Gulf of St. Lawrence (Jackson, 2002; Marillier et al., 1989). The geometries of this body are constrained by one seismic refraction profile of Jackson et al. (1998) (Fig 2.8). Its spatial extrapolation beyond the profile follows the studies of Funck et al. (2001) and Hall et al. (1998).

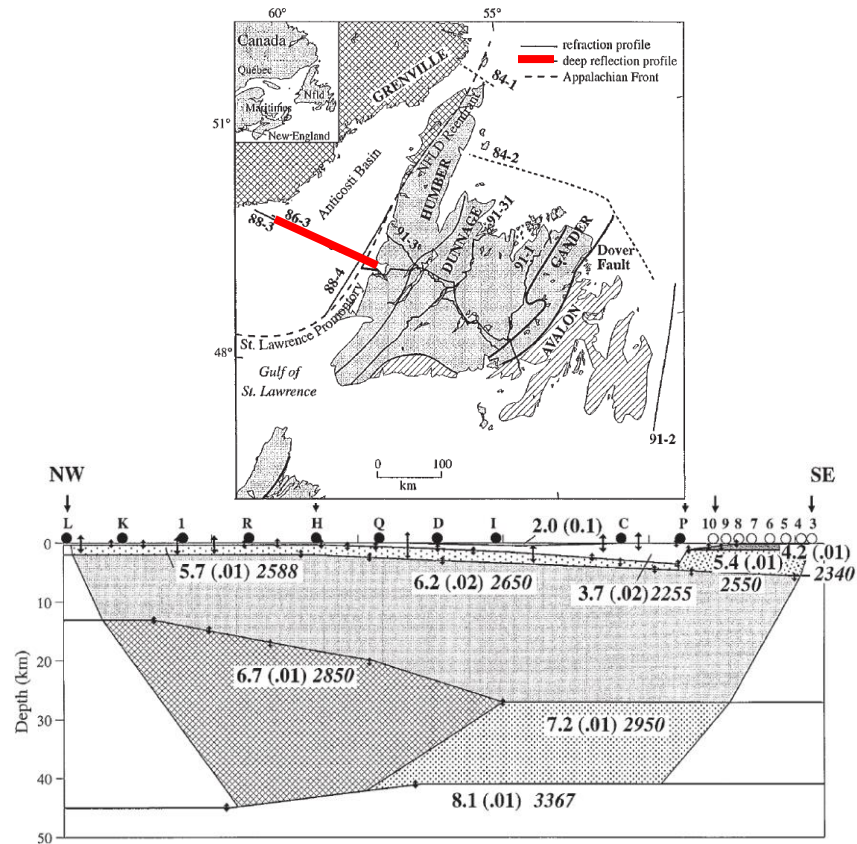


Figure 2. 8: (Top) Location of seismic line 86-3, red line. (Bottom) Interpretation of seismic line 86-3 from Jackson et al. (1998).

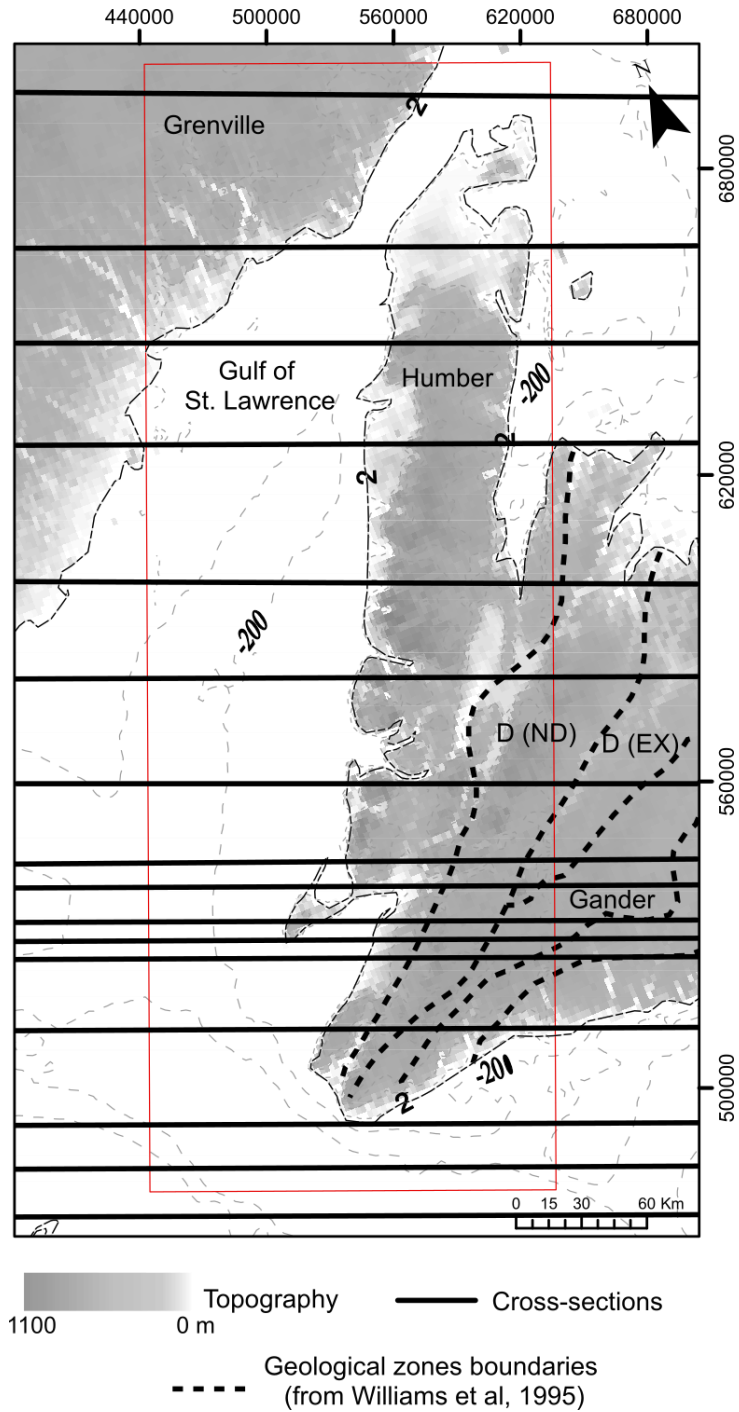


Figure 2. 9: Map of E-W parallel initial sections (thick black lines). Map shows surface geological zones of the Appalachian Orogen in Newfoundland (Williams, 1995). Dashed grey lines correspond to bathymetric and topographic contours (m). The red square outlines the model area used for this project. Abbreviations: D (Ex), Exploits subzone of the Dunnage zone; D (ND), Notre Dame subzone of the Dunnage zone.

2.3 Gravity Inversion

The inverse problem involves using the observed data to directly generate a density model using a physical relationship that connects both parameters. This physical relationship can be expressed linearly or non-linearly and provides a direct theoretical link between the model and the observed data.

Inverse problems are non-unique. For gravity, different mass distributions can generate identical gravity anomalies. Therefore, it is necessary to add constraints to the inversion process in order to limit the non-uniqueness and generate geologically reasonable models that satisfy all available datasets. These constraints can be based on other geophysical information and they allow for a better characterization with higher certainty.

The inverse problem can be described linearly if there is a linear relationship between the data vector d of length D , and the model vector with P parameters, m :

$$d = Am + e \quad (8)$$

A is a $D \times P$ matrix which is often referred to as the theory operator and is independent of both data and model, and e is a vector of length D with the measurement errors (Snieder and Trampert, 1999). Equation 8 can be written out in full as:

$$d_i = \sum_{j=1}^P A_{ij}m_j + e_i \quad (9)$$

If $D = P$, the number of equations is equal to the number of unknowns and such a problem is called equi-determined. If $D > P$, there are more independent equations than unknowns, the problem is said to be over-determined. When $D < P$, the problem is said to be under-determined (Gubbins, 2004).

The over-determined problem can be solved using least squares. Writing the matrix notation of the least squares solution of equation 9 results in:

$$m = (A^T A)^{-1} A^T d \quad (10)$$

This means that the least squares solution is given by the model m that minimizes the following cost function (Strang, 1980):

$$S = \|d - Am\|^2 \quad (11)$$

Minimization is accomplished by differentiating S with respect to the model parameters and setting the derivatives equal to zero (Meju, 1994).

The gravity inversion is tested both with and without the seismic constraints. This process creates density models that can be compared with the results obtained from the forward modelling. Because the gravity inversion results have full 3D coverage, they constrain areas lacking previous geophysical information and complement the sparser forward modelling. The gravity inversion also produces models with smooth density variations that can be used to test the appropriateness of the blocky constant density models from the gravity forward modelling. The gravity inversion can also generate a large number of alternative models by varying the inversion parameters. These can be used to help assess the non-uniqueness of the final model.

2.3.1 GRAV3D

The program GRAV3D version 2.0 is based on the algorithm from Li and Oldenburg (1998, 1996) which is summarized as follows:

- 1) Division of the Earth into rectangular cells of constant but unknown densities.

2) Densities are found by minimizing a model objective function subject to fitting the observed data.

3) The objective function includes smoothing in different spatial directions, a depth weighting function which distributes the density with depth, and an additional depth weighting function to incorporate density constraints from previous geophysical information.

A detailed explanation of the algorithm can be found in the UBC-Geophysical Inversion Facility help document. However, some important concepts are highlighted here.

The inverse problem for this software is formulated as an optimization problem where a global objective function, $\Phi(\rho)$, is minimized subject to constraints. Therefore, the inverse problem is solved by finding a density $\rho(r)$ which minimizes Φ_m and misfits the data according to the noise level. This is accomplished by minimizing equation 12 by using a generalized technique:

$$\Phi(\rho) = \Phi_d + \mu\Phi_m \quad (12)$$

where $\mu \in [0, \infty]$ is a regularization parameter that controls the relative importance of data misfit Φ_d and model objective function Φ_m . The algorithm also restricts the density solution to lie between a lower and upper density bound. Thus, the solution is obtained according to the following constrained minimization problem:

$$\begin{aligned} \text{minimize: } & \Phi(\rho) = \Phi_d + \mu\Phi_m \\ \text{subject to: } & \rho_{min} \leq \rho \leq \rho_{max} \end{aligned}$$

ρ_{min} and ρ_{max} are vectors containing the lower and upper bounds on the model values.

2.3.2 Probabilistic Inversion Approach

Probability density functions, for the probability distribution of parameters prior to the solution and the observed data uncertainties, are introduced in the probabilistic approach. Additionally, information contained in the theoretical relationship between model parameters and data is also represented by a probability distribution (Hadidi and Gucunski, 2009). Hence, the solution of an inverse problem, through a probabilistic approach, can be defined as a probability distribution combining the a priori information, with the information obtained from the theoretical relationship (Tarantola, 2005).

Dr. Meixia Geng, from the Department of Earth Sciences at Memorial University, recently developed a 3D gravity inversion code based on the probabilistic inversion approach (Geng et al., 2017, submitted). The objective function for this code has the form (Geng et al., submitted; Tarantola, 2005):

$$\varphi = (Gm - d_{obs})^T C_d^{-1} (Gm - d_{obs}) + (m - m_{apr})^T C_M^{-1} (m - m_{apr}) \quad (13)$$

where T indicates transpose. The first term of equation 13 is the data misfit function, which includes a diagonal matrix, C_d , with the standard deviation error of the data points. The second term in equation 13 represents the deviation of model parameters away from a reference model m_{apr} (Geng et al., 2017, submitted).

This probabilistic approach results in inverted models that can more easily incorporate density jumps without imposing hard boundaries in the model, in contrast with GRAV3D (Welford et al., 2018).

2.3.3 Inversion Process

The gravity anomaly dataset is gridded to 5 by 5 km for the study area. With this new gridded data, the gravity files “.grv” are created as input for GRAV3D. The mesh cells are 5 km by 5 km by 700 m in depth. At first, the gravity file and the mesh are the only inputs for the inversion in this software. Subsequently, different meshes, topography, and

bathymetry are added. Finally, the density bounds, length scales and depth weighting function are varied to generate models that are more geologically reasonable.

The same previously gridded gravity anomaly dataset can also be used in a probabilistic approach. For this method, the depth to the basement and bathymetry are used to constrain the inversion process.

2.4 Summary

This chapter introduced the methodology that this research project follows. The first section describes the data sets used and how they were combined. This is followed by the statistical analysis, the separation of residual and regional anomalies, the Euler deconvolution, and the Curvature analysis. These techniques were used to enhance trends not easily seen in the gravity and magnetic datasets. Finally, the construction of the initial density model is described, along with the constraints used. The gravity inversion process and the prescribed parameters are described as well.

The next chapter, Chapter III, will present the results from the statistical analysis, the separation of residual and regional anomalies, the Euler deconvolution and the Curvature analysis.

Chapter 3: Description of the gravity and magnetic anomalies

The first results of this research are presented in this chapter. It starts with a description of the study area in terms of topography and bathymetry. The gravity and magnetic anomaly maps are then quantitatively and qualitatively analyzed. The results from the curvature and Euler deconvolution techniques are also shown.

3.1 Maps and description of anomalies

Figure 3.1 shows that the topography and bathymetry of the study area do not vary greatly. The highest elevation, 745 m, is located in Gros Morne National Park, whereas the deepest bathymetry is found in the southwest corner of the study area, in the Gulf of St. Lawrence.

The Free Air gravity anomaly captures the vertical gradient of gravity and mimics the bathymetry and topography with fidelity. Positive values of the Free Air anomaly are related to structural highs while low values correspond to submerged or depressed areas. Figure 3.2 shows the gravity anomalies and the bathymetry/topography. The highest Free Air gravity anomaly in the external Humber zone (Fig. 3.2a), associated with granites from Laurentian basement, does not correspond with the highest topographical point. To the north of this anomaly (Fig. 3.2a and 3.2b), the high values decrease gradually due to the increase in the thickness of the shelf successions. Other important positive anomalies found on land in Western Newfoundland (Fig. 3.2a and 3.2b) are likely linked to ophiolite complexes and mafic volcanic assemblages in the Notre Dame subzone (Newfoundland and Labrador Geological Survey, 2013). The Precambrian Grenville area, as shown in Figure 3.2, has positive Bouguer anomalies of approximately 110 mGal that are related to Mesoproterozoic granitic intrusions (Newfoundland and Labrador Geological Survey, 2013).

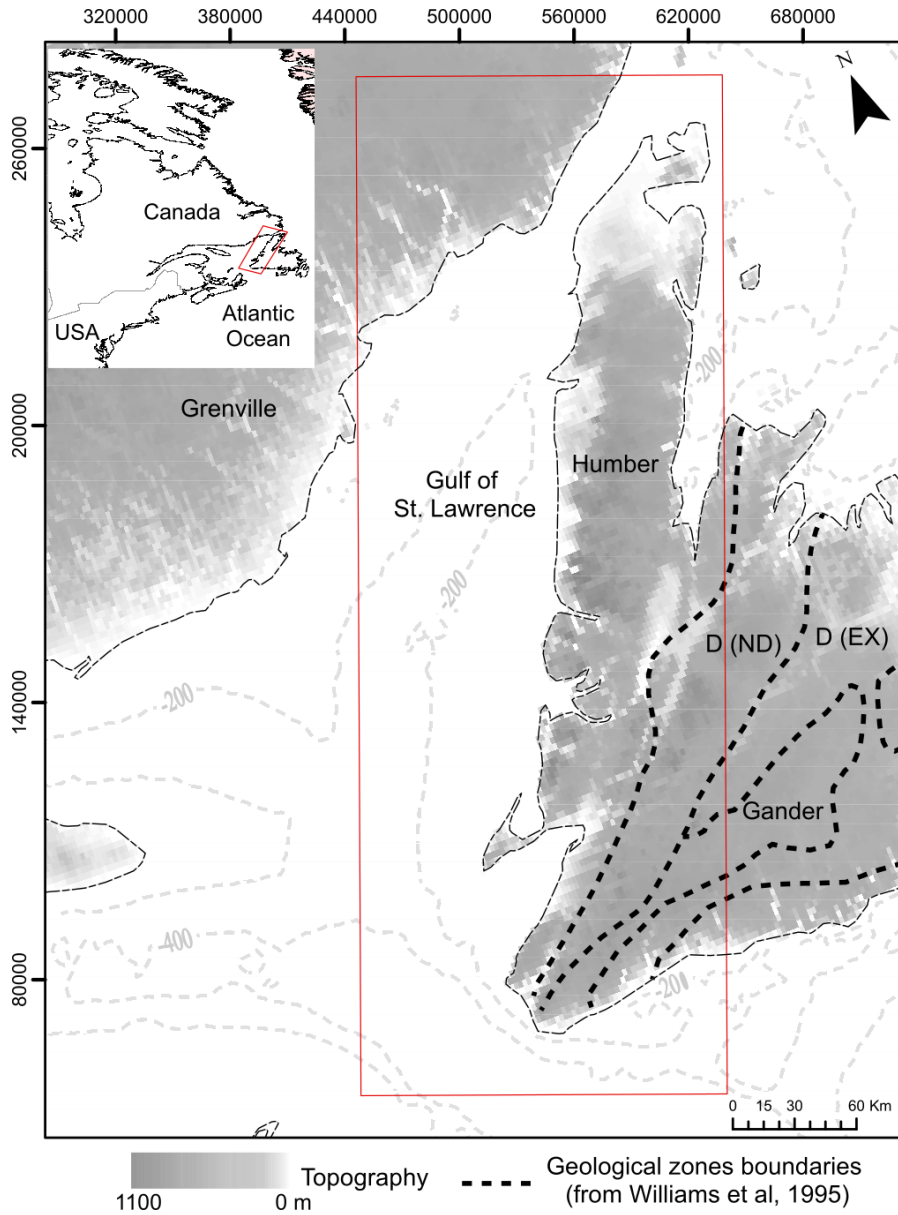


Figure 3. 1: Western Newfoundland topographic and bathymetric map (Ante and Eakins, 2009). Map shows surface geological zones of the Appalachian Orogen in Newfoundland (Williams, 1995), outlined by dashed black lines. The red box shows the limits of the 3D model generated for this project. Abbreviations: D (Ex), Exploits subzone of the Dunnage zone; D (ND), Notre Dame subzone of the Dunnage zone.

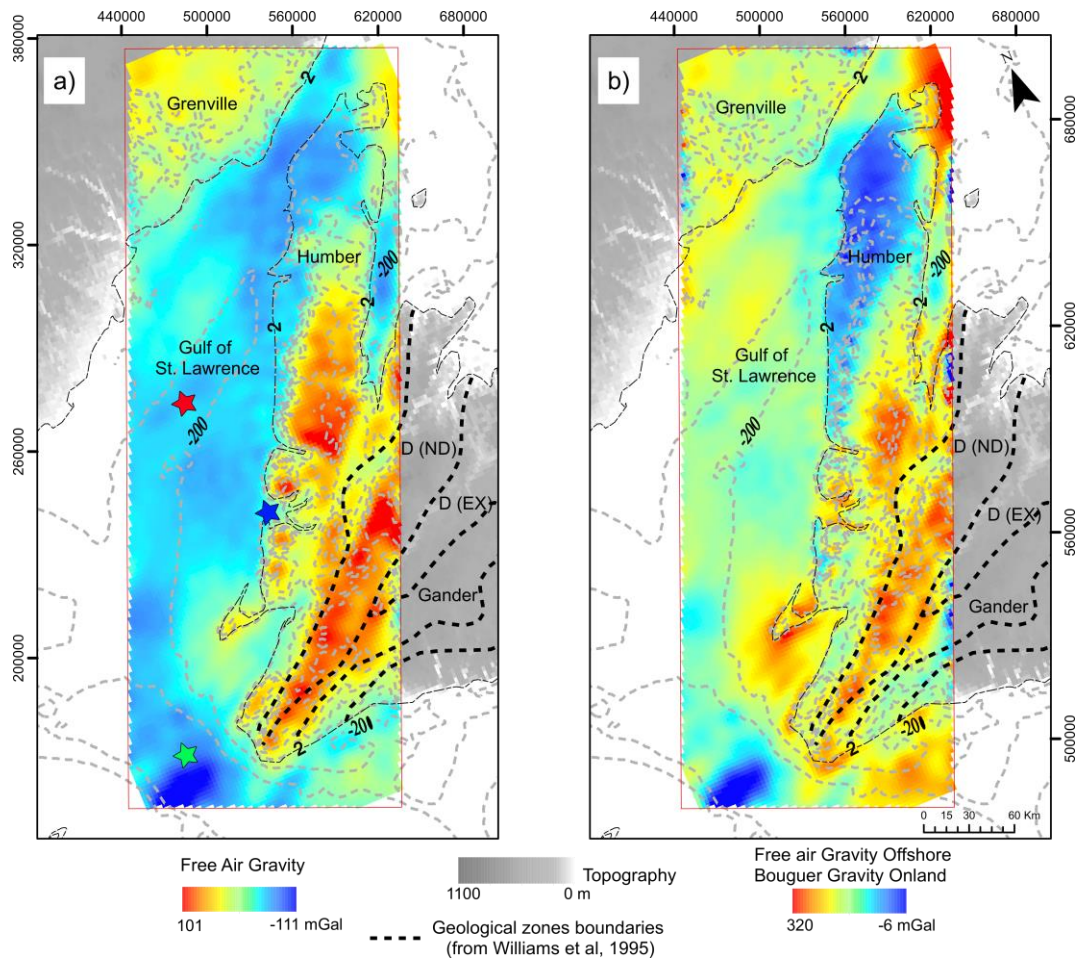


Figure 3. 2: Western Newfoundland gravity map. Map shows surface geological zones of the Appalachian Orogen in Newfoundland (Williams, 1995). Dashed grey lines correspond to bathymetric and topographic contours (m). Different color stars correspond to Free Air gravity anomalies described in text. a) Free Air anomaly, b) Free Air anomaly offshore and Bouguer anomaly on land. Abbreviations: D (Ex), Exploits subzone of the Dunnage zone; D (ND), Notre Dame subzone of the Dunnage zone.

In the Gulf of St. Lawrence, low Free Air anomalies cover most of this region. They correlate to the bathymetric variations in the area other than the low anomaly values found in the Esquiman Trough (red star, Fig. 3.2). The Bay of Islands gravity low (blue star, Fig. 3.2) is related to an increase in the thickness of Paleozoic sedimentary rocks (Haworth, 1978). The lowest free air gravity anomaly (as shown in Fig 3.2 by the green star), found offshore, to the south, is likely from a thick accumulation of sediments in the Maritime Basin.

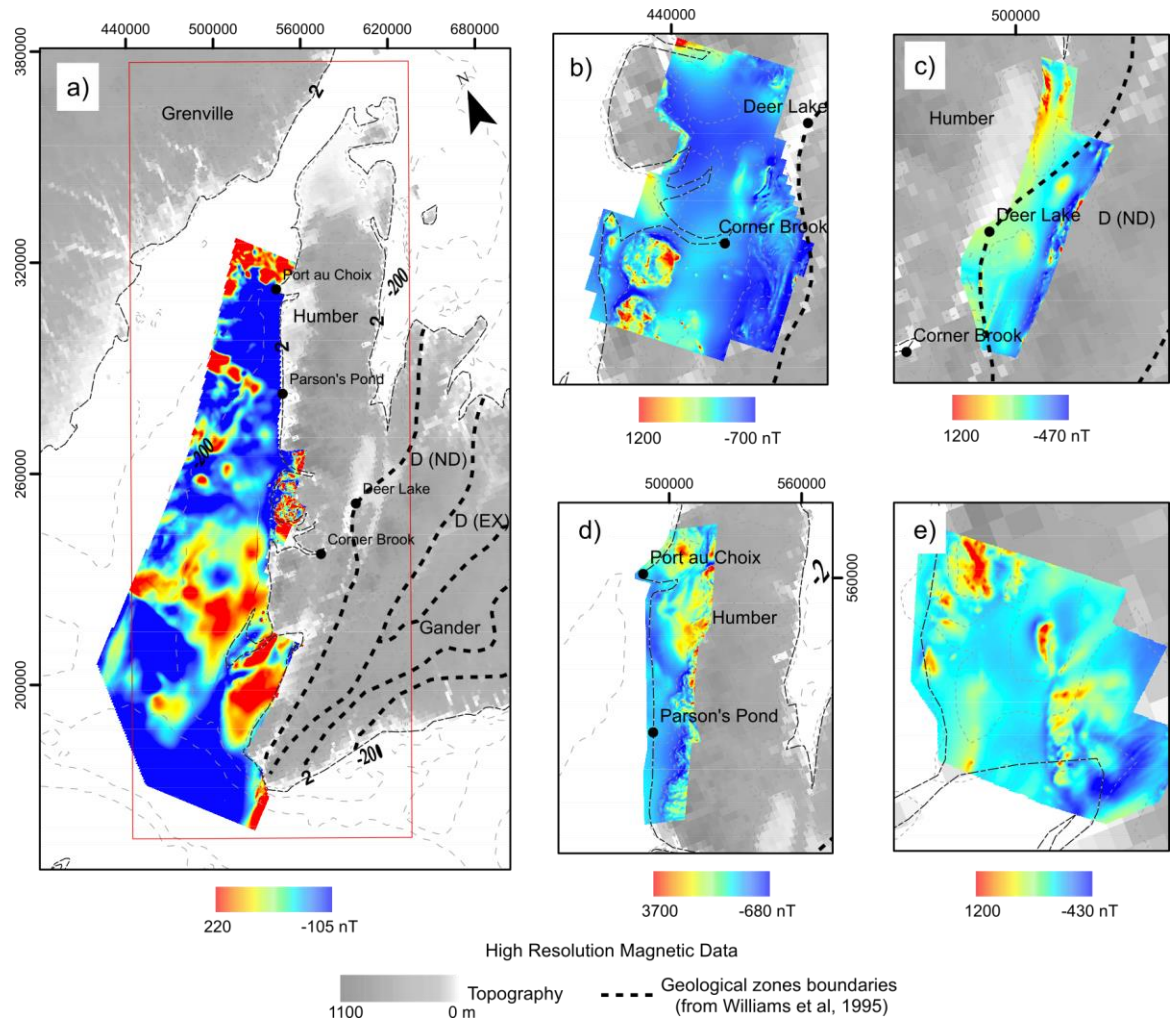


Figure 3.3: Western Newfoundland high resolution residual magnetic maps. Maps show surface geological zones of the Appalachian Orogen in Newfoundland (Williams, 1995). Dashed grey lines correspond to bathymetric contours (m). a) Offshore Western Newfoundland, b) Corner Brook, c) Deer Lake, d) Gros Morne, e) Indian Head. Abbreviations: D (Ex), Exploits subzone of the Dunnage zone; D (ND), Notre Dame subzone of the Dunnage zone.

Residual high resolution magnetic anomaly maps (Fig. 3.3) show high anomalies related to ophiolite complexes near Corner Brook and north of the Bay of Islands (Fig. 3.3b). Figure 3.4b shows a zoomed-in view of the high anomalies. In the Gros Morne area (Fig. 3.3d and Fig. 3.4b), high magnetic values are linked to outcrops of the Laurentian basement. However, in regions adjacent to these anomalies (Parsons Pond, Portland Creek and Port-au-Choix), a negative N-S magnetic anomaly extends offshore (red star in Fig. 3.4). Northwest of Port-au-Choix, an oval-shaped and high positive anomaly (orange in star Fig. 3.4) is attributed to Grenvillian granitoid rocks of the Laurentian margin. North of this

anomaly, high positive values dominate and are also clustered in oval-shaped anomalies. These correspond to carbonates and carbonate limestone shelf successions.

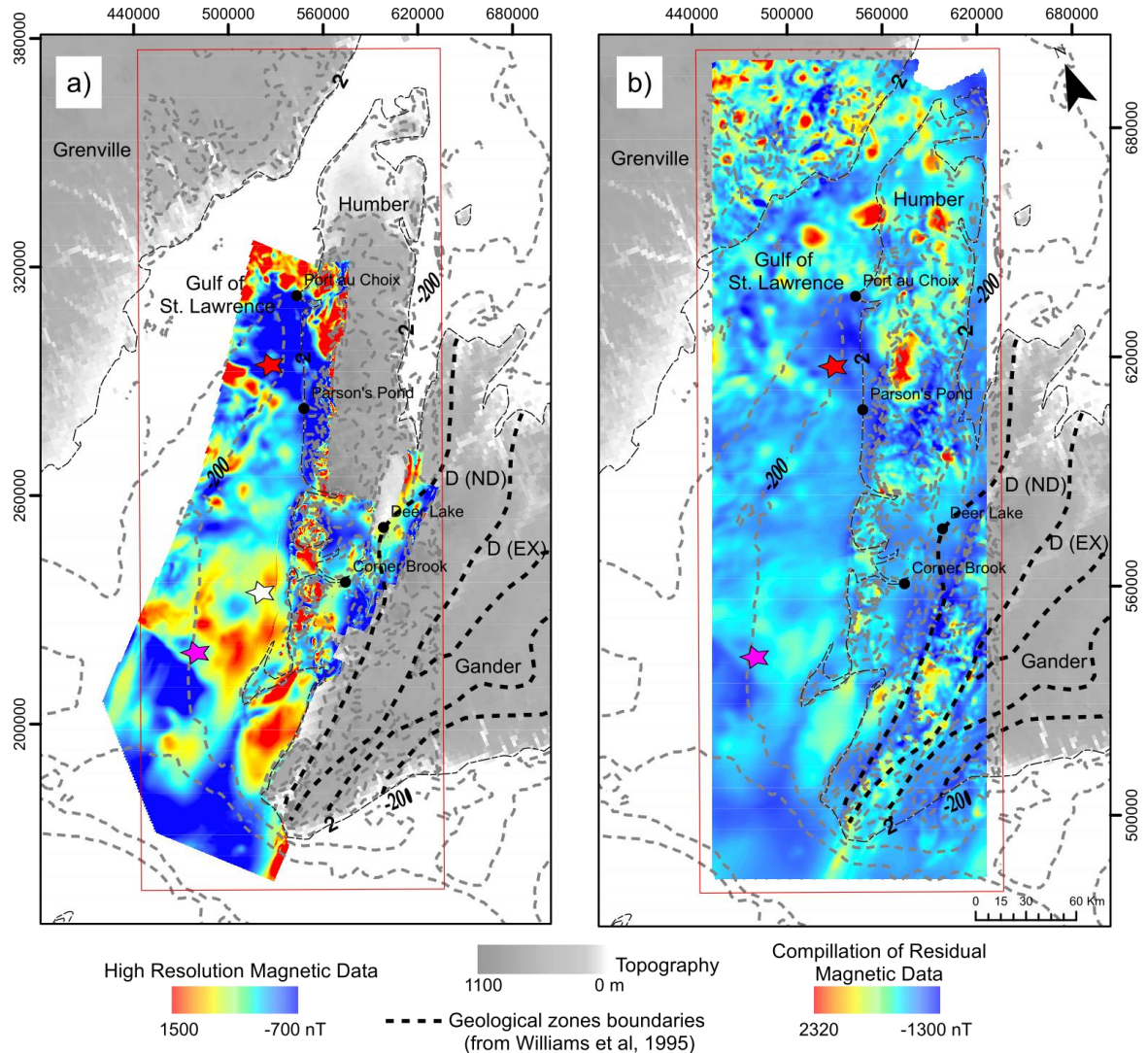


Figure 3. 4: Western Newfoundland residual magnetic maps. Maps show surface geological zones of the Appalachian Orogen in Newfoundland (Williams, 1995). Dashed grey lines correspond to bathymetric and topographic contours (m). Different color stars correspond to magnetic anomalies described in text. a) High resolution magnetic map, b) compilation of residual magnetic data for Western Newfoundland. Abbreviations: D (Ex), Exploits subzone of the Dunnage zone; D (ND), Notre Dame subzone of the Dunnage zone.

The separation between the Dunnage zone and the Humber zone is associated with negative magnetic anomaly values (Fig. 3.4b). High positive anomalies in the Dunnage zone are igneous rocks related to the closing of the Iapetus Ocean. Portions of the St.

George Basin and the Deer Lake Basin show low negative magnetic anomalies (yellow star in Fig. 3.4b).

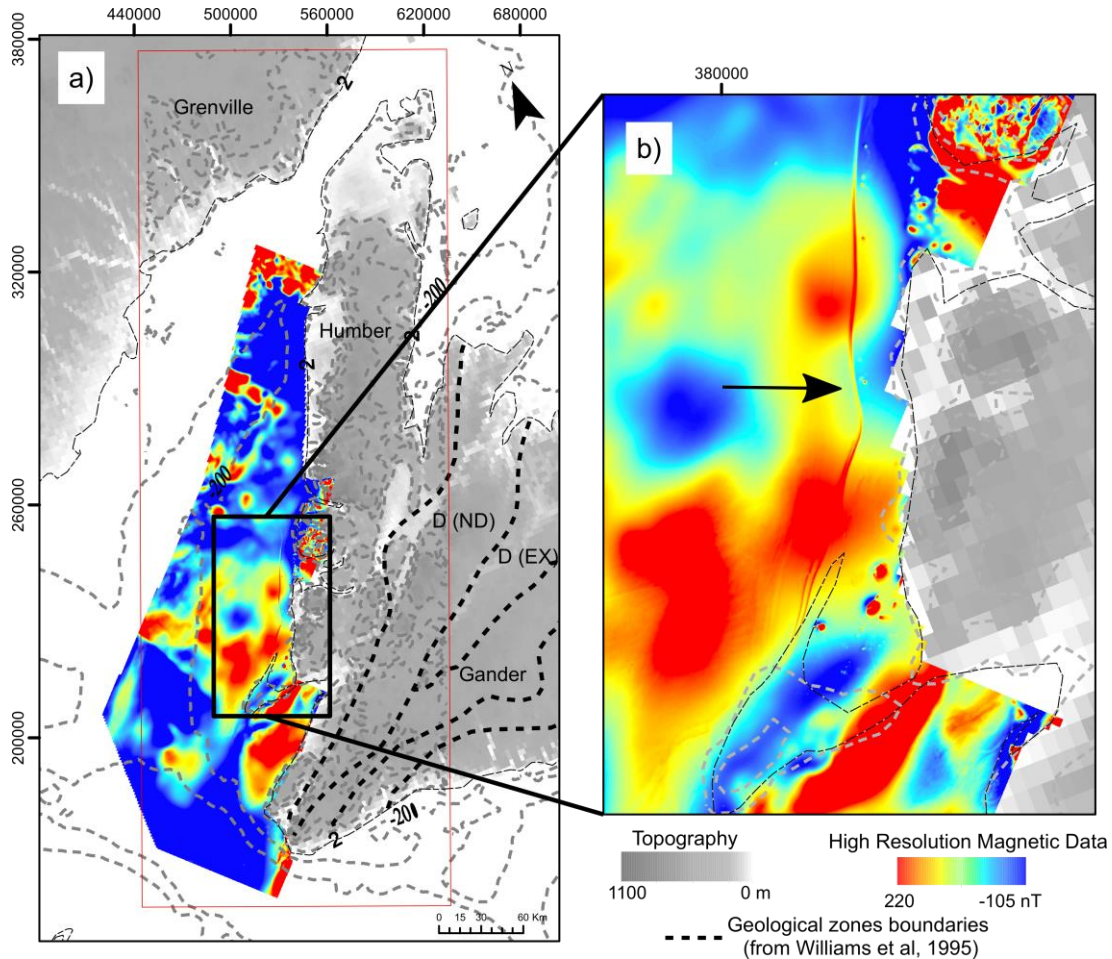


Figure 3. 5: Western Newfoundland high resolution residual magnetic map. Maps show surface geological zones of the Appalachian Orogen in Newfoundland (Williams, 1995). Dashed grey lines correspond to bathymetric and topographic contours (m). a) Offshore Western Newfoundland and b) zoomed in map showing the Odd Twins Anomaly. Black arrow shows the position of the Odd Twins Anomaly. Abbreviations: D (Ex), Exploits subzone of the Dunnage zone; D (ND), Notre Dame subzone of the Dunnage zone.

Offshore, two strong magnetic markers are called the Odd Twins Anomaly (White star in Fig. 3.4a, Fig. 3.5b). This feature coincides with two sandstone units, rich in magnetic mineral sand grains (Waldron et al., 2002). Next to this anomaly, a weaker magnetic anomaly may approximate the trace of the Tea Cove Thrust, a feature marking the front of the Humber allochthon (Hinchey et al., 2015; Waldron et al., 2002).

South of the study area, in the Gulf of St. Lawrence, low negative magnetic anomalies are truncated by a NW-SE trending positive trend anomaly (purple star in Fig. 3.4). In the central offshore area, positive magnetic anomalies are truncated by a similar set of NW-SE trending anomalies like the one to the south (Fig. 3.4). Northwest of Port-au-Choix and along the Quebec margin, large circular anomalies are commonly associated with igneous rocks (black star in Fig. 3.4b).

The grids from Figure 4a and 4b were knitted together with a 50 m sampling and the resulting map is shown in Figure 4.8.

3.2 Statistical analysis

The maximum residual magnetic anomaly value, 1570 nT, is associated with an ophiolite complex. The lowest value, -653 nT, lies within the offshore negative anomalies. Overall, the average anomaly is negative, -15 nT, as is the median value, -55 nT. The deviation and variance values are high. It is thus deduced that the area is complex with significant data variability. The asymmetry of the data distribution is positive, which means that the data tend to cluster to the left of the mean value. The kurtosis value is positive, which means that the data are centered in the central region of the distribution (Fig. 3.6). It can be surmised that even though the study area is known for complex surface geology, the residual magnetic anomaly values are clustered in the -500 to 500 nT range. This range is largely due to the ophiolite complexes which are found in the study area.

Figure 3.6a shows the histogram for the merged Free Air and Bouguer gravity anomalies. The minimum value is 54 mGal, related to a cluster of low anomalies in the southwestern part of the study area (Fig. 3.2), and the maximum value is 184 mGal, related to igneous rocks in the Humber zone (Fig. 3.2). The mean value of the data is 123 mGal and the data distribution is almost symmetric (Fig. 3.6a). However, the values are slightly clustered to the left of the mean value and are concentrated around the mean value. These

results mimic the distribution of the residual magnetic anomaly data histogram. Both anomalies seem to vary within a reasonable range with no separate clusters. This suggests that there are no major lithology changes in the study area.

3.3 Spectral analysis and filtering

Figure 3.7 shows the power spectrum vs the radial wavenumber, obtained through spectral analysis of the potential field data (see section 2.3, Chapter II for more details). In the study area, there are three main trends. For the gravity data (Fig. 3.7a), the broad scale spectrum corresponds to source depths of ~39 km, with the shallowest sources occurring at ~ 6 km. The deeper sources may correspond with the mean depth for the Moho, a finding that agrees with previous seismic studies (Hall et al., 1998; Hughes et al., 1994; Jackson et al., 1998; Marillier et al., 1994). The intermediate source depth of ~17 km may be related to a discontinuity within the crust while the shallowest depth of 6 km may be related to the mean depth of basement in the study area.

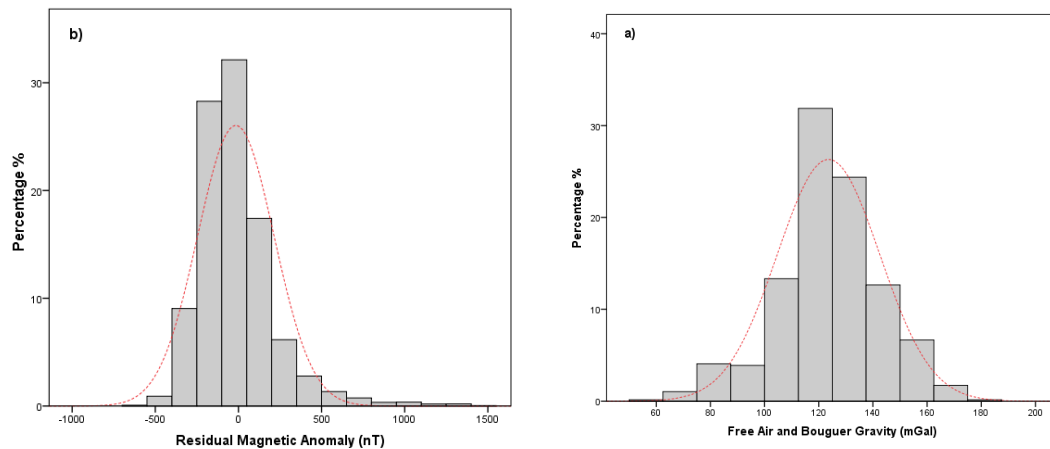


Figure 3. 6: Histograms of a) Free Air and Bouguer anomaly data values and b) Residual Magnetic anomaly data values

The power spectrum for the knitted high resolution magnetic anomaly data is shown in Figure 3.6b. The first trend is related to source depths of ~25 km. This depth may be the deepest extent of static magnetic sources. The other two trends are related to shallower magnetic sources. The surface geology of Western Newfoundland and the magnetic

residual map of the area (Fig. 3.4) show the presence of ophiolite complexes that may extend to those depths.

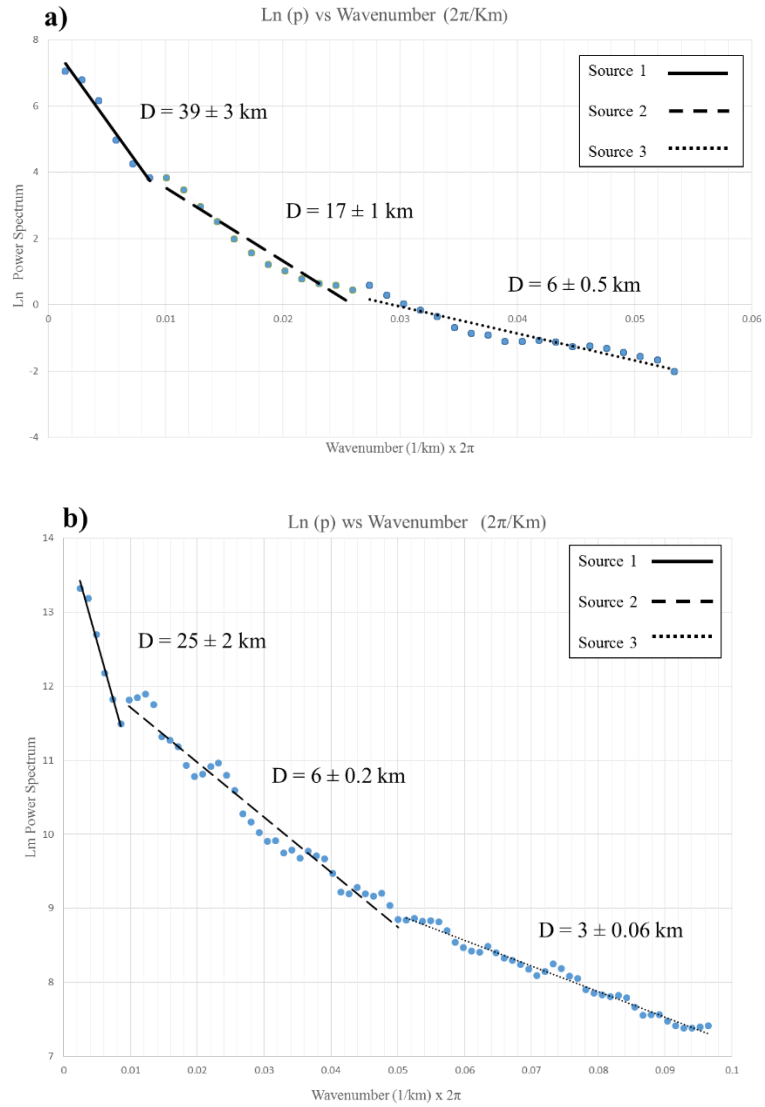


Figure 3. 7: Power Spectra of a) Free Air and Bouguer gravity anomaly data and b) Residual Magnetic anomaly data.

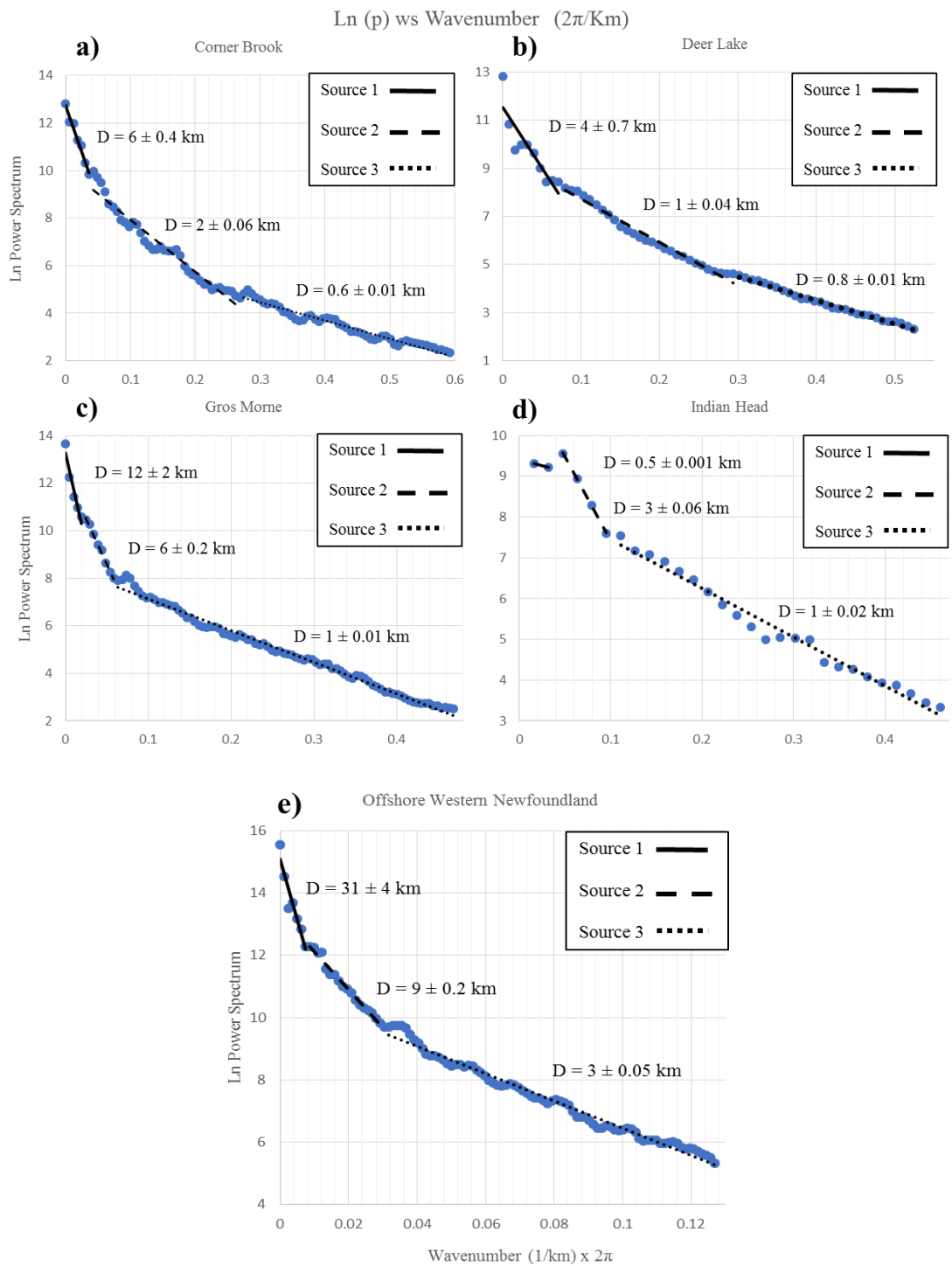


Figure 3. 8: Power Spectra of a) Corner Brook, b) Deer Lake, c) Gros Morne, d) Indian Head and e) Offshore Western Newfoundland.

The power spectra for each of the high resolution magnetic surveys were also computed and are shown in Figure 3.8. The magnetic anomalies in the Corner Brook area (Fig 3.3b & Fig. 3.8a), associated with the Humber Arm Allochthon ophiolite complexes, may involve stacking of ophiolite sheets to a thickness of 6 km. In the Gros Morne area and offshore Western Newfoundland, the deepest sources (Fig 3.3a and d, Figs. 3.8c and e) may be related to the deepest extent of static magnetic sources. If so, and assuming a thermal conductivity of 2.5 W/m°C as the average for igneous rocks (Stacey, 1977), the Curie temperatures for Western Newfoundland will vary between 930 and 490 °C.

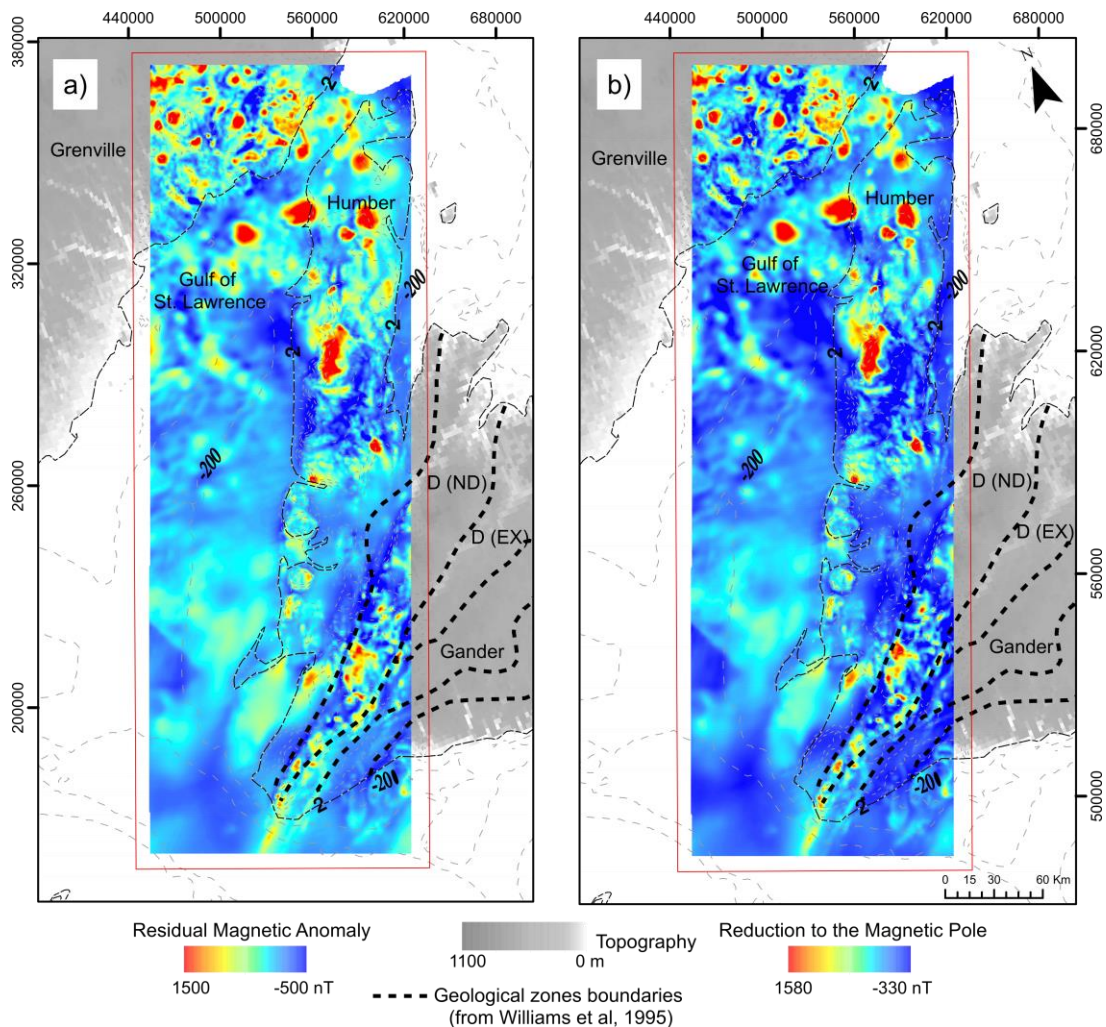


Figure 3. 9: Reduction to the Pole of the magnetic anomaly data: a) residual magnetic anomaly data, b) reduced to the pole magnetic anomaly. Map shows surface geological zones of the Appalachian Orogen in Newfoundland (Williams, 1995). Dashed grey lines correspond to bathymetric and topographic contours (m). Abbreviations: D (Ex), Exploits subzone of the Dunnage zone; D (ND), Notre Dame subzone of the Dunnage zone.

In order to correct for the magnetic data dependence on the magnetic inclination, the data were reduced to the pole (RTP) (Fig. 3.9) using the Oasis Montaj software. The inclination and declination used were 69.77° and -19.28° respectively, which are automatically calculated by the software. As shown in Figure 3.9b, the reduction to the pole reduced asymmetries in the anomalies. However, no major changes were observed.

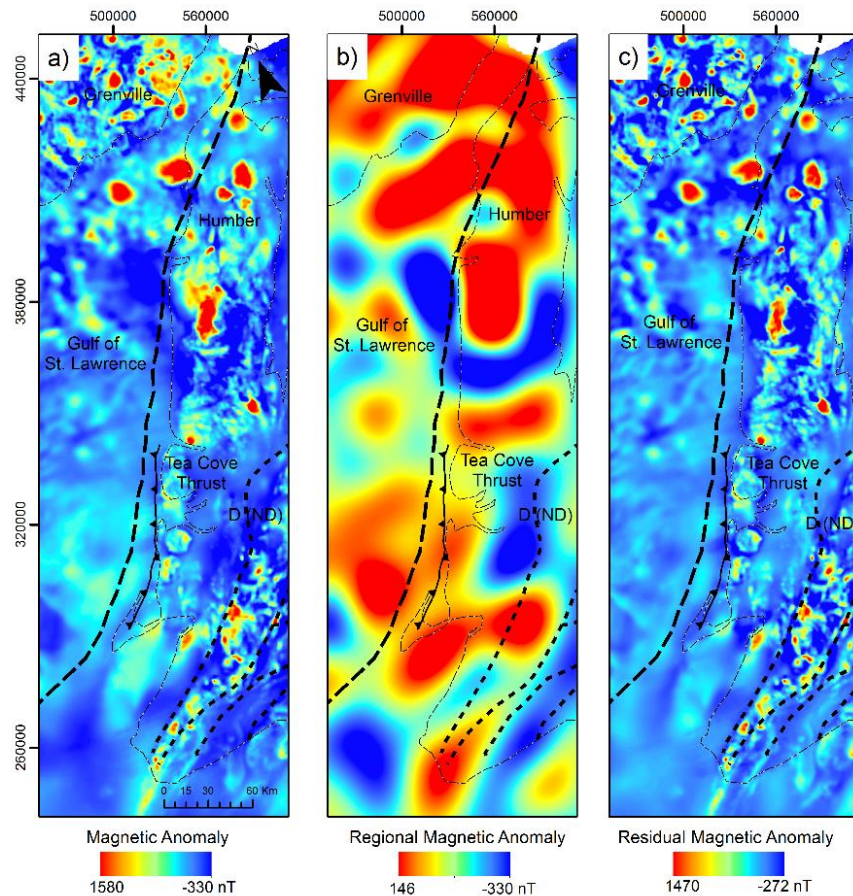


Figure 3. 10: Separation of the Regional/Residual field from the Magnetic anomaly data using the Power Spectrum: a) Magnetic anomaly data, b) Regional Magnetic anomaly data and c) Residual magnetic anomaly data. Map shows surface geological zones of the Appalachian Orogen in Newfoundland (Williams, 1995). Abbreviations: D (Ex), Exploits subzone of the Dunnage zone; D (ND), Notre Dame subzone of the Dunnage zone.

Using the Power Spectrum for the knitted magnetic anomaly data (Fig. 3.7b), the lower frequencies (first trend) were chosen for removal using a band pass filter. The filter was applied to the grid shown in Figure 3.10a. The residual was calculated by subtracting the complete magnetic anomaly from the regional magnetic anomaly (Fig. 3.10c). The

frequencies corresponding to the two other trends (Fig. 3.7b) correspond with the anomalies shown in Figure 3.9c. Therefore, the magnetic bodies causing these anomalies likely reside in the sediment layers and in the crystalline layers of the upper crust. The regional magnetic anomaly map does not show any geologically-significant trends.

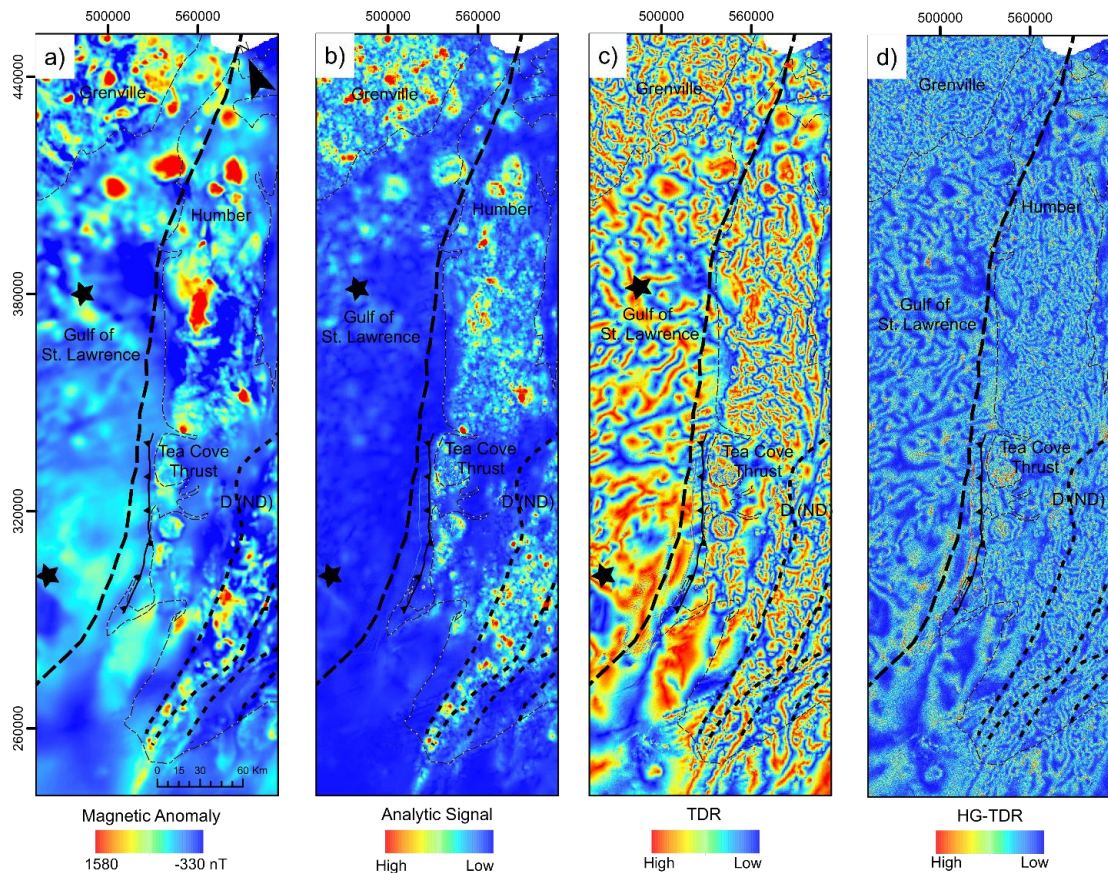


Figure 3.11: Special filters applied to the Magnetic anomaly data, a) Magnetic anomaly data, b) Analytic Signal, c) Tilt derivative (TDR) and d) Horizontal derivative of the tilt derivative (HD-TDR). Maps show surface geological zones of the Appalachian Orogen in Newfoundland (Williams, 1995). Black stars correspond to magnetic anomalies described in text. Abbreviations: D (Ex), Exploits subzone of the Dunnage zone; D (ND), Notre Dame subzone of the Dunnage zone.

Figure 3.11 shows the special filters applied to the magnetic anomaly data. The analytic signal (Fig. 3.11b), tilt derivative (Fig. 3.11c), and the horizontal derivative of the tilt derivative (HD-TDR; Fig. 3.11d) help to highlight the features discussed in previous sections, such as the Odd Twins Anomaly and the ophiolite complexes. Two W-E linear anomalies (black stars in Fig. 3.11), seen offshore Western Newfoundland, also stand out

in the Analytic Signal (Fig. 3.11b) and Tilt derivative (Fig. 3.11c). These linear features may represent boundaries between different crustal blocks.

A band-pass filter is applied to the gravity data to separate the regional and residual components (Fig. 3.12). Once again, the filter is based on the Power spectrum shown in Figure 3.6a, assuming that lower frequencies are typically associated with deeper layers. Figure 3.12c shows that the residual gravity anomaly data do not contribute significantly to the total gravity signal of the area. This behaviour is expected due to the coarse 3 km spacing of the satellite gravity data, which is appropriate for regional studies.

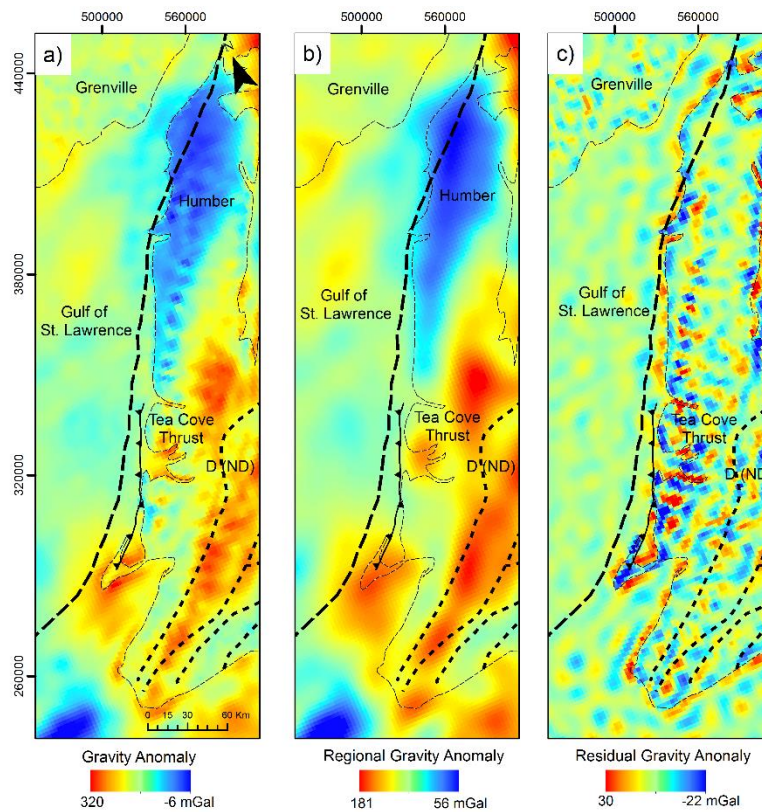


Figure 3. 12: Separation of the Regional/Residual fields from the Gravity anomaly map using the Power Spectrum: a) Gravity anomaly data, b) Regional Gravity anomaly data and c) Residual gravity anomaly data. Map shows surface geological zones of the Appalachian Orogen in Newfoundland (Williams, 1995). Abbreviations: D (Ex), Exploits subzone of the Dunnage zone; D (ND), Notre Dame subzone of the Dunnage zone.

Computation of the Analytic Signal, Tilt derivative (TDR) and Horizontal derivative of the tilt derivative (HD-TDR) is also performed for the Free Air offshore and Bouguer onshore gravity anomaly data. The Analytic Signal (Figure 3.13b) clearly resolves the Humber allochthon while the TDR highlights the trace of the Appalachian front (black arrow in Fig. 3.13c) and the density variability within the Long Range Massif (red arrow in Fig. 3.13c) in the Humber Arm. Figure 3.13 does not show any variability offshore Western Newfoundland. This may indicate that the densities are uniform in the material beneath this area.

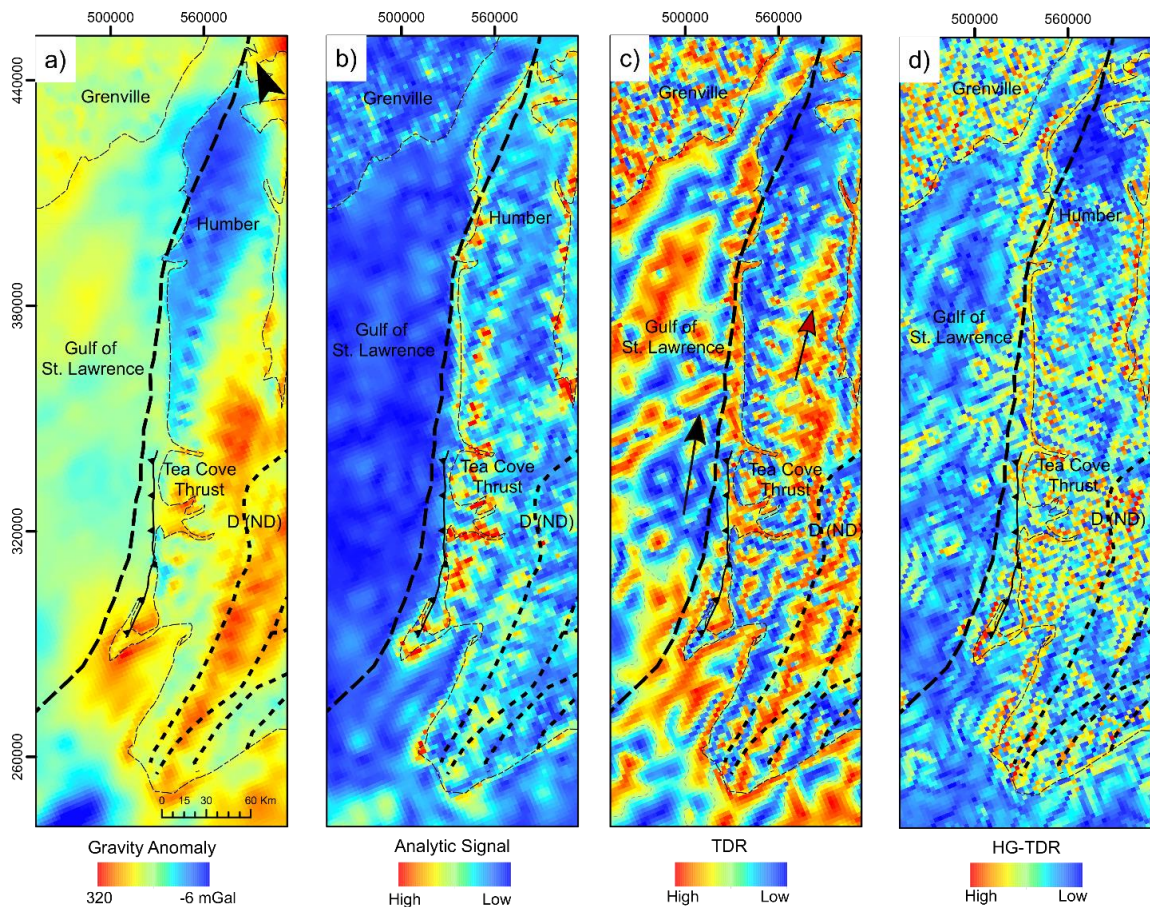


Figure 3. 13: Special filters applied to the Free Air offshore and Bouguer onshore Gravity anomaly data: a) Gravity anomaly data, b) Analytic Signal, c) Tilt derivative (TDR) and d) Horizontal derivative of the tilt derivative (HD-TDR). Map shows surface geological zones of the Appalachian Orogen in Newfoundland (Williams, 1995). Arrows correspond to gravity anomalies described in text. Abbreviations: D (Ex), Exploits subzone of the Dunnage zone; D (ND), Notre Dame subzone of the Dunnage zone.

3.4 Curvature

In general, all of the calculated curvature attributes succeed in highlighting the main features observed in the gravity and magnetic data. Figure 3.14 shows the dip angle curvature for the high resolution residual magnetic grids. This attribute can be used to detect linear features that separate geological domains with different magnetic susceptibilities. In Figure 3.14a, the dip angle highlights the extent of the Odd Twins Anomaly (purple star in Fig. 3.15a), which seems to vanish close to the coast of Western Newfoundland. West of the Port-au Port area, a trend (white star in Fig. 3.15b) correlates with the boundary between the high and low values in the same area as Figure 3.3a.

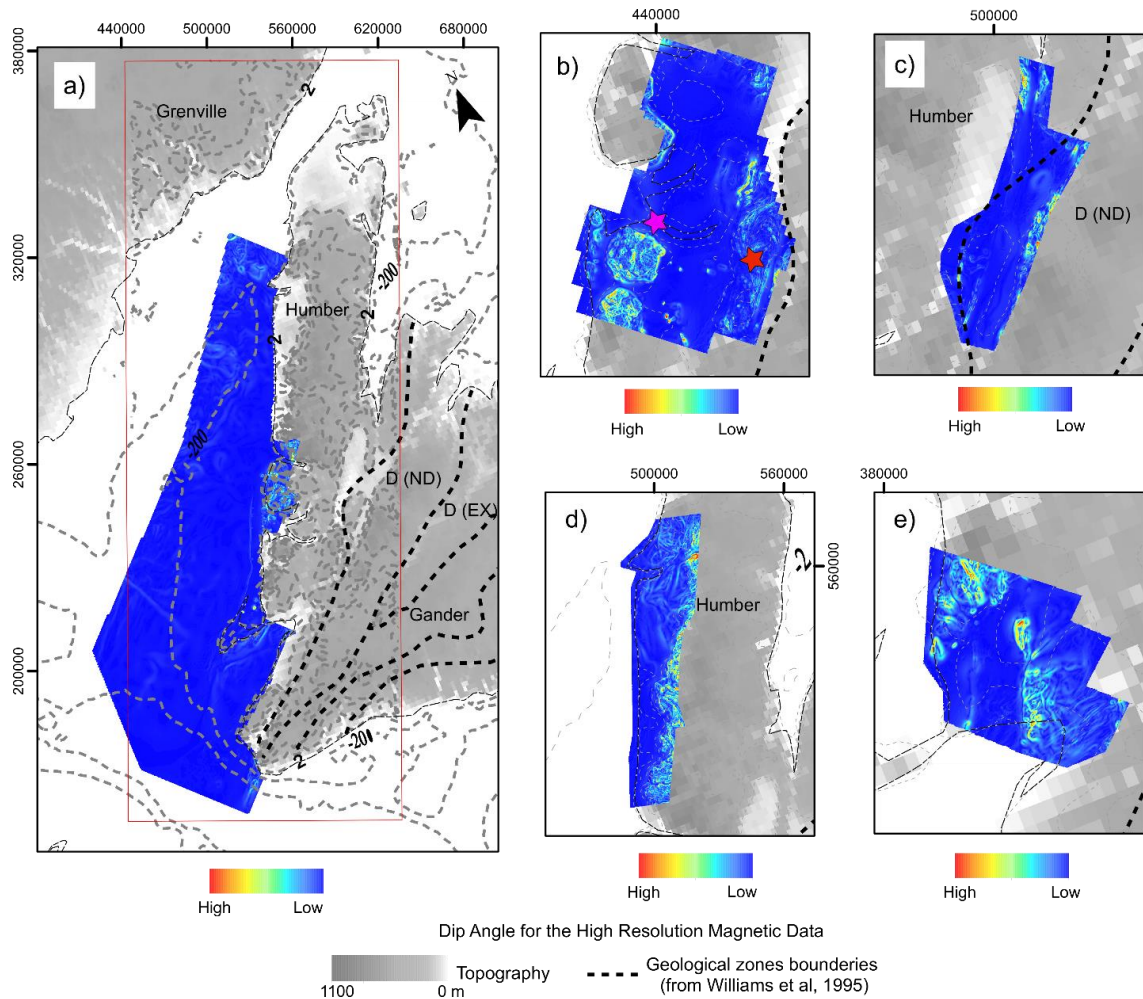


Figure 3. 14: Dip Angle Curvature results for the high resolution magnetic data. Map shows surface geological zones of the Appalachian Orogen in Newfoundland (Williams, 1995). Dashed grey lines correspond to bathymetric and topographic contours (m). Color stars correspond to magnetic anomalies described in text. a) Offshore Western Newfoundland, b) Corner Brook, c) Deer Lake, d) Gros Morne, e) Indian Head. Abbreviations: D (Ex), Exploits subzone of the Dunnage zone; D (ND), Notre Dame subzone of the Dunnage zone.

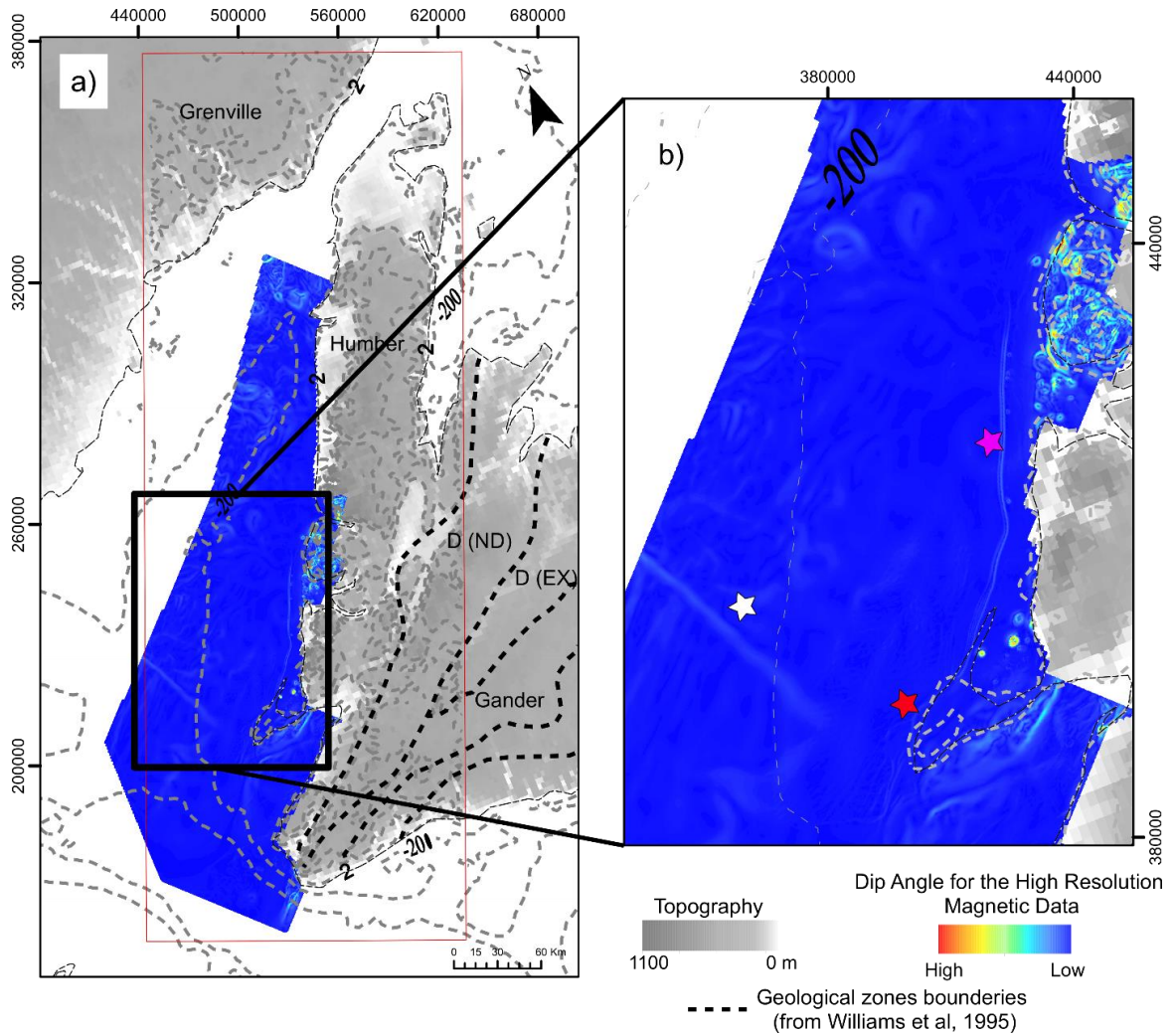


Figure 3. 15: Dip Angle Curvature results for the high resolution magnetic data. Maps show surface geological zones of the Appalachian Orogen in Newfoundland (Williams, 1995). Dashed grey lines correspond to bathymetric and topographic contours (m). Color stars correspond to anomalies described in text. a) Offshore Western Newfoundland and b) zoomed in map showing the Odd Twins Anomaly and other features. Abbreviations: D (Ex), Exploits subzone of the Dunnage zone; D (ND), Notre Dame subzone of the Dunnage zone.

The Dip angle for the Corner Brook area (Fig. 3.14b) clearly defines the boundaries of the ophiolite complexes in the area (purple star in Fig. 14b). An oval-elongated shape also demarcates the presence of the Fleur de Lys Super Group (red star in Fig 3.14b). Similar patterns are also found in Figure 3.14c, d and e where the attribute highlights different rock unit outcrops.

To calculate the curvature attributes for the knitted magnetic data, it was necessary to create a grid with a 3 km data point spacing. Dip angle and dip curvature attributes are shown for the knitted dataset in Figure 3.16. Both attributes show similar results and mainly highlight ophiolites complexes on land and offshore Western Newfoundland.

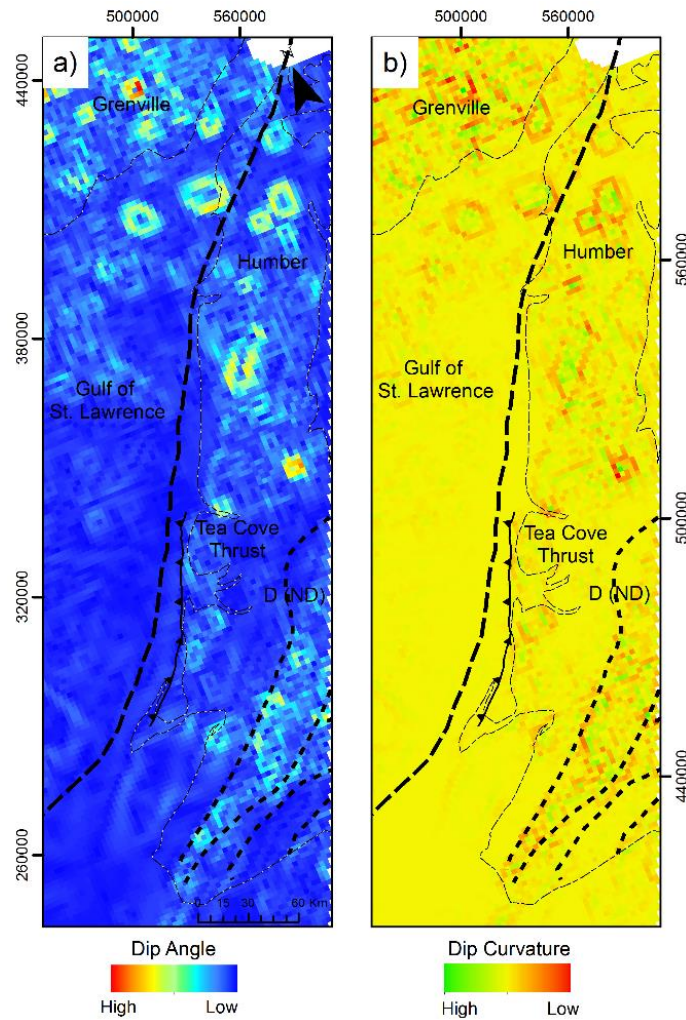


Figure 3. 16: Map of a) dip angle and b) dip curvature of the Western Newfoundland Magnetic anomaly data. Maps show surface geological zones of the Appalachian Orogen in Newfoundland (Williams, 1995). Abbreviations: D (Ex), Exploits subzone of the Dunnage zone; D (ND), Notre Dame subzone of the Dunnage zone.

The dip angle and dip curvature attributes were also calculated for the Bouguer data on land and the Free Air data offshore (Fig. 3.17). However, the results shown in Figure 3.17 are not very informative. Due to the knitting of the Bouguer onshore and Free Air

offshore datasets, it was thought that this would have created artefacts that could obstruct the curvature analysis. Therefore, the curvature analysis was also performed on just the Free Air anomaly data alone (Fig. 3.18). The dip angle and dip curvature attributes are very similar. Within the Humber Arm, a strong positive trend seems to separate zones of differing density and also follows the trace of the Tea Cove thrust. Nevertheless, the thrust ends and the trend continues on land. In general, density variability and the ophiolites are strongly highlighted on land. Offshore Western Newfoundland and in the Grenville region of Quebec, the curvature attributes are not as variable. However, the southern depocenter in the Gulf of St. Lawrence does stand out due to the density contrast between the thick Carboniferous basin and the surrounding sediments.

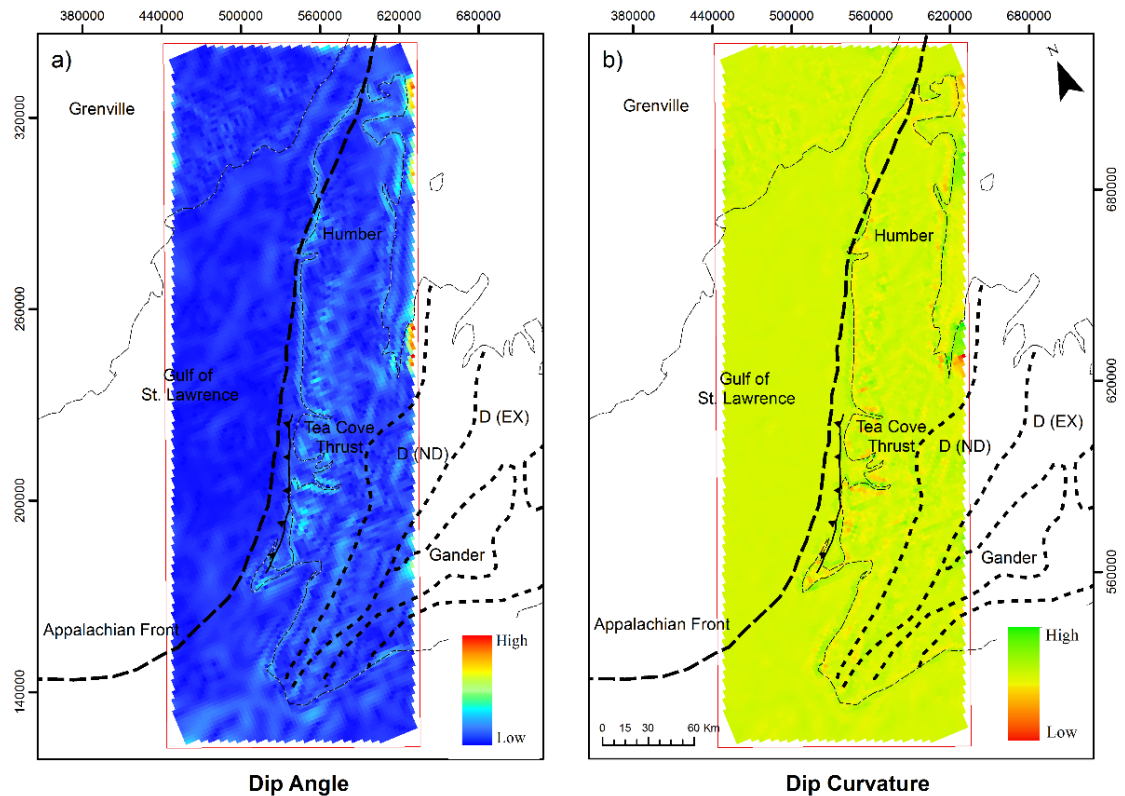


Figure 3. 17: Map of a) dip angle and b) dip curvature for the Western Newfoundland combined Bouguer/ Free Air gravity map. Maps show surface geological zones of the Appalachian Orogen in Newfoundland (Williams, 1995). Abbreviations: D (Ex), Exploits subzone of the Dunnage zone; D (ND), Notre Dame subzone of the Dunnage zone

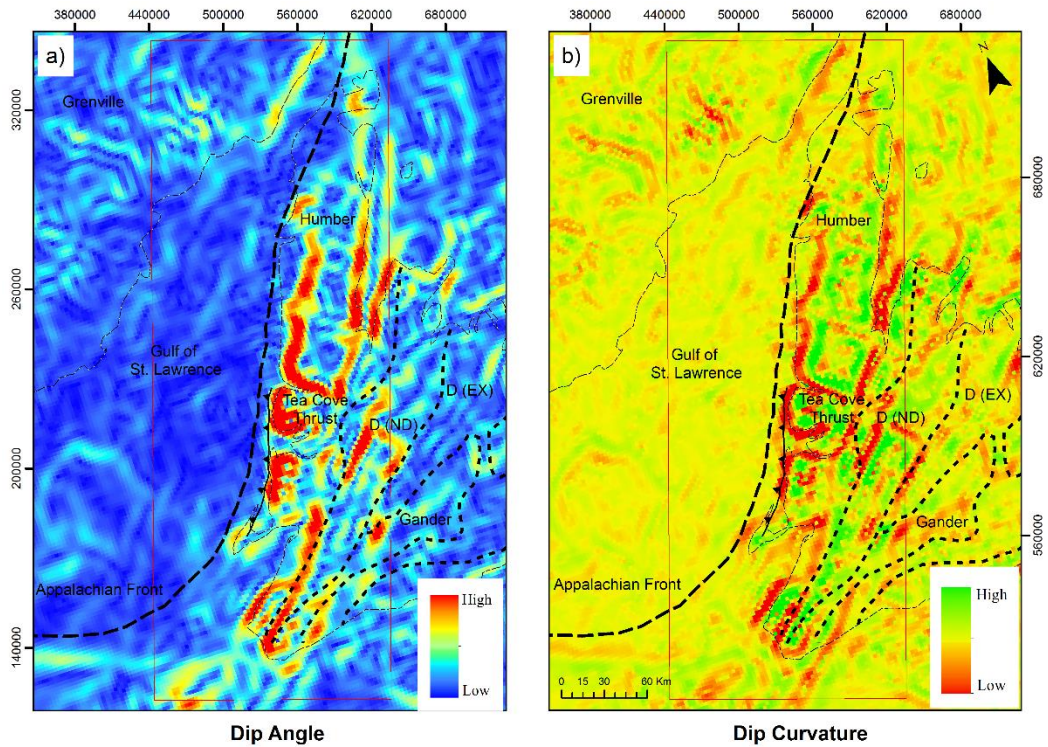


Figure 3. 18: Map of a) dip angle and b) dip curvature of the Western Newfoundland Free Air anomaly data. Maps show surface geological zones of the Appalachian Orogen in Newfoundland (Williams, 1995). Abbreviations: D (Ex), Exploits subzone of the Dunnage zone; D (ND), Notre Dame subzone of the Dunnage zone.

3.5 Euler Deconvolution

The Euler Deconvolution method is a trial and error process that depends on three parameters: the structural index (SI), the window size, and the tolerance of the obtained solutions. Figure 3.19 shows the Euler deconvolution results obtained by varying the SI from 0 to 2 and keeping the other parameters constant for the combined Free Air/ Bouguer gravity anomaly datasets. Increasing the SI leads to an increase in the amount of points resolved by the Euler deconvolution. Although, the choice of SI implies a model interpretation (Section 2.4, Chapter II), the clusters shown in Figure 3.19 do not provide any interpretable information about the underlying structures in the study area.

After testing all parameters, the preferred solutions are shown in Figure 3.20. The clusters are located in the offshore area and they border gravity anomalies. The results, nonetheless, are not geologically intuitive or interpretable.

The Euler deconvolution testing process is also applied to the magnetic datasets. Figure 3.21 shows the preferred solutions for the compilation magnetic data, high resolution magnetic data, and the knitted dataset. Figure 3.21a and Figure 3.21b show clusters that border the E-W linear anomalies (red circles in Fig. 3.21a and 21b). The depths of those clusters extend to 7.9 km. Therefore, these anomalies appear to originate from the upper crust. Clusters also border certain oval shaped anomalies in the northern part of the study area (Fig. 3.21a) with shallower depths, which suggest that these bodies are found in sedimentary layers or the upper crust.

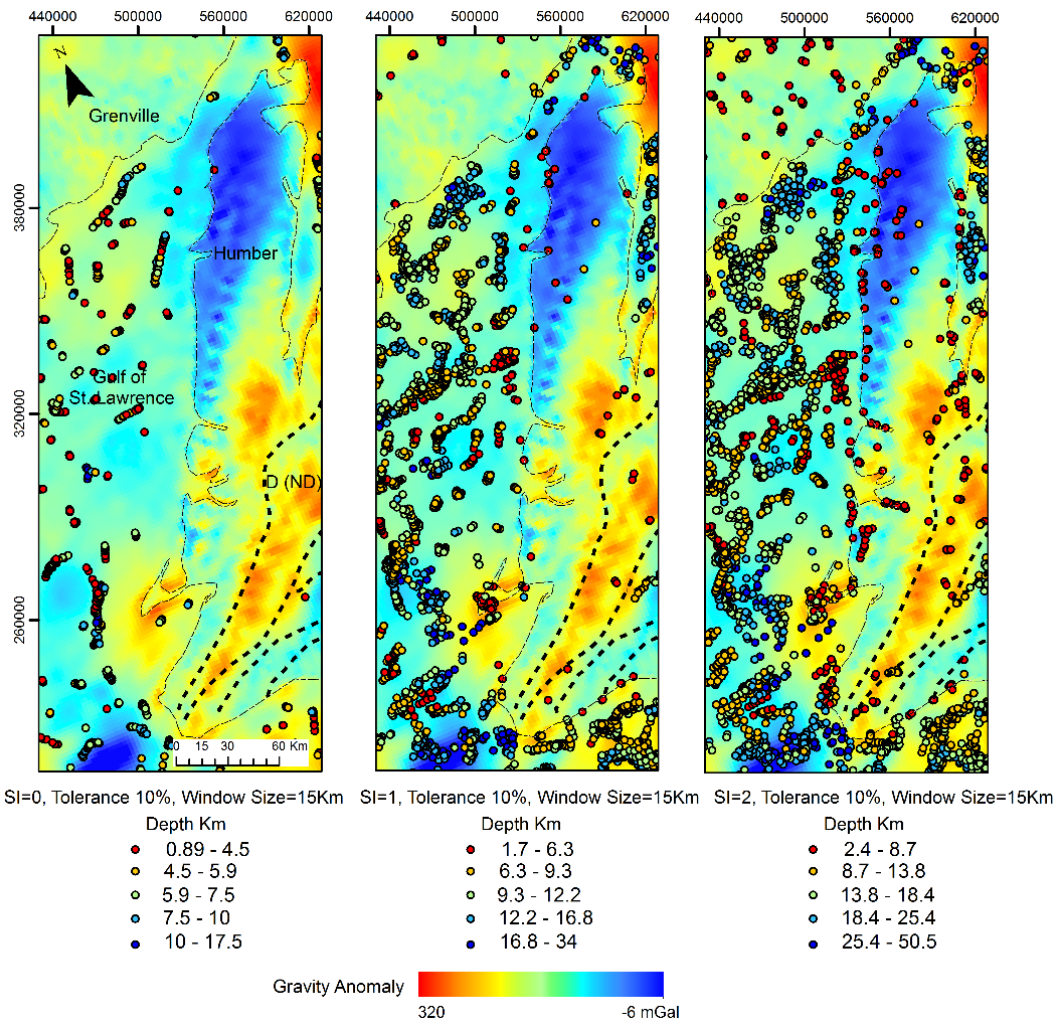


Figure 3. 19: Maps of tests of the Euler deconvolution results for the combined Bouguer/ Free Air gravity data from varying the Structural Index (SI). a) SI = 0, Tolerance = 10% and Windows size= 15 km, b) SI = 1, Tolerance = 10% and Windows size= 15 km and c) SI=2, Tolerance= 10% and Windows size= 15 km. Maps show surface geological zones of the Appalachian Orogen in Newfoundland (Williams, 1995). Abbreviations: D (Ex), Exploits subzone of the Dunnage zone; D (ND), Notre Dame subzone of the Dunnage zone.

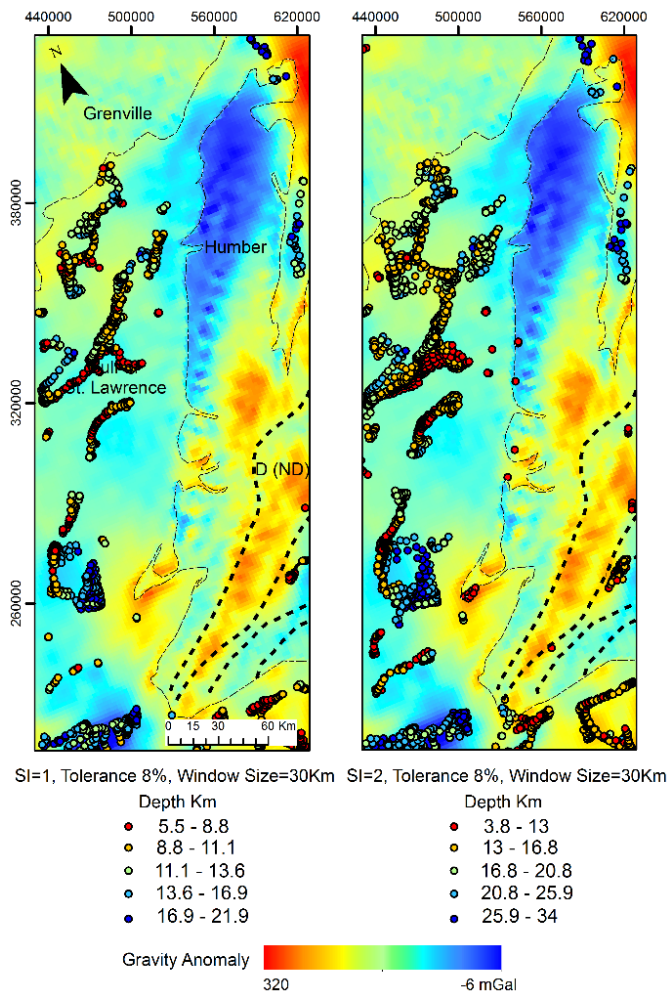


Figure 3. 20: Maps of Euler deconvolution for the combined Bouguer/ Free Air gravity data. a) $SI = 1$, Tolerance = 8% and Windows size= 30 km and b) $SI = 2$, Tolerance = 8% and Windows size= 30 km. Maps show surface geological zones of the Appalachian Orogen in Newfoundland (Williams, 1995). Abbreviations: D (Ex), Exploits subzone of the Dunnage zone; D (ND), Notre Dame subzone of the Dunnage zone.

The Euler deconvolution tests were also performed on the Free Air anomaly data of the study area. Figure 3.22 shows the preferred solution for this case. This figure shows more interpretable results in comparison to Figure 3.20. In the Notre Dame subzone of the Dunnage zone, a large accumulation of points is shown (Fig. 3.22). The behaviour of these points may provide information about the major faults in the area. Similarly, a cluster that parallels the trace of the Tea Cove Thrust is shown in Figure 3.22, despite the lack of surface evidence for this feature.

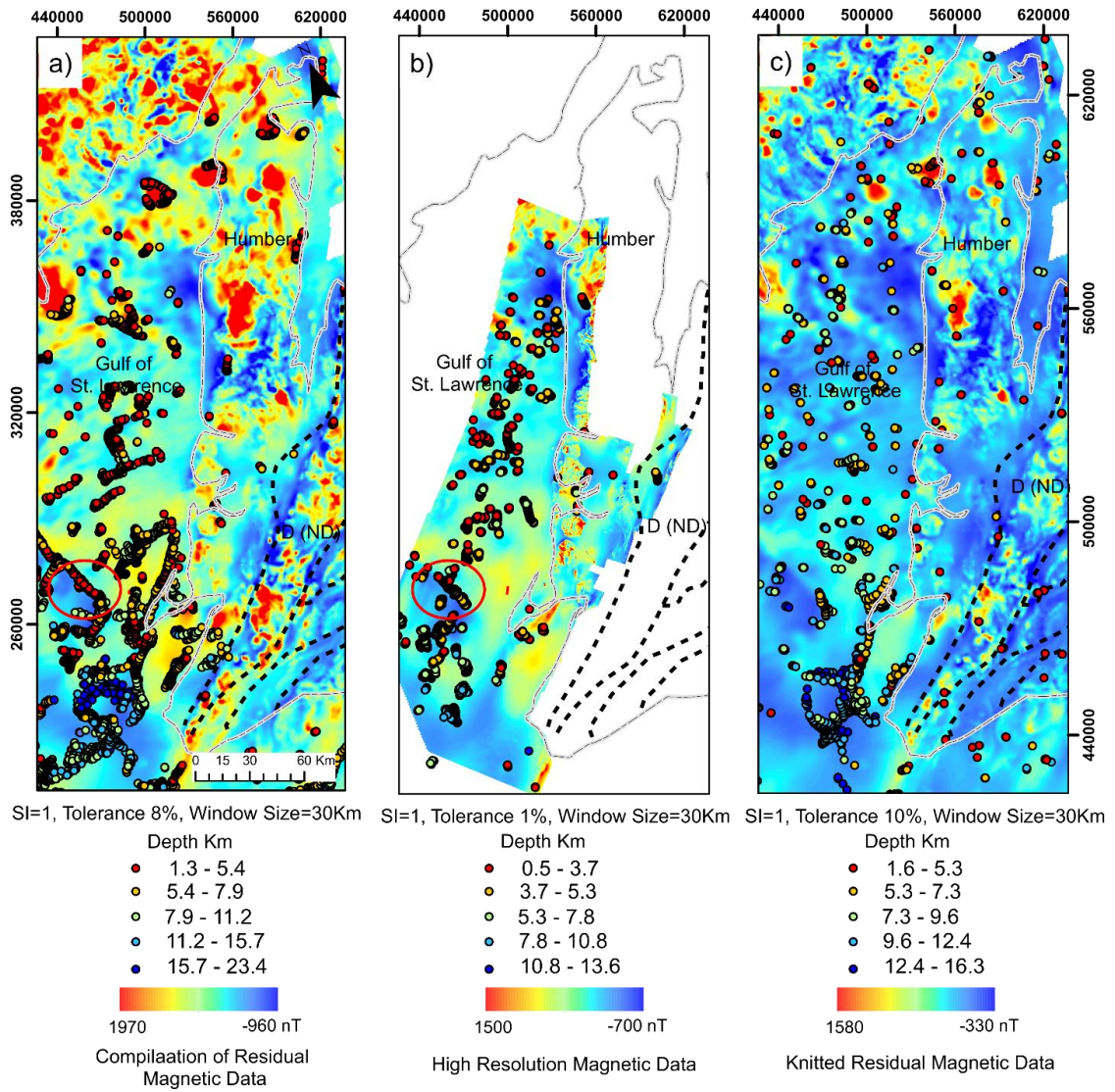


Figure 3.21: Map of Euler's deconvolution for magnetic data. a) $SI = 1$, Tolerance = 8% and Window size= 30 km and b) $SI = 1$, Tolerance = 1% and Window size= 30 km, and c) $SI = 1$, Tolerance 10% and Window size =30 km. Maps show surface geological zones of the Appalachian Orogen in Newfoundland (Williams, 1995). Red circle corresponds to anomalies described in text. Abbreviations: D (Ex), Exploits subzone of the Dunnage zone; D (ND), Notre Dame subzone of the Dunnage zone.

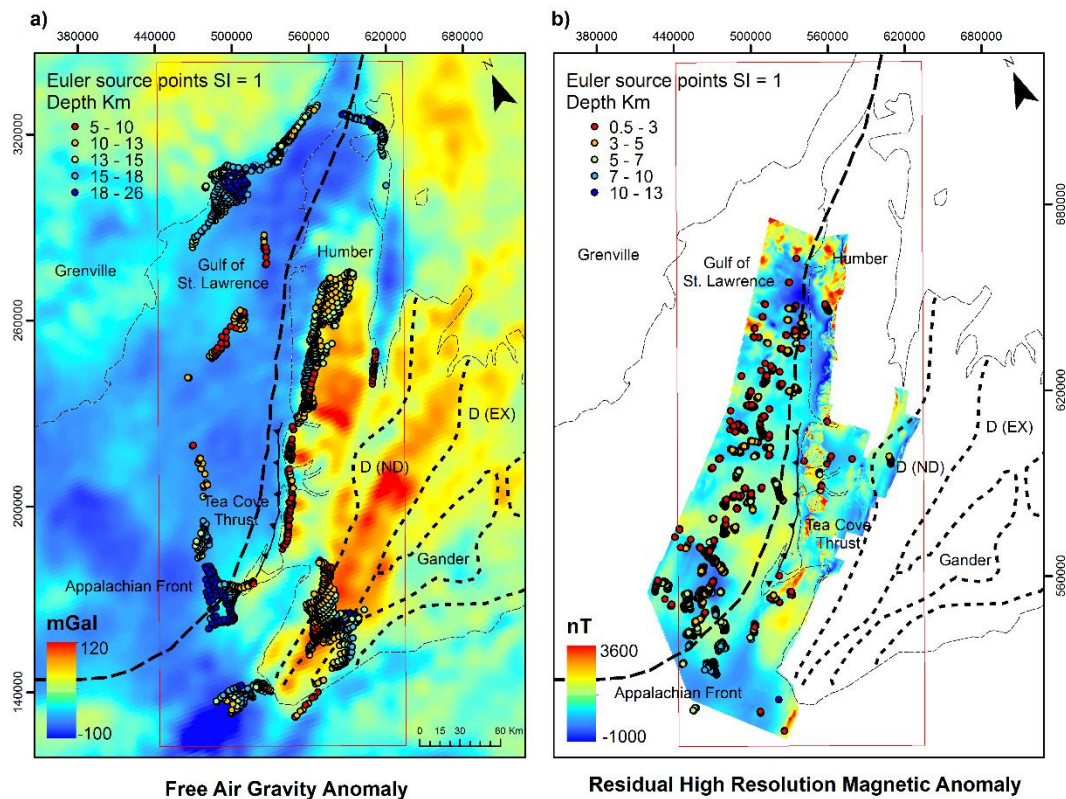


Figure 3. 22: Map of Euler's deconvolution for Free Air anomaly and high resolution magnetic data. a) $SI = 1$, Tolerance = 8% and Window size= 30 km and b) $SI = 1$, Tolerance = 2% and Window size= 30 km. Maps show surface geological zones of the Appalachian Orogen in Newfoundland (Williams, 1995). Abbreviations: D (Ex), Exploits subzone of the Dunnage zone; D (ND), Notre Dame subzone of the Dunnage zone.

3.6 Summary

The Free Air anomaly generally corresponds with the topography and bathymetry. The Free Air offshore and Bouguer onshore gravity maps show high positive anomalies related to ophiolite complexes in the Notre Dame subzone whereas low negative anomalies cover most of the Gulf of St. Lawrence. Similarly, the residual magnetic anomaly also shows the same behavior. The Odd Twins Anomaly is highlighted by the High resolution magnetic data and by the Curvature attributes. The spectral analysis for both potential data showed a broad scale (>25 km) for the first spectrum trend. These depths may be related to the mean Moho depth and deepest extent of static magnetic sources for the study area. A more detailed power spectrum analysis was also performed for each of the high resolution

magnetic surveys. The Euler deconvolution final results may provide information about faults in the study area.

The following chapter, chapter IV, introduces the core research results. The 3D gravity modelling and seismic interpretation results are analyzed.

Chapter 4: Seismic Interpretation and Gravity modelling

In this chapter, the core research results are presented. First, the seismic interpretation results are discussed. These are used to constrain the sedimentary structure in the Gulf of St. Lawrence. The results from the 3D gravity forward modelling are presented as evolving sections. Standard basic statistics are computed for the residual gravity anomaly of the final model. Sections of the final model are also explained. Finally, derived Moho depth and basement depth maps are shown and discussed. The evidence for the high-density lower crustal body is also addressed.

4.1 Seismic Interpretation

The interpreted general structure of the sedimentary layers as well as the faults that modify the basement are shown in the final stages of the forward gravity modelling.

In general, all seismic lines are characterized by chaotic reflectivity and poor continuity. However, for all northern seismic lines, four different patterns were observable (Figs. 4.1 and 4.2). In Figures 4.1 and 4.2, letter A denotes parallel reflections that are marked as horizons 1 and 2 and that correspond to Cambro-Ordovician platform successions and the Grenville basement. Along the east side of the seismic lines, from 250 to 1250 ms, an area of chaotic reflectors stands out. This behavior contrasts with the discontinuous reflectivity seen to the west, and denoted by letter C, that corresponds to foreland basin sediments. Low angle reflections that terminate against a steeper seismic surface, well known as onlap, are found between C and B. This pattern of onlap indicates two different strata coexisting in the area. The shallower area, from 0 to almost 500 ms, is characterized by strong continuous reflectors. These distinct patterns allowed for three main horizons to be interpreted and the chaotic character shown by letter B to be interpreted as the Humber Arm Allochthon (HAA) (Cooper et al., 2001; Hinchey et al., 2015; Stockmal et al., 1998). Figure 4.2 shows the interpretation of seismic line 91-1493 and it is shown how the Humber Arm Allochthon is still present in the south. Stockmal et al. (1998) interpreted the same seismic lines, as well

as others in the study area, and found that the tectonic wedge (Triangle zone or Humber Arm Allochthon) is of a thin-skinned nature. This can be seen in Figure 4.1 and Figure 4.2, where the HAA seems to be bounded at the top by the Tea Cove Thrust. The parallel reflections marked as A, and the sub-parallel reflections marked as C suggest that the arrival of the HAA disrupted these sedimentary packages. The emplacement of the HAA took place after these layers were deposited. Therefore, the HAA was emplaced during the post-Silurian or the Early Devonian (Stockmal et al., 1998).

Further south in the study area at line CAH91-20 from the Port-au-Port Peninsula (Fig. 4.3), parallel and subparallel reflector geometries with strong amplitudes are observed. These horizons are deformed and the chaotic geometry of the HAA is not clear since there are clear faults that mask the seismic reflectivity. However, Stockmal et al. (1998) interpreted the presence of the HAA, as shown in Figure 4.3, with a dashed circle.

The faults shown in Figure 4.3 cut through the sedimentary layers and also the basement. These faults are characterized as thick-skinned faults (Stockmal et al., 2004, 1998). Examples are the Round Head Thrust and the St. George Thrust. Stockmal et al. (2004, 1998) interpreted the Round Head Thrust as a reactivated normal fault during the Acadian Orogen.

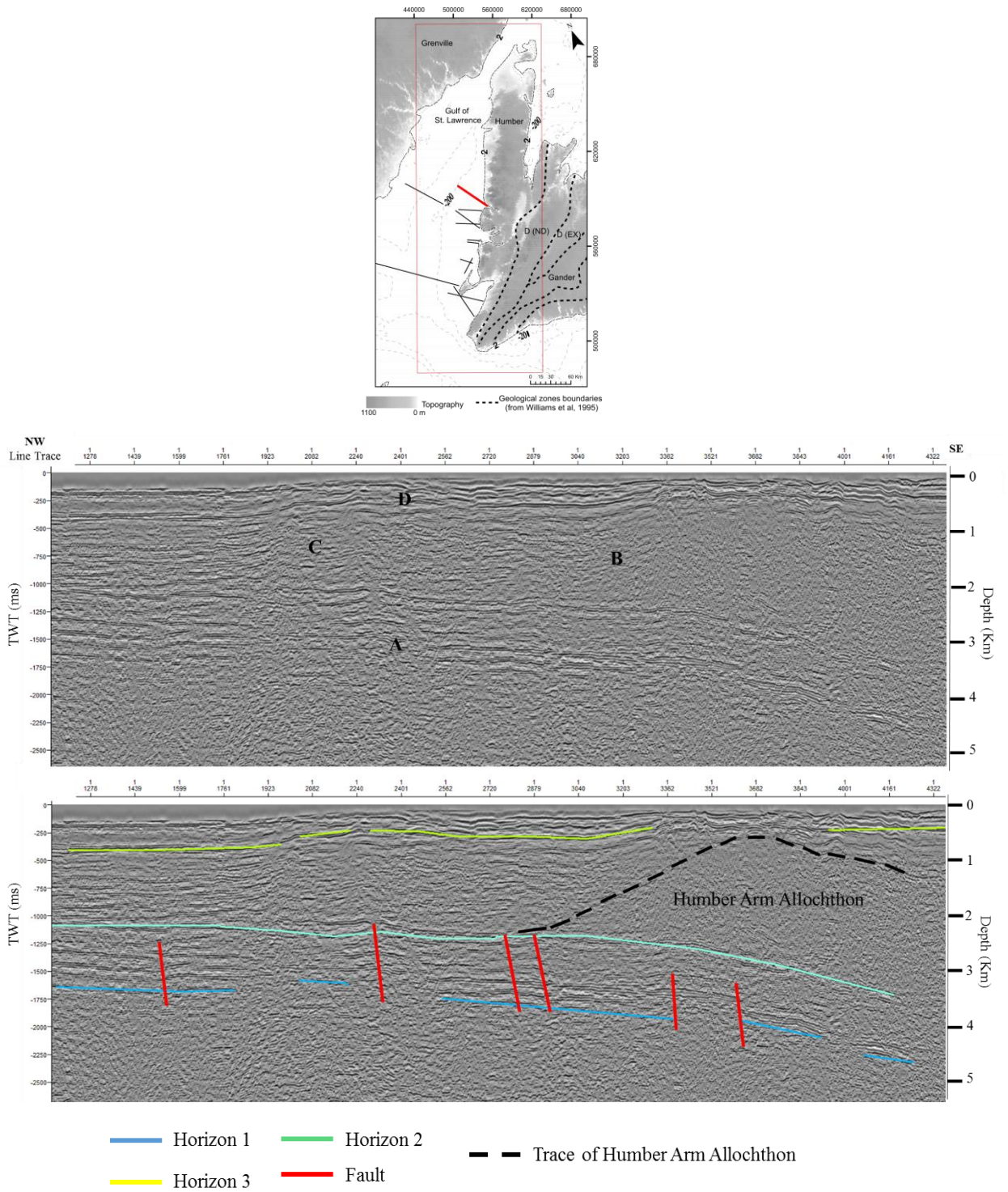


Figure 4. 1: (Top) Location of seismic line CAH90-01, red line. (Bottom) Uninterpreted and interpreted seismic line CAH90-01.

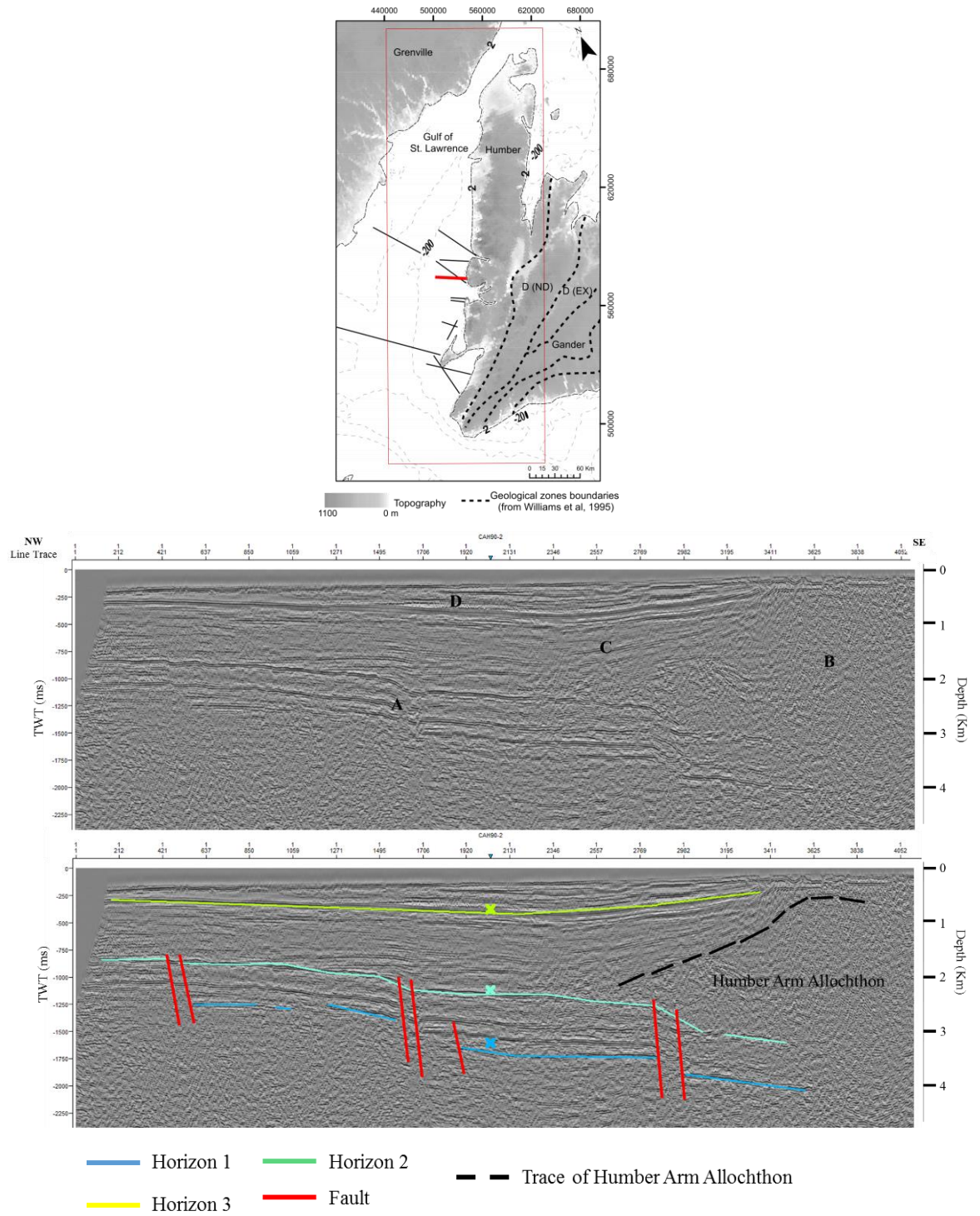


Figure 4. 2: (Top) Location of seismic line 91-1493, red line. (Bottom) Uninterpreted and interpreted seismic line 91-1493.

4.2 Forward Modelling

The gravity forward model was improved by adding more constraints. The first model (Table 4.1, Fig. 4.5a) only included 18 sections with variations in topography and bathymetry. The sediment depths were set to 3 km and 40 km respectively, following the seismic refraction model from Jackson et al. (1998) and Marillier et al. (1994). Figure 4.5a shows the residual gravity map for this overly simple preliminary model. The correlation factor between the measured and calculated gravity anomaly was 0.63. A second model (Table 4.1, Fig. 4.5b) was constructed by varying Moho depth and depth to basement, to reproduce the gravity anomalies along each section. The correlation factor increased to 0.78.

A better fit was achieved by including more model sections, for a total of 28 sections (Table 4.1, Fig. 4.5c), and by dividing the crust into an upper and a lower crust based on the seismic refraction model. The correlation factor between the measured and calculated gravity anomaly increased to 0.93. To fit the observations, this model did not require a clear separation between the lower crust of the Grenville zone and the Humber zone, or an underplated crust in the Humber zone, as has been previously proposed (Hall et al., 1998; Jackson et al., 1998; Marillier et al., 1994; Quinlan et al., 1992).

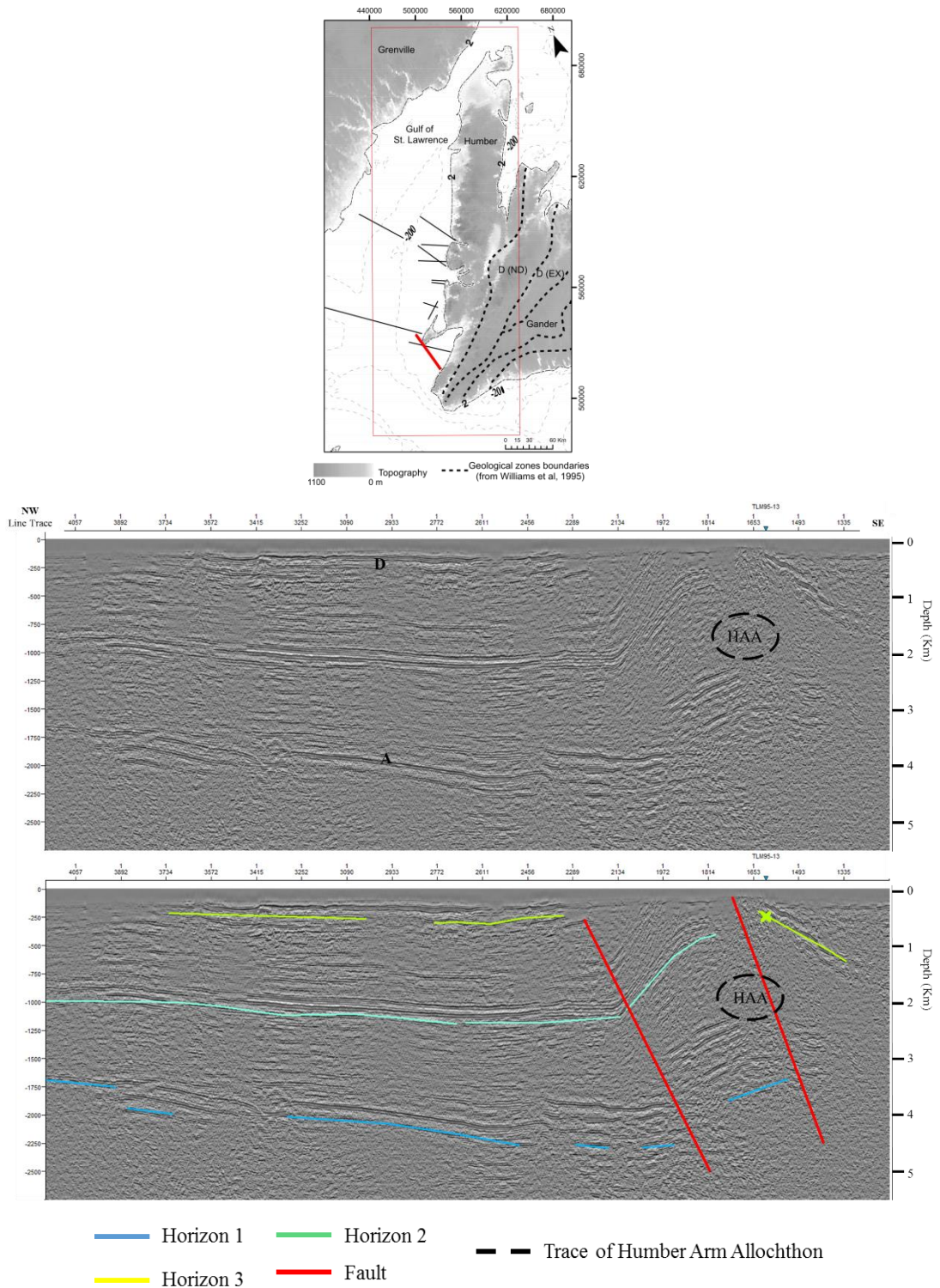


Figure 4. 3: (Top) Location of seismic line CAH91-20, red line. (Bottom) Uninterpreted and interpreted seismic line CAH91-20.

Based on previous work, a high density body was included beneath the former Laurentia continental margin, and the lower crust was separated into lower-crustal blocks (LCBs) (Hall et al., 1998; Jackson et al., 1998; Marillier et al., 1989). More sections, for a total of 30 (Table 4.1, Fig. 4.5d), were added to better constrain the geometry and extent of the high density lower crustal body. The correlation factor increased to 0.96.

These four preliminary models (Table 4.1, Fig 4.5) were tested against the observed Free Air anomaly data (Fig. 4.4). These models show that the density structure in Western Newfoundland is very simple. With a simple sedimentary layer with a density of 2.4 g/cm^3 , a good fit is obtained for the western part of the study area in the Gulf of St. Lawrence (Fig. 4.5). The depth to the Moho and the separation between the upper and lower crust also reproduce the regional trends of the gravity anomaly well. To improve the model for the eastern part of the study area, the models were adjusted using the combined Free Air anomaly data offshore and Bouguer anomaly data on land. Figure 4.6 documents the evolution of the forward model until the final model is reached.

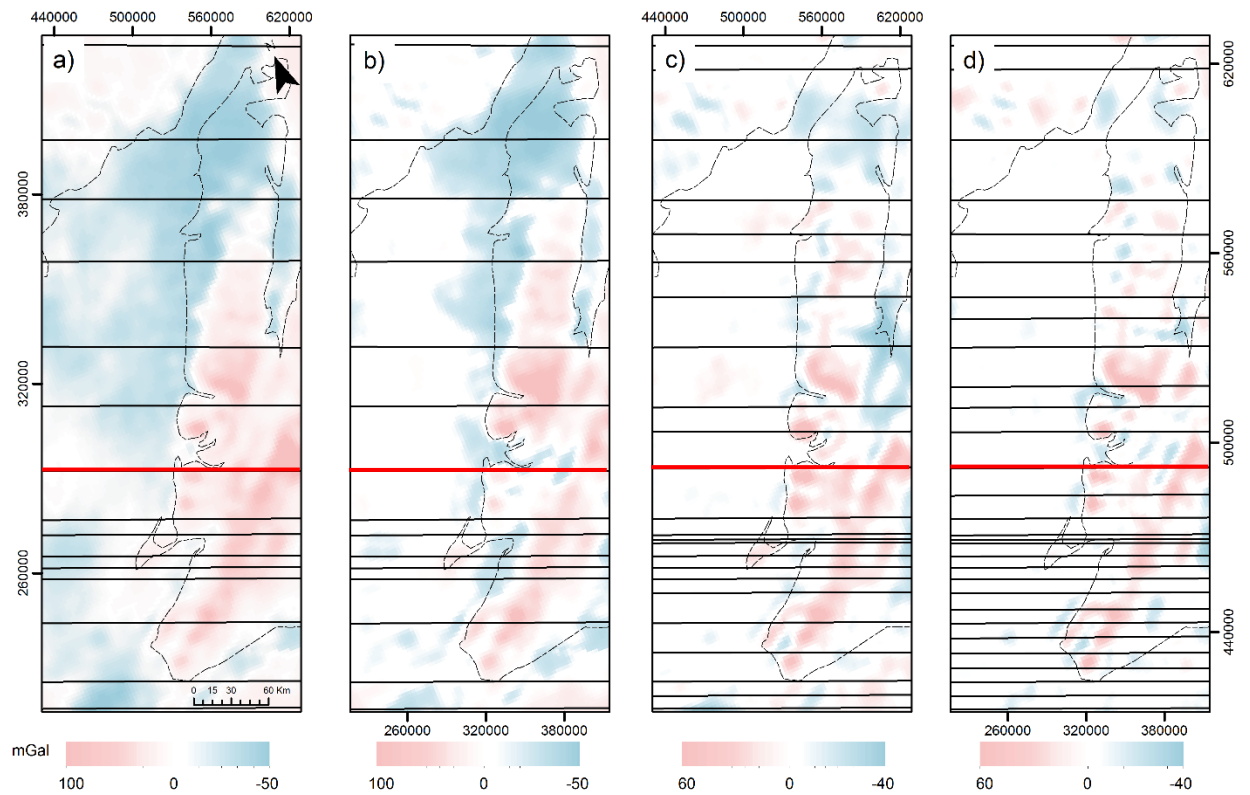


Figure 4.4: Western Newfoundland Residual gravity maps for the preliminary models 1 to 4. a) Correlation of 0.63, b) correlation of 0.78, c) correlation of 0.93 and d) correlation of 0.96. Red line indicates position of the section shown in Figure 4.5.

Figure 4.6a shows the fifth version of the forward model (Table 4.1), constructed using the same 30 sections. However, changes in topography were not taken into account on land since the Bouguer anomaly data are already corrected for topography. The correlation factor dropped from 0.96 to 0.88 and as it is shown in Figure 4.6a, the main differences in the residual anomaly are found on land. This discovery suggests that the sedimentary structure for Western Newfoundland cannot be defined using only a simple sedimentary layer. The surface geology of the study area (Williams, 1995) divides the area into different tectonic domains that may each have different density characteristics and that may differ from the sediments in the offshore area.

Table 4. 1: Summary of 3D gravity forward models and final model.

Model	Number of 2D sections	Free Air Anomaly	Free Air and Bouguer Anomaly	Topography/ Bathymetry	Division of Upper and Lower Crust	High density body	Division of Sediments	Euler constraints	Seismic constraints
1	18	x		x					
2	18	x		x					
3	28	x		x	x				
4	30	x		x	x	x			
5	30		x	x	x	x			
6	48		x	x	x	x	x	x	x
7 (Final model)	50		x	x	x	x	x	x	x

To improve the fit between the measured and observed gravity data, Euler deconvolution points (Fig. 3.20 from Chapter III) were projected into the model. Seismic refraction lines 91/3 and 91/4 were also used to better constrain the evolving model (Fig. 1.1 from Chapter I). Figures 4.7a and 4.7b show how the Euler Deconvolution points appear in the 3D window of the IGMAS software. An explanation could be proposed for the distribution of Euler Deconvolution points in the northern area (Fig. 4.7), however, this is highly speculative given the lack of other constraints. Figure 4.7b shows an example section with projected Euler deconvolution points within 5 km of the section. As shown in Figure 4.8a, the points seem to follow the upper-lower crustal boundary, although this may be coincidental. The large accumulation of points in the southern part of the study area (Fig. 4.7b) could be interpreted as major faults in the Notre Dame subzone since the points reach depths down to 20 km. The Burgeo Road Transect deep seismic reflection profile (Fig. 1.1 from Chapter I) shows changes in reflectivity (van der Velden et al., 2004) that may support the fault interpretation in the Notre Dame subzone. For example, the Bay Verte line- Cabot fault system is expressed as a vertical feature that cuts the entire crust. The Little Grand Lake Fault, the Lloyds River Fault and the Red Indian line also cut the crust (van der Velden et al., 2004). Despite this area appearing structurally complex on the seismic data, the density structure does not show abrupt lateral variability (Fig. 4.8b). Therefore, mean

densities of 2.65 and 2.85 g/cm³ for the upper crust and lower crust were assigned, without further lateral subdivisions.

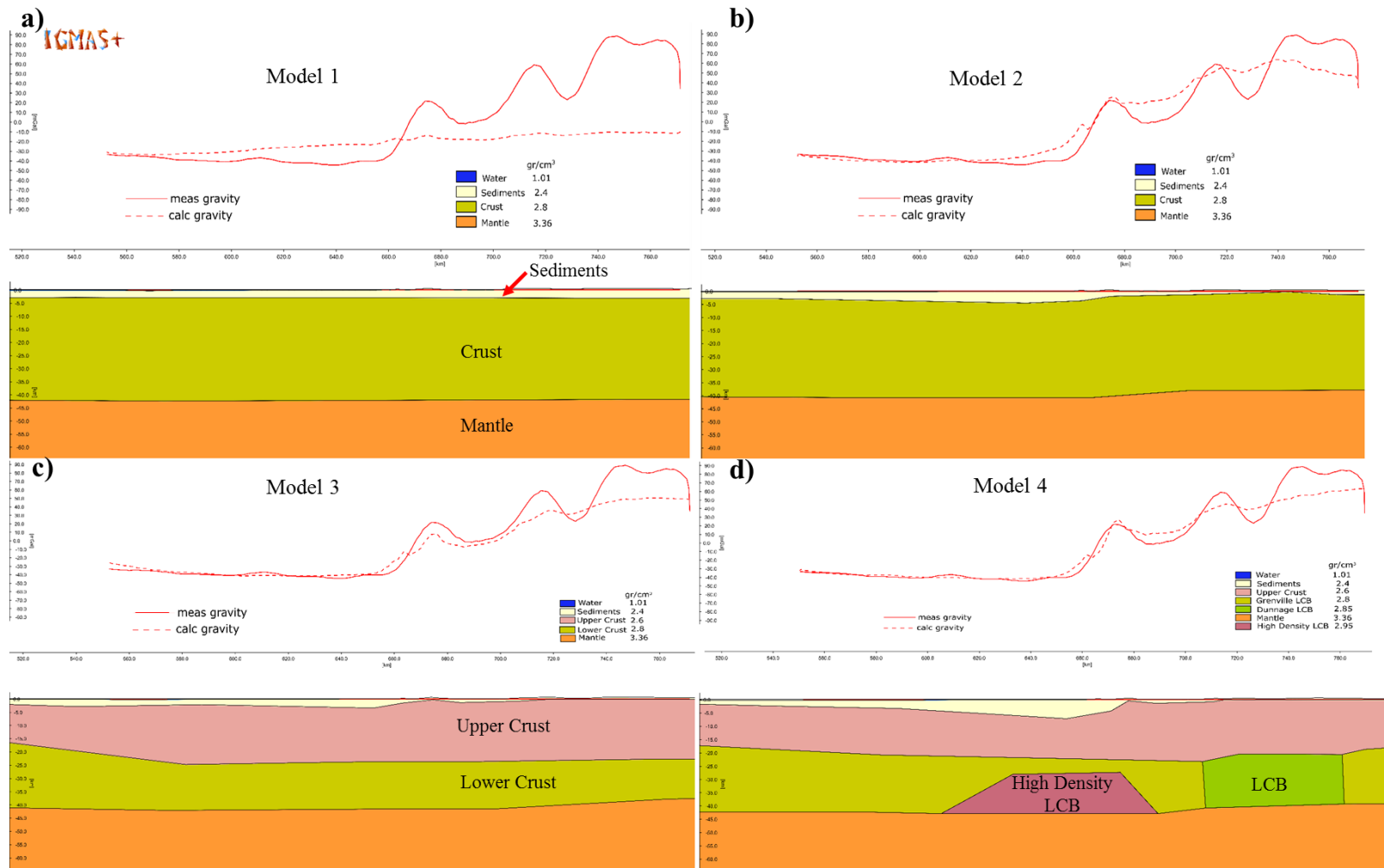


Figure 4. 5: Evolution of a 2D section through the preliminary models 1 to 4, with the match between the observed and calculated data plotted above each model section. a) Correlation of 0.63 between observed and calculated anomaly, b) correlation of 0.78, c) correlation of 0.93 and d) correlation of 0.96. Location of this section is found in Figure 4.4.

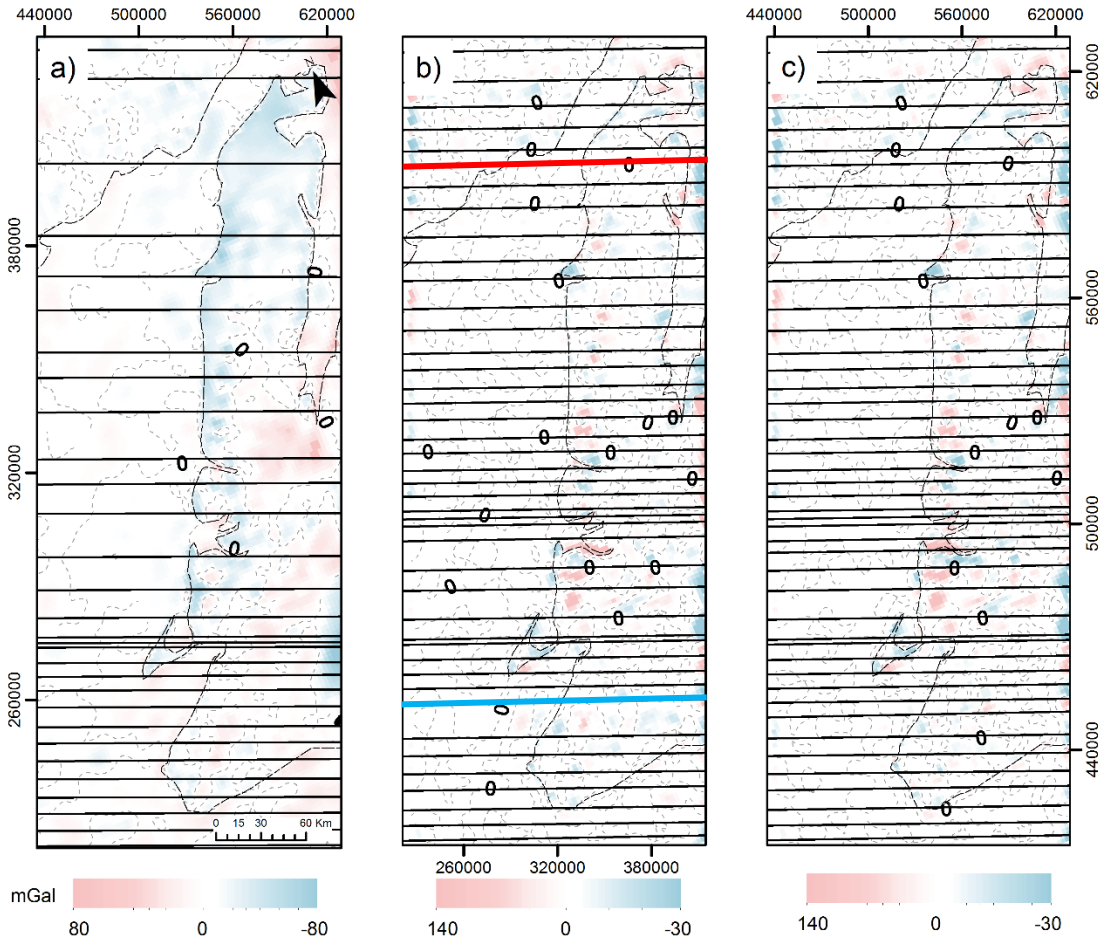


Figure 4. 6: Western Newfoundland Residual gravity maps of Free Air anomaly offshore and Bouguer anomaly on land for models 5 to 7 with 0 contour labelled. a) Correlation of 0.88, b) correlation of 0.97 and c) correlation of 0.97. Blue line and Red line are shown in Figure 4.8.

The surface geology was placed on Figure 4.8 using the surface geology maps of Western Newfoundland (Colman-Sadd et al., 2000; Waldron et al., 1993) and the tectonic division of Williams (1995). As shown in Figure 4.8, different regions in the study area have different densities that were adjusted to better fit the gravity signal. Along the coastline, where the Free Air anomaly and Bouguer anomaly were knitted together, anomalous geometry structures for the sediment layer were needed to reach a better fit. This situation is caused by the knitting algorithm and the complex Newfoundland coastline that do not allow a clear meshing between both anomaly datasets. The anomalous structures do not have a geological meaning and are not interpreted. Hence, the results along the coastline are marked by a white square on the sections (Fig. 4.8 and 4.9).

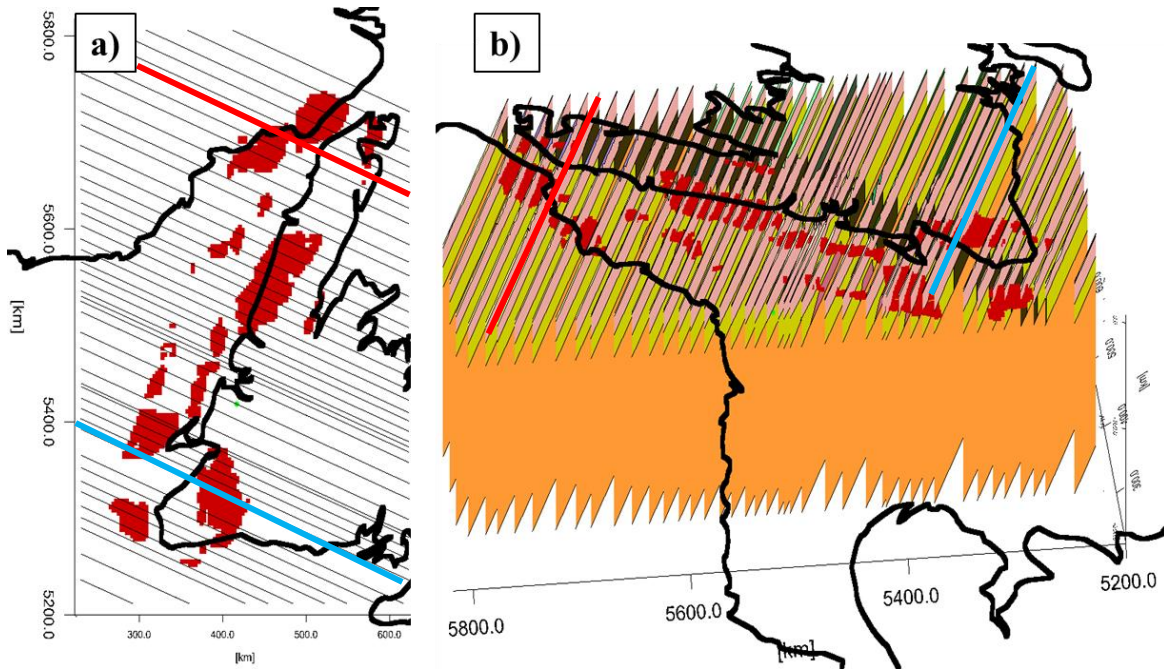


Figure 4. 7: Western Newfoundland modelling area with Euler deconvolution points (red dots) in a) 2D and b) 3D. Red line shows position of Figure 4.8a and blue line shows position of Figure 4.8b.

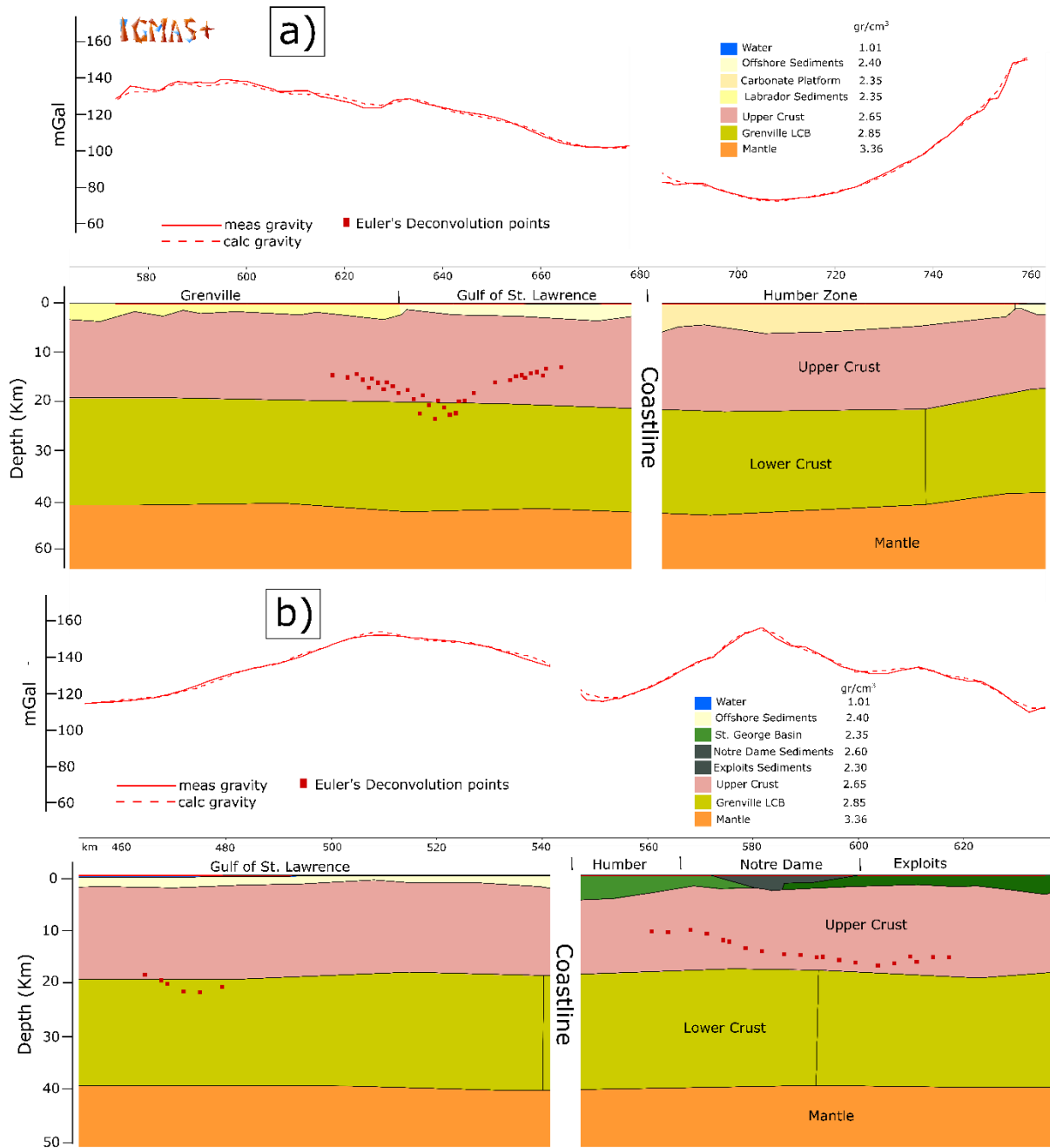


Figure 4.8: Example sections of model 5, corresponding to Figure 4.6. a) Section in the north of the study area, marked as red in Figure 4.6b and 4.7, and b) section in the south of the study area, marked as blue in Figure 4.6b and 4.7.

Figure 4.9 shows the section that follows seismic refraction profile 88-3 (Figure 1, Chapter I). The Moho depth is approximately 40 km for the shown slice. The geometry of the high density body is not fully captured by seismic profile 88-3 (Hall et al., 1998; Jackson et al., 1998). However,

this body, with a seismically derived density of 3.03 g/cm³, is modelled within the Grenville basement and underneath the Humber zone. The depth of the sedimentary layer is shown by the thick dashed line (Fig. 4.9).

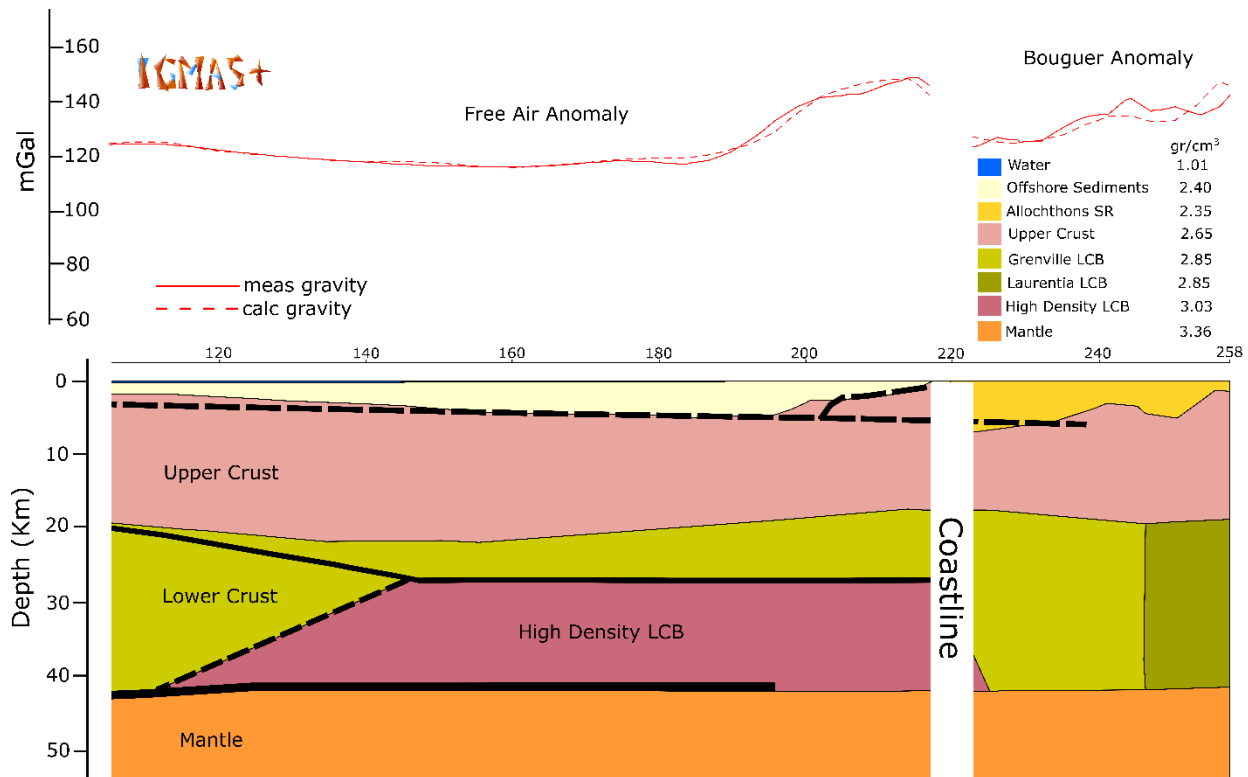


Figure 4. 9: Section from model 5, coincident with seismic refraction line 88-3. (Top) Comparison of the observed gravity and calculated gravity data. (Bottom) Density model for this line. Black lines (solid and dashed) identify the configuration of the layers given by seismic refraction line 88-3 (Jackson et al., 1998). Solid black lines are reflectors. Base of the crust (Moho) identified by black thicker line. Dashed black lines are model boundaries.

After adding the independent constraints already discussed and adjusting the geometry of the sediments to produce a better fit between the model and observed gravity data, the correlation factor improved from 0.88 to 0.97. The final model 7 (Figure 4.6c, Table 4.1) included the seismically interpreted horizons and necessary model adjustments to improve the fit. In the following section, the final model is discussed.

4.1.1 Model precision and limitations

In order to assess the precision of the regional density model, a statistical analysis of the misfit between the observed gravity (Combined Free Air anomaly offshore / Bouguer anomaly on land) and the calculated gravity from the model was undertaken. Figure 4.10b shows the histogram of the misfit (Fig. 4.10a), which shows a high concentration of values around 5.28×10^{-9} mGal (arithmetic mean) with a standard deviation of 3.97 mGal, and a correlation factor of 0.97 between calculated and observed gravity anomalies.

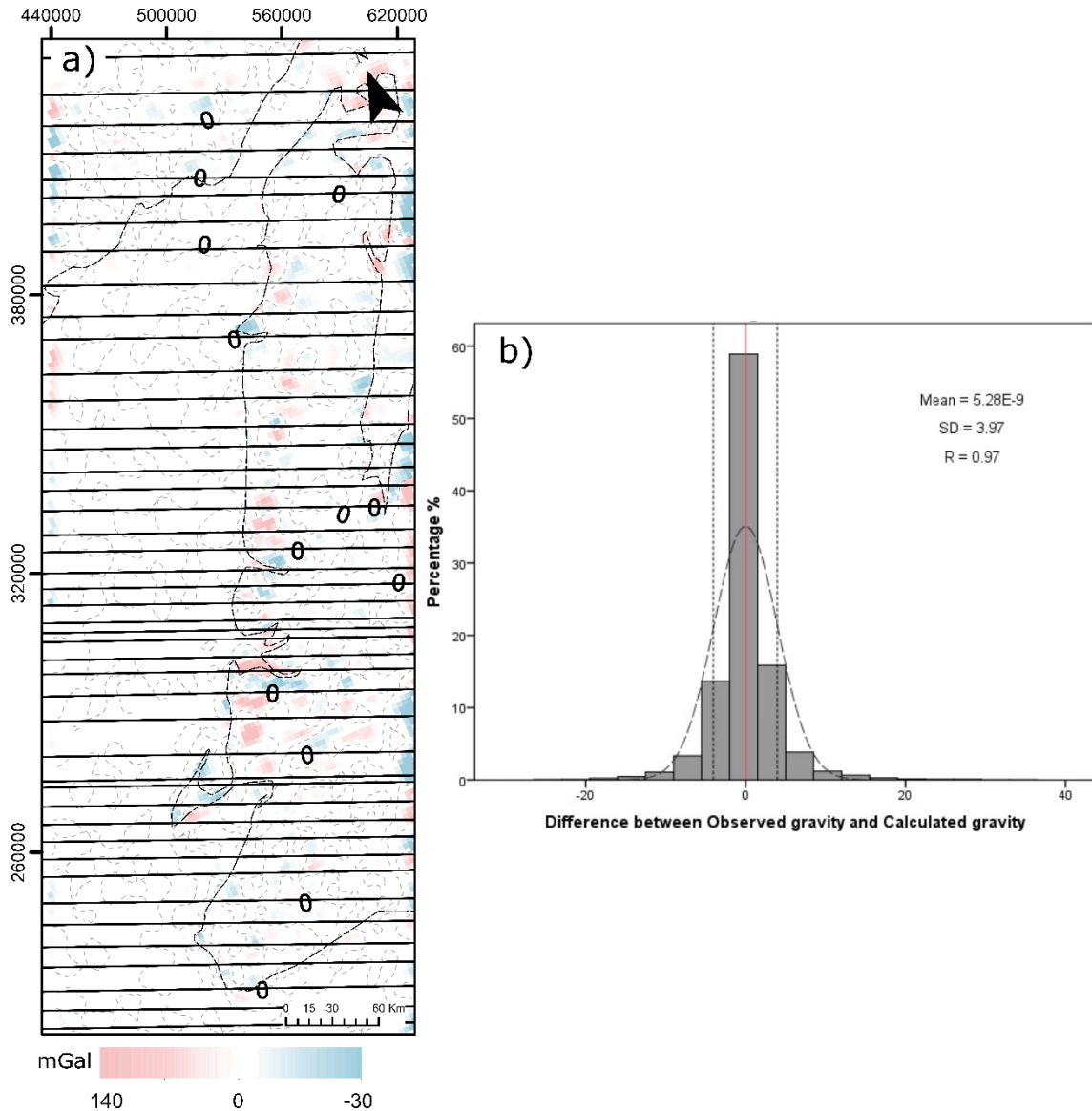


Figure 4. 10: a) Residual gravity field of the study area obtained by subtracting the calculated gravity effect of the 3D model from the observed gravity field (black lines indicate position of the W-E sections used to define the model geometry), b) histogram of residual gravity, arithmetic mean, standard deviation (SD), and correlation coefficient (R).

The greatest differences in the residual map (Fig. 4.10a) are found along the sections where the geology of the bodies has been interpolated. The average separation between sections is ~10 km, so smaller geological structures were not taken into account. For instance, values higher than the standard deviation are observed in the ophiolite complexes of the Humber Arm Allochthon, indicating that the material should have a higher local density value than the selected density value for the regional structure.

Despite the discrepancies discussed, the statistical analyses show that the observed misfit is not regionally significant. Tassara et al. (2006) developed a 3D density model for the Nazca plate and the Andean continental margin and according to their results, the expected uncertainty for the depth to discontinuities is ~20% and for density uncertainties range from 0.15 to 10%. Considering those uncertainties, the 3D density model from this study is non-unique and represents one of the many possible models for Western Newfoundland. However, the high-resolution gravity data and the seismic constraints allow this model to satisfy the regional tectonic structures of the study area.

4.2.2 Model sections

Four E-W sections and 5 arbitrarily oriented sections are presented to illustrate the main characteristics of the 3D gravity model and its consistency with the constraining data (Fig. 4.11).

Section 1 (Fig. 4.12) crosses the southern part of the study area, specifically the Gulf of Saint Lawrence, and it is in the vicinity of seismic profile 91/4. The seismic velocities from seismic profile 91/4 were used as the main input for the density selection for the area. The sediments are divided in two layers with densities of 2.30 and 2.60 g/cm³. The upper crust is also divided into two layers of 2.74 and 2.80 g/cm³. The derived densities from seismic velocities for the lower crust were higher (2.91 g/cm³) compared to what was required to reach a better fit. A density of 2.88 for the lower crustal bodies was assigned to the Laurentia and Dunnage margins. The Moho depths, less than 40 km, agree with profile 91/4 (Hall et al., 1998).

Section 2 (Fig. 4.13) is the same section shown in Figure 4.8b with the final layer divisions. This section crosses the Gulf of St. Lawrence, St. George Basin and the Dunnage surface zones.

The separation of the St. George Basin and the Notre Dame sub-zone corresponds to the Cabot fault, which is a dextral strike-slip fault. van der Velden et al. (2004) interpreted this fault as a near vertical feature that extends from the surface to the Moho, meaning that this fault cuts the entire crust. The Cabot fault is shown in Figure 4.13 as black dots. There is a clear near vertical separation within the sedimentary provinces with different densities but there is not a clear separation in the crust within this model. The Euler deconvolution points are also plotted in Figure 4.13 as green dots which may relate to the extensive crustal scale faults as interpreted in the area by van der Velden et al. (2004).

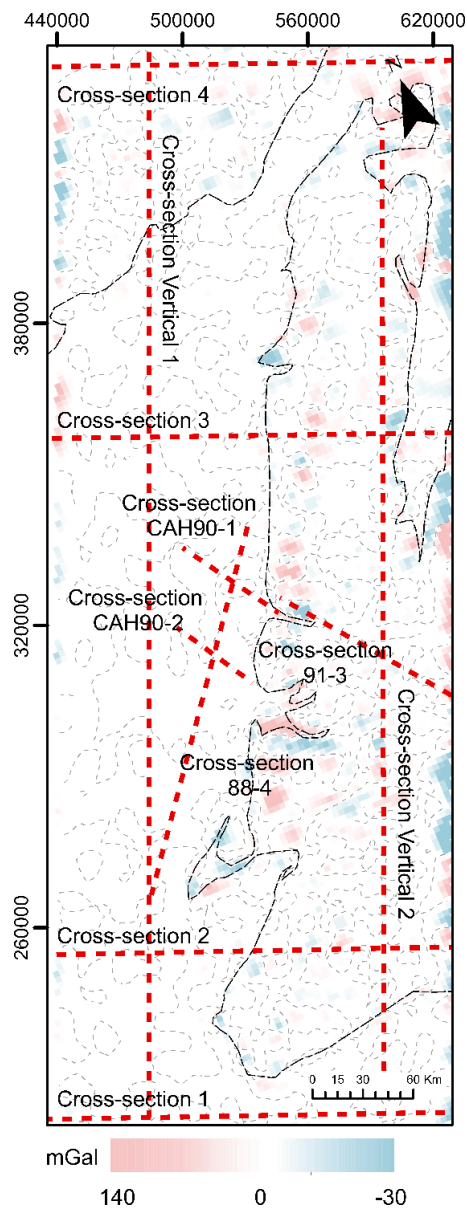


Figure 4. 11: Residual gravity field of the study area obtained by subtracting the calculated gravity effect of the 3D model from the observed gravity field, with sections in later figures shown by red dashed lines.

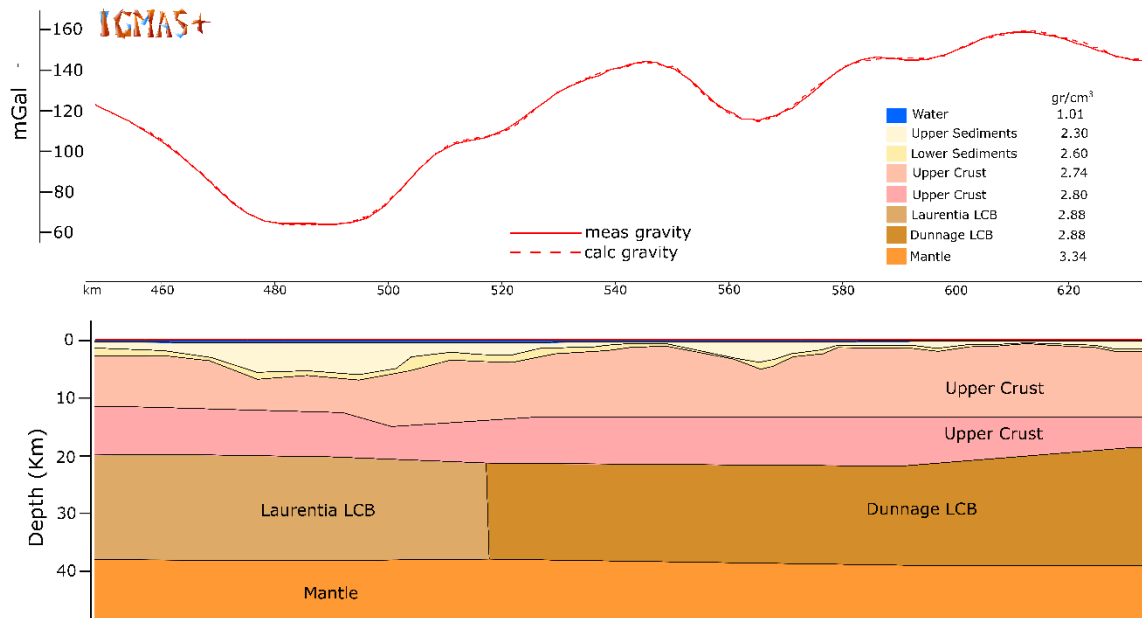


Figure 4. 12: E-W Section 1 at the southern end of the study area. Location in Figure 4.11. (Top) Comparison of the observed gravity and calculated gravity data. (Bottom) Density model for this line. See Figure 4.22 for the contribution in the gravity signal of the sediments in the area.

Sections CAH90-1 and CAH90-2 (Fig. 4.14) are extracted along the seismic lines CAH90-1 (Fig. 4.1) and CAH 90-2, which both contain the Humber Arm Allochthon (HAA). Beneath the seismically imaged HAA, the basement had to be adjusted to better match the observed and calculated gravity. This shifted the model basement by ~ 2 km in comparison with the seismically interpreted basement. The interpreted basement was converted to depth using a 4 km/s standard velocity for sediments that may not be appropriate for the entire sedimentary structure of the area. In general, the HAA is composed of mainly sediments deposited on the continental shelf slope. The HAA and the offshore sediments seem to have the same general 2.4 g/cm³ density.

Section 3 (Fig. 4.15) crosses the northern part of the Humber external zone and White Bay. This section crosses the shelf and foreland basin rocks of the autochthon and the Long Range Massif. Figure 4.15 shows the separation between the LCBs and the separation of the upper crust, although the densities remain the same. The densities for the Grenville LCB and Laurentia LCB were obtained from profiles 88-3, 88-4 and 91-3 (Hall et al., 1998). The densities and structure for

the Long Range Massif and the carbonate successions were based on gravity forward modelling adjustments. Section 3 also shows the high density lower crustal body which was previously inferred from seismic data investigations (Jackson et al., 1998). This body extends along the Humber peninsula and seems to exist beneath the Humber arm region as it was imaged for seismic refraction lines 88/3 and 88/4 (Hall et al., 1998; Jackson et al., 1998).

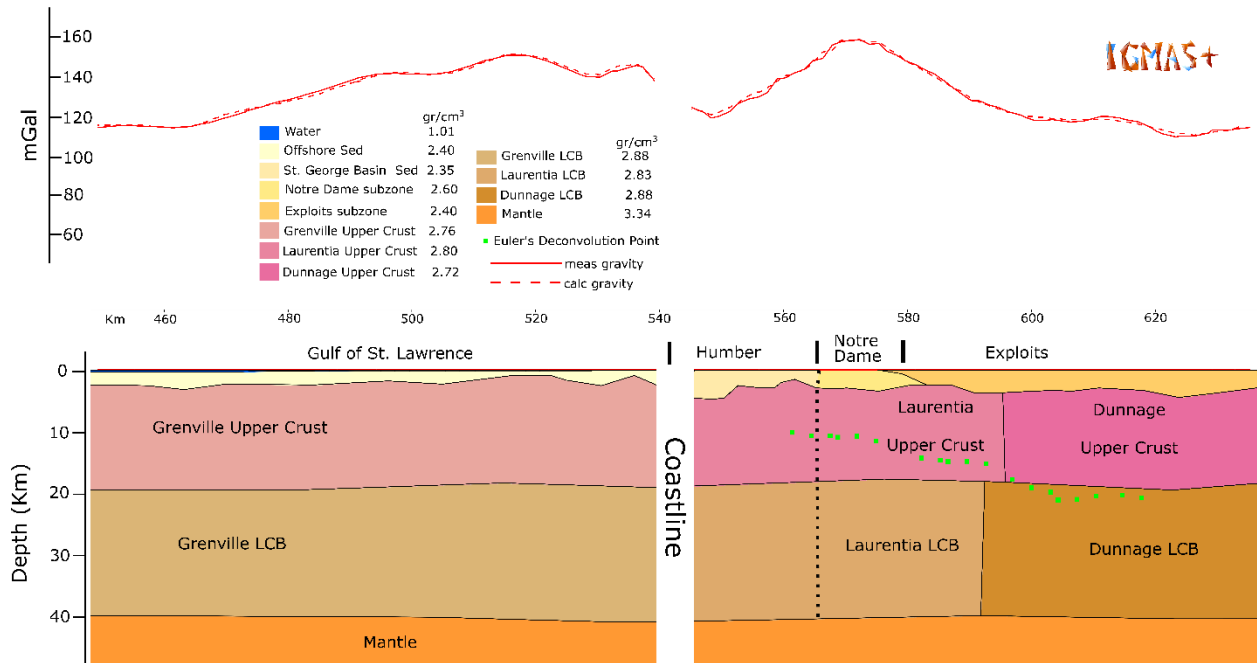


Figure 4.13: Section 2. (Top) Comparison of the observed gravity and calculated gravity data. (Bottom) Density model for this line. Green square dots are Euler deconvolution points. Dotted black line represents the position of the strike-slip Cabot fault. Location in Figure 4.11.

Section 4 (Fig. 4.16) is from the northern part of the study area. It crosses the Labrador region and extends into the Atlantic Ocean. The densities obtained from profile 88-3 for the upper and lower crust are still kept for the Grenville Province in this area, for lack of other constraints. North of the study area, Funck et al. (2001) found similar densities for the Grenville Province. The shallowest crust of the Grenville has a higher density than the offshore sediments since igneous rocks are present based on the residual magnetic maps (Fig. 4.4 from Section III, Chapter III).

Profile 88-4 is shown in Figure 4.17. This seismic profile runs parallel to the Humber Arm peninsula and crosses perpendicular to profile 88-3 (Figure 1, chapter I). The Moho depths and the

top of the high density lower crustal body are well constrained and correlate with seismic refraction line 88-4. The dashed line represents a layer that has a slightly higher density than the density chosen for the entire structure based on profile 88-3. However, the sedimentary structure is consistent with both profiles.

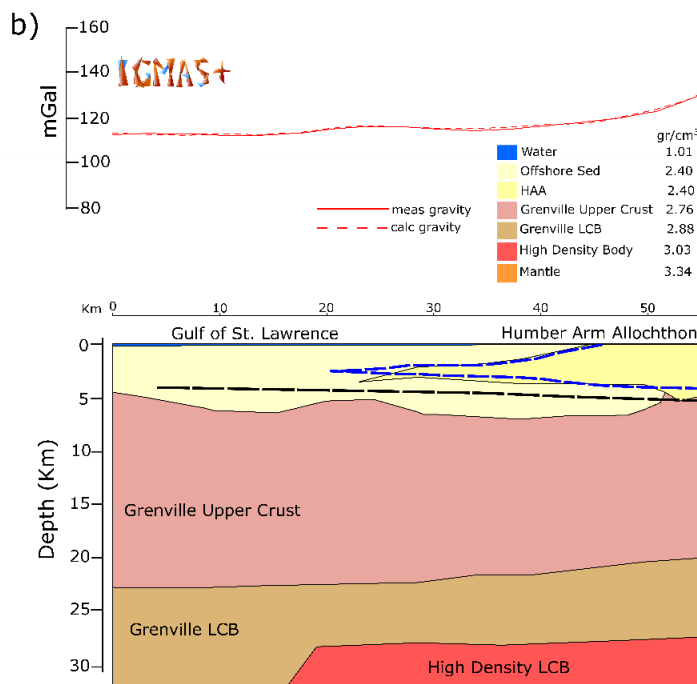
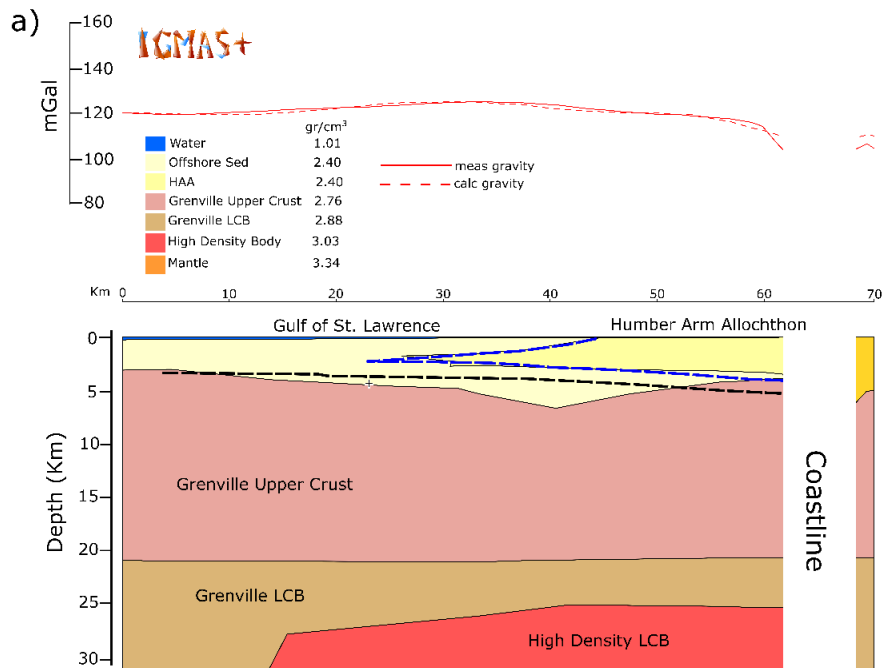


Figure 4. 14: Sections along seismic profiles (a) CAH90-1 and (b) CAH90-2. Black dashed line is the depth to the basement from seismic interpretation. Blue dashed line is the position of the Humber Arm Allochthon from seismic interpretation. Location in Figure 4.11.

The eastern part of seismic profile 91-3 was also used to constrain the onshore structure for Western Newfoundland, as shown in Figure 4.18. The Moho does not exactly follow the Moho constrained by the seismic profile (Fig. 4.18). However, estimated errors for the depth to the top of the interface in profile 91-3 correspond to about 10% of the layer boundary depth. In that sense, the ~3 km misfit between the modelled Moho and the constrained Moho is still within an acceptable difference. Differences between the calculated and observed gravity for the HAA, which are caused by the ophiolite complexes, are smaller than the section separation and were not modelled.

The western part of profile 91-3 shows a misfit of ~ 20 mGal between the calculated and observed gravity. This difference suggests that the density of the Humber Arm Allochthon (2.40 g/cm³) is higher than needed.

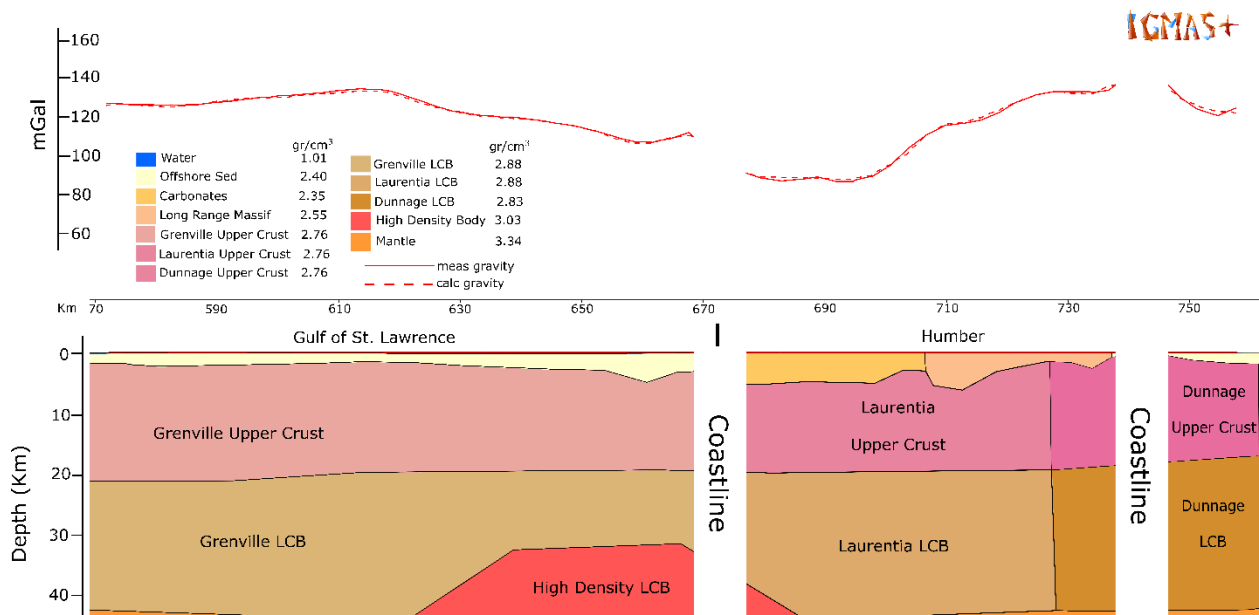


Figure 4. 15: E-W section 3 near the centre of the study area. (Top) Comparison of the observed gravity and calculated gravity data. (Bottom) Density model for this line. Location in Figure 4.11.

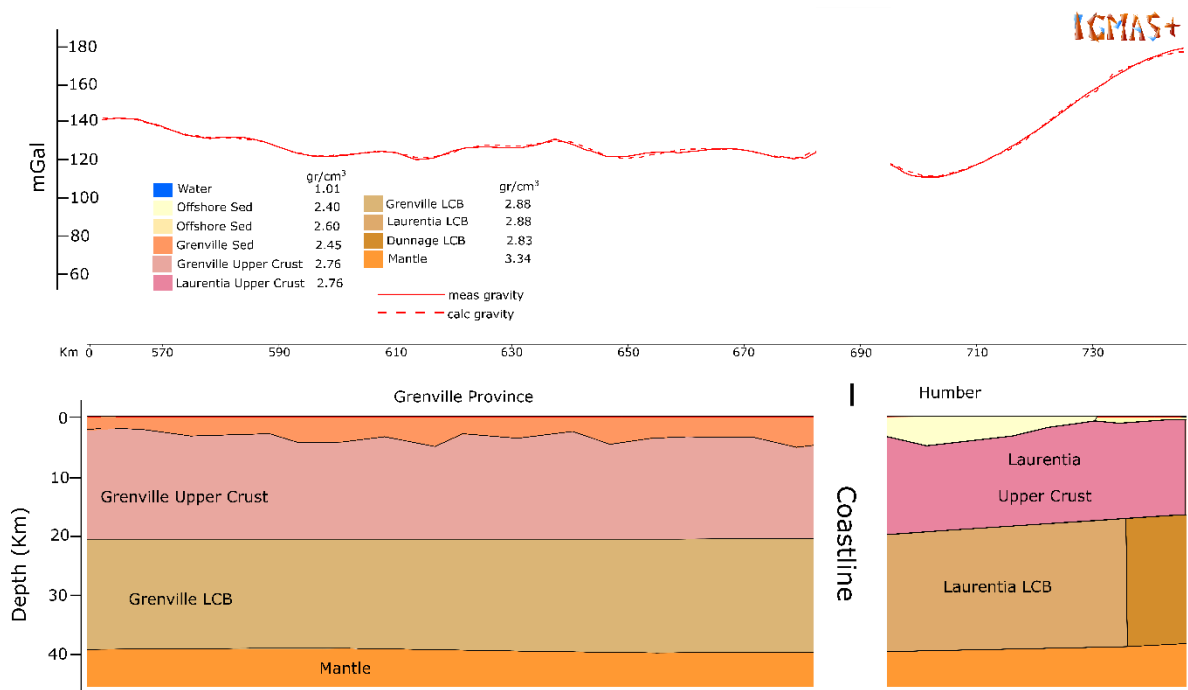


Figure 4. 16: E-W section 4 at the northern end of the study area. (Top) Comparison of the observed gravity and calculated gravity data. (Bottom) Density model for this line. Location in Figure 4.11.

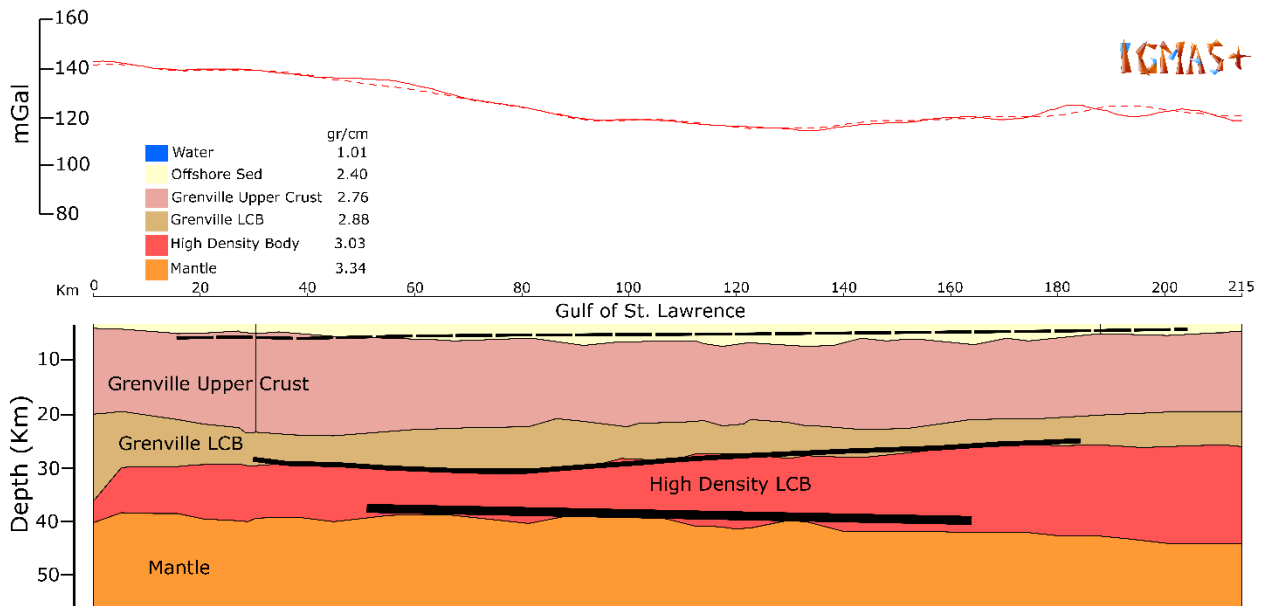


Figure 4. 17: Section 88-4, parallel to the coastline. (Top) Comparison of the observed gravity and calculated gravity data. (Bottom) Density model for this line. Solid black lines are reflectors. Base of the crust (Moho) identified by black thicker lines. Dashed black lines are model boundaries. Location in Figure 4.11.

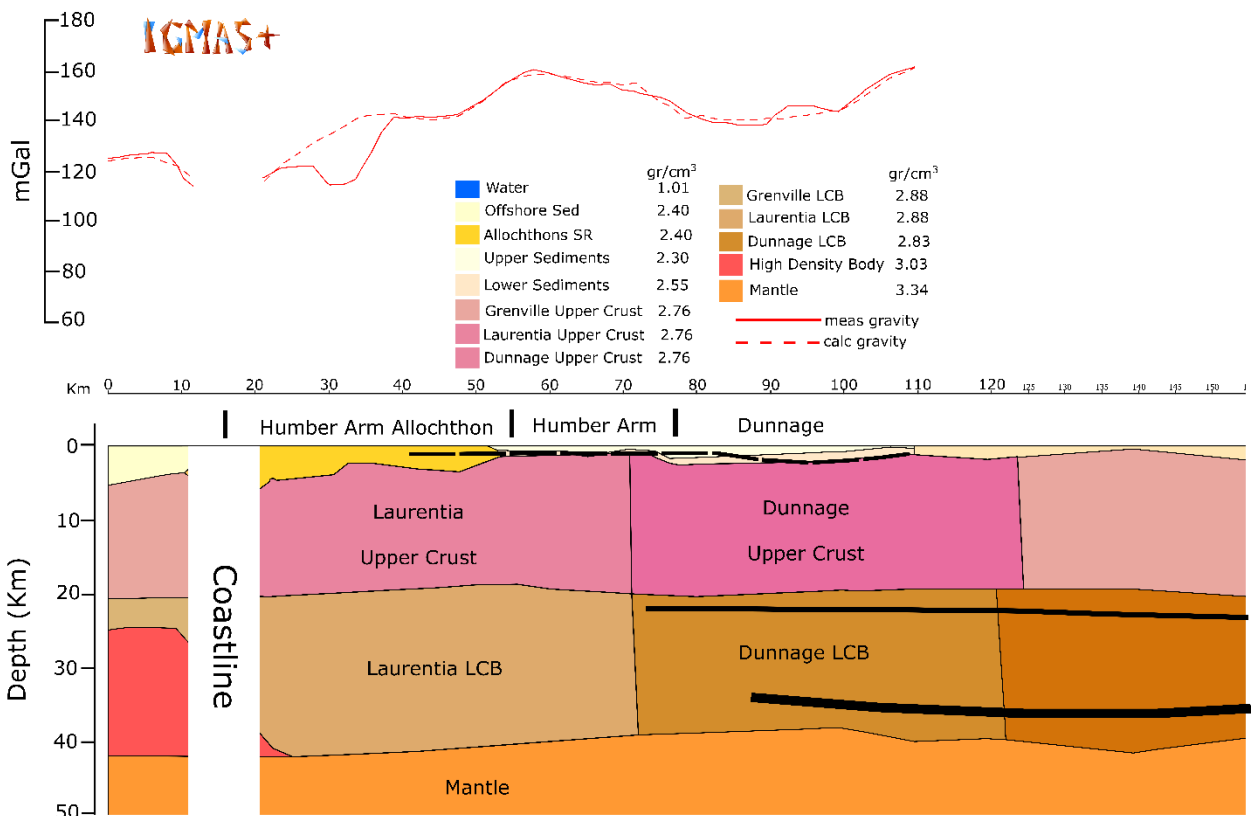


Figure 4.18: Results for profile 91-3. (Top) Comparison of the observed gravity and calculated gravity data. (Bottom) Density model for this line. Thick solid black lines are reflectors. Dashed black lines are model boundaries. Base of the crust (Moho) identified by black thicker lines. Dashed black lines are model boundaries. Location in Figure 4.11

Finally, regional north-south sections that cross the entire study area are shown in Figure 4.19 and Figure 4.20. As shown in these figures, the Moho depths do not vary significantly. Figure 19 shows a large accumulation of sediments toward the middle of the study area in the Gulf of St. Lawrence. The high density body extends for almost 150 km north-south. At the southern end of the study area, the upper crust exhibits more differentiated densities, in agreement with profile 91-4 (see location of profile 91-4 in Figure 1, chapter I).

Despite differences of up to 5 mGal between the observed and calculated gravity shown in Figure 4.20, the model follows the regional gravity trend. This means that the 3D gravity forward model satisfies the regional tectonic structures of the study area.

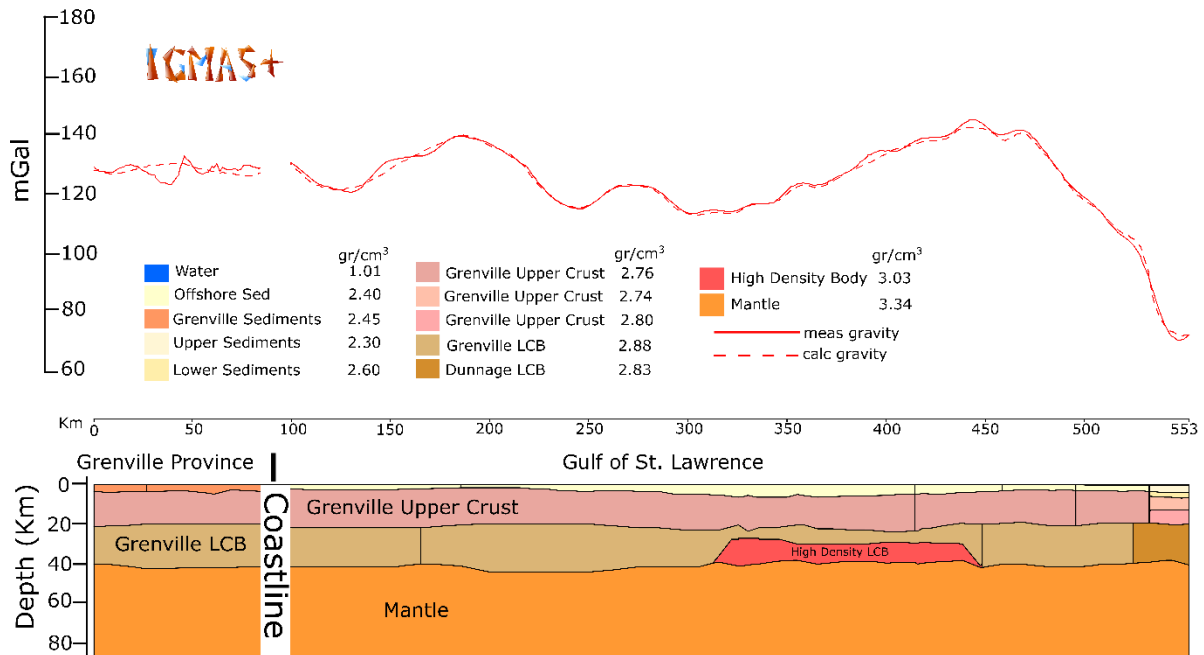


Figure 4. 19: Vertical section 1 from N to S across the full study area. (Top) Comparison of the observed gravity and calculated gravity data. (Bottom) Density model for this line. Location in Figure 4.11

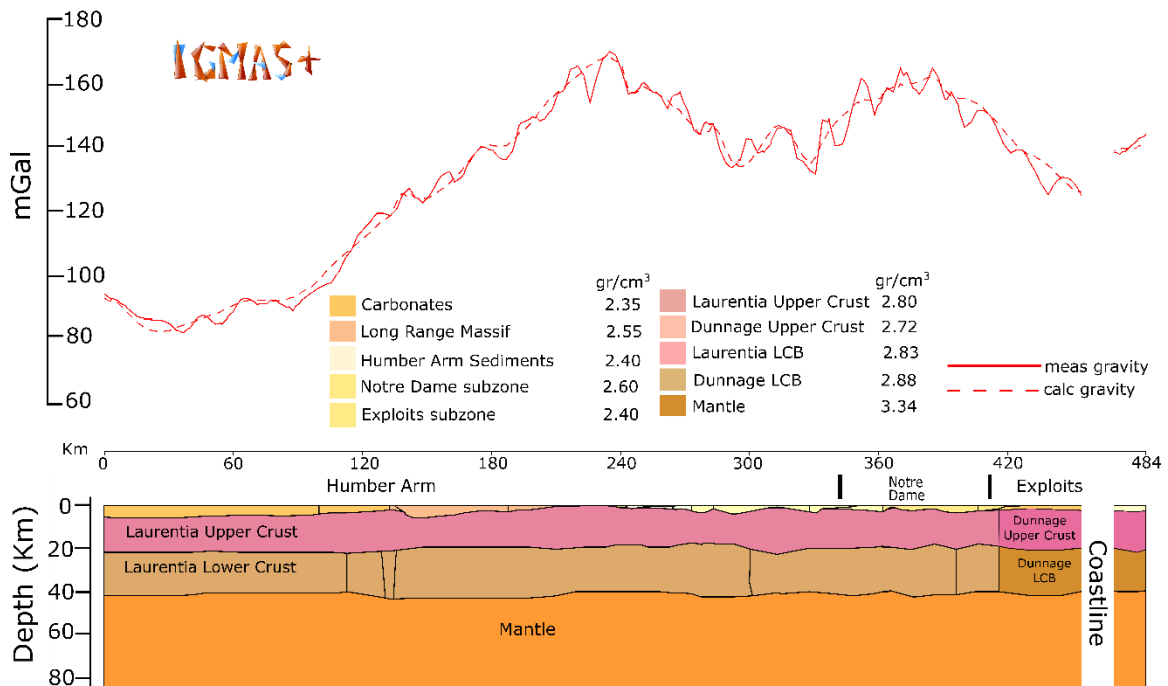


Figure 4. 20: Vertical section 2 from N to S across the full study area. (Top) Comparison of the observed gravity and calculated gravity data. (Bottom) Density model for this line. Location in Figure 4.11

4.2.3 Moho and Depth to the Basement Maps

Figure 4.21 shows the Moho depths and depth to the basement obtained from the 3D final model (Fig. 4.10). The Moho varies in depth (Fig. 4.21b) from approximately 38 km to 45 km. The parts of the model for which the Moho was constrained by the seismic profiles did not require much modification of the model geometry to obtain a good fit between the modelled and observed gravity fields. The depths shown in Figure 4.20b are in agreement with a stable and thick continental crust as expected for Western Newfoundland. The Moho is shallower in the south of the study area and increases in depth towards the Humber Arm until it becomes more flat in the northern study area. The presence of the high density lower crustal body seems to have an effect on the Moho depth since its presence coincides with the Moho depth change towards the center of the study area. Although, the sediments in the southern part of the study area thicken, the Moho depth does not deepen in this area.

The depth to the basement variations in the study area correlate with the shape of the gravity anomaly, suggesting that they have a significant impact on the gravity field of the area. The depth to the basement is deeper (> 4 km) in the western part of the Humber Arm and its continuation offshore into the Anticosti Basin, which follows seismic refraction line 88-3. In the southern part of the study area, the depth to the basement deepens (> 5 km) due to the presence of the Magdalen Basin depocenter. Similarly, in the St. George Sub-basin, the depth to the basement increases. The depth to the basement onshore Western Newfoundland is very shallow, with the exception of areas where ophiolite complexes occur at the surface. In the Grenville Province of the Labrador Province, the top of basement is consistently deep. However, there are small variations that may be caused by igneous rocks inferred from the residual magnetic map.

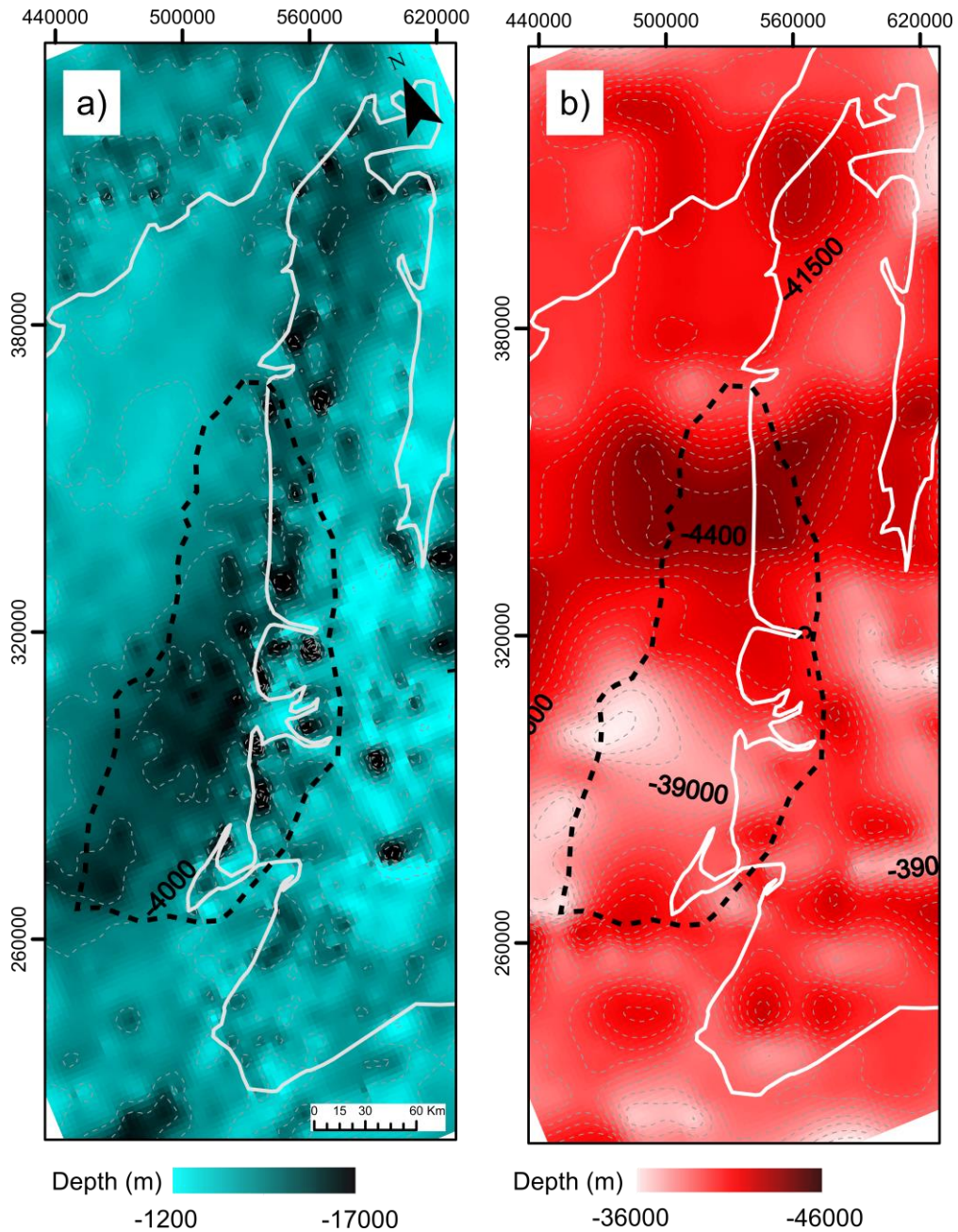


Figure 4. 21: a) Depth to the basement and b) Moho depth map for Western Newfoundland. Dash black lines represent the modelled position of the high density lower crustal body.

4.4.4 High density lower crustal body

The high density lower crustal body (Fig. 4.19) was first imaged along seismic lines 88-3 and 88-4 by Michel et al. (1992) (See figure I, chapter I for location). However, the offshore extent of this body could not be estimated due to the lack of deep seismic profiles in the Gulf of St.

Lawrence. Hall et al. (1998) proposed that this lower crustal body extended along seismic profile 88-4. Based on this earlier work, the high density lower crustal body was included in the 3D model. The density chosen was 3.03 g/cm^3 based on the cited seismic profiles. The body appears at the Port-au Port Peninsula and runs parallel to the west coast. It extends $\sim 200 \text{ km}$ N-S and $\sim 80 \text{ km}$ E-W. However, to the north, it narrows. This body extends into parts of the Humber Arm surface zone.

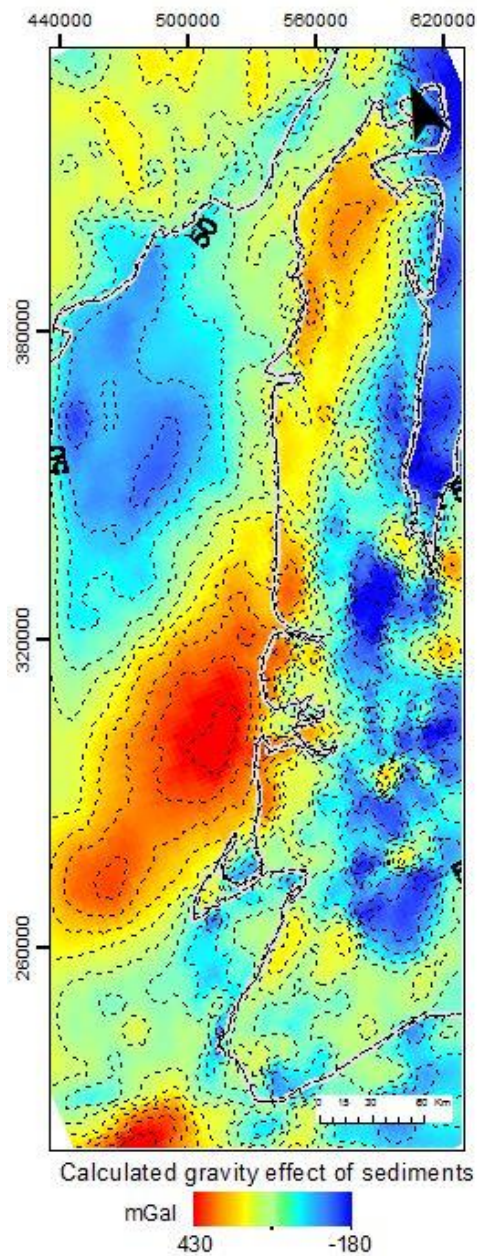


Figure 4. 22: Calculated gravity effect of sediments. Dashed black lines correspond to contours each 50 mGal.

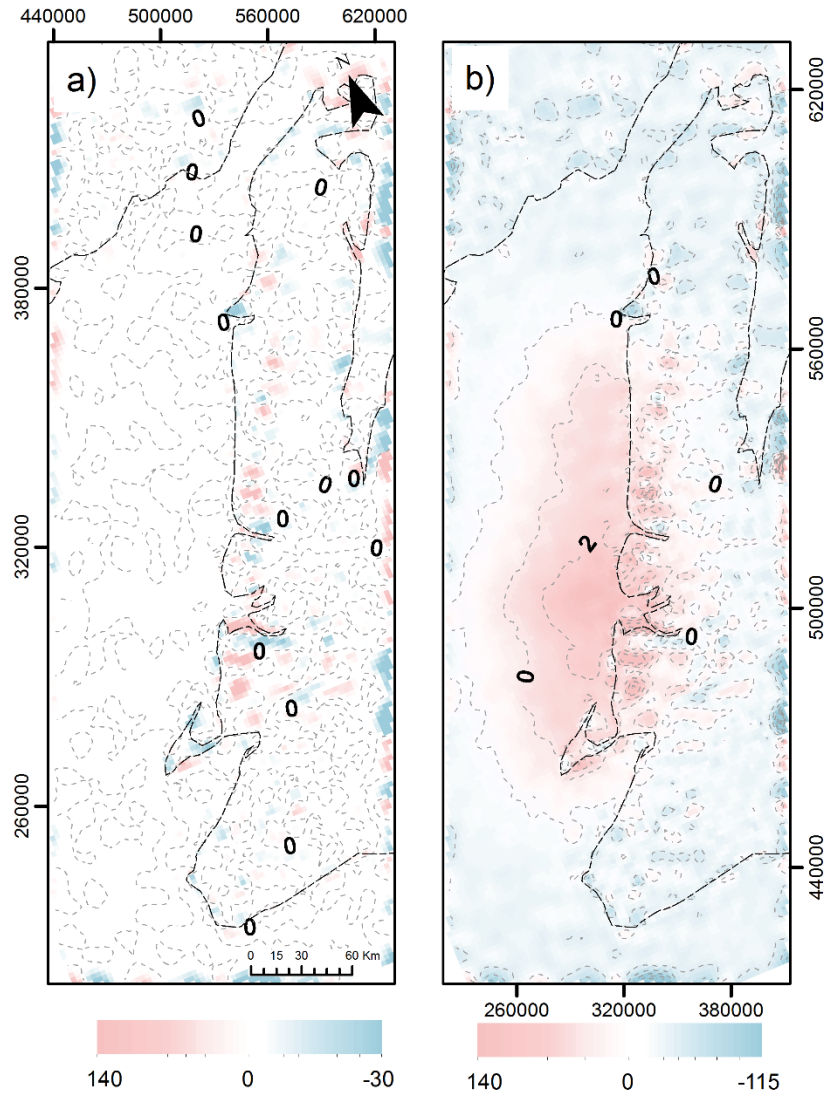


Figure 4. 23: a) Residual gravity field of the study area obtained by subtracting the calculated gravity effect of the 3D model from the observed gravity field for the final model with the presence of the High density body and b) Residual gravity field for the same model with a lower crust without the High density body, correlation factor = 0.89

An alternative model with a continuous lower crust in which the high density body does not exist was also tested. The density distribution was assumed to be equal to the densities from the base model. The results from the alternative model (Fig. 4.23b) show that the contribution of the high density lower crustal body does have a significant effect on the gravity signal in the area. In fact, the correlation factor between the observed gravity and calculated gravity decreased from 0.97 to 0.89. Therefore, the high density lower crustal body is included in the final model.

4.3 Summary

This chapter introduced the 3D gravity forward modelling results. The first section described the results obtained for the seismic interpretation which constrained the depth to the basement and geometry of the Humber Arm Allochthon. This was followed by an explanation and description of the required steps and input constraints to reach a correlation factor of 0.97 between the observed and calculated gravity. The final model (model 7) was then analyzed by describing ten 2D sections. 4 sections run E-W while 2 sections run N-S across the full study area. The remaining 4 sections were extracted along different seismic profiles.

Having described the final model geometry and densities, the Moho depths and depth to the basement were discussed. The Moho varies from approximately 38 km to 45 km while the depth to the basement seems more variable. The sediments thicken in the Gulf of St. Lawrence, especially in the southern part of the study area.

Finally, the contribution from the high density lower crustal body to the full gravity signal was tested with an alternative model with a continuous lower crust in which the high density body does not exist. The results show that the high density lower crustal body does indeed have a significant effect on the gravity signal in the area.

The following chapter, chapter VI, introduces the results from the 3D gravity inversion using the Grav3D algorithm and an algorithm created by a Post-doctoral fellow, Dr. Meixia Geng, in the Earth Sciences Department of Memorial University.

Chapter 5: Gravity Inversion

In this chapter, the inversion of the gravity data is presented. First, the 3D gravity inversion results using the GRAV3D algorithm are discussed. The 3D gravity inversion is presented as evolving sections. Finally, the gravity inversion results constructed from an inversion algorithm developed in the Department of Earth Sciences of Memorial University are compared with the gravity forward model and the GRAV3D results.

5.1 3D Gravity Inversion

All gravity inversions were performed using the combined Free Air anomaly offshore and Bouguer anomaly on land dataset. The first 3D gravity inversion is obtained by using the mesh created automatically by the GRAV3D program with no other constraints. The input parameters for the mesh are the width of the cells, set to 5 km, and the height of each cell, which is set to 600 m. As shown in Figure 5.1, the results obtained from this first inversion approach are not geologically interpretable, despite fitting the observed gravity data (Fig 5.2). The depth of the auto-generated mesh is too deep and does not correspond with the focus of this research. For more interpretable results, the depth of the mesh is restricted to 60 km (Fig. 5.3a).

Upon creating a satisfactory mesh, one default parameter is changed each time that a 3D gravity inversion is performed. The second gravity inversion takes into account the bathymetry of the study area (Fig. 5.3b). The bathymetry and a depth weighting function are included in the third inversion (Fig. 5.3c). The density contrast bounds are set to -2 and 0.6 g/cm³ relative to a crustal density of 2.85 g/cm³. The lower negative density bound is related to the most negative contrast related to the water layer which usually has a density of 1.03 g/cm³. The higher positive density bound is related to the mantle layer which usually has a density range of 3.1-3.5 g/cm³. These density bounds are introduced into a fourth model (Fig. 5.3d) that also includes the previously mentioned parameters.

For inversions five to seven (Fig. 5.4), the length scales or smoothness (L_x , L_y and L_z) are modified to highlight geological structures in a preferred axis direction. Specifying greater values

for a certain length scale produces smoother models in that direction. The x-length scale is increased from 1 to 2 for the fifth inversion (Fig. 5.4a) while the y-length scale is increased by the same amount for the sixth inversion (Fig. 5.4b). Finally, the seventh inversion includes both increased x and y length scales and all parameters previously discussed (Fig. 5.4c).

Table 5. 1: Summary of 3D gravity inversion parameters

Inversion	Default Mesh	Modified Mesh	Bathymetry	Depth weighting function	Density contrast bounds	Length scales	Reference model	Probabilistic approach
1	x							
2		x	x					
3		x	x	x				
4		x	x	x	x			
5		x	x	x	x	x		
6		x	x	x	x	x		
7		x	x	x	x	x		
8		x					x	
9		x	x				x	
10		x	x	x		x	x	
11		x	x	x			x	
12		x	x	x		x	x	
13		x	x	x		x	x	
14		x	x	x				x

The first seven 3D gravity inversions (Table 5.1) do not include the final 3D forward model discussed in chapter IV. This forward model is used as a reference model to constrain the 3D gravity inversion from the eighth to eleventh inversions (Table 5.1). The reference model is constructed using the Moho depths and depths to the basement from the final forward modelled density model. It also included the top of the high density lower crustal body structure. The density contrasts are calculated relative to the densities assigned for the final 3D forward model.

The eighth gravity inversion is performed using only the reference model and the default parameters (Fig. 5.4d). The ninth gravity inversion includes the bathymetry (Fig. 5.5a) while the tenth gravity inversion includes a modification in the length scales. A depth weighting function, and the y-length scale is increased to emphasize the along-margin structure of the high density

lower crustal body (Fig. 5.5b). The eleventh inversion (Fig. 5.5c) uses all of the same parameters but the depth weighting function's exponent is changed from 3 to 2.

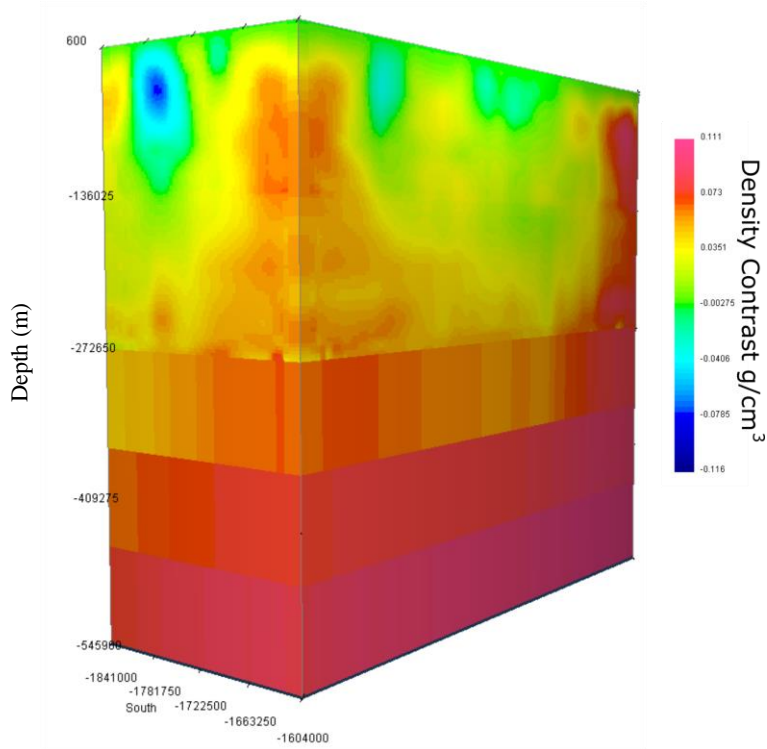


Figure 5. 1: First inversion using the mesh auto-generated by GRAV3D.

Table 5. 2: Summary of reference density contrast bounds in g/cm^3

Inversion	Water	Sediments	Crust	High density body	Moho
8-11	-0.05, 0.05	-0.2, 0.2	-0.2, 0.2	-0.15, 0.15	-0.2, 0.3
12	-0.05, 0.05	-0.2, 0.2	-0.4, 0.3	-0.1, 0.1	-0.01,0.3
13	0.05, 0.05	-0.4, 0.4	-0.3,0.3	-0.1, 0.1	-0.01,0.3

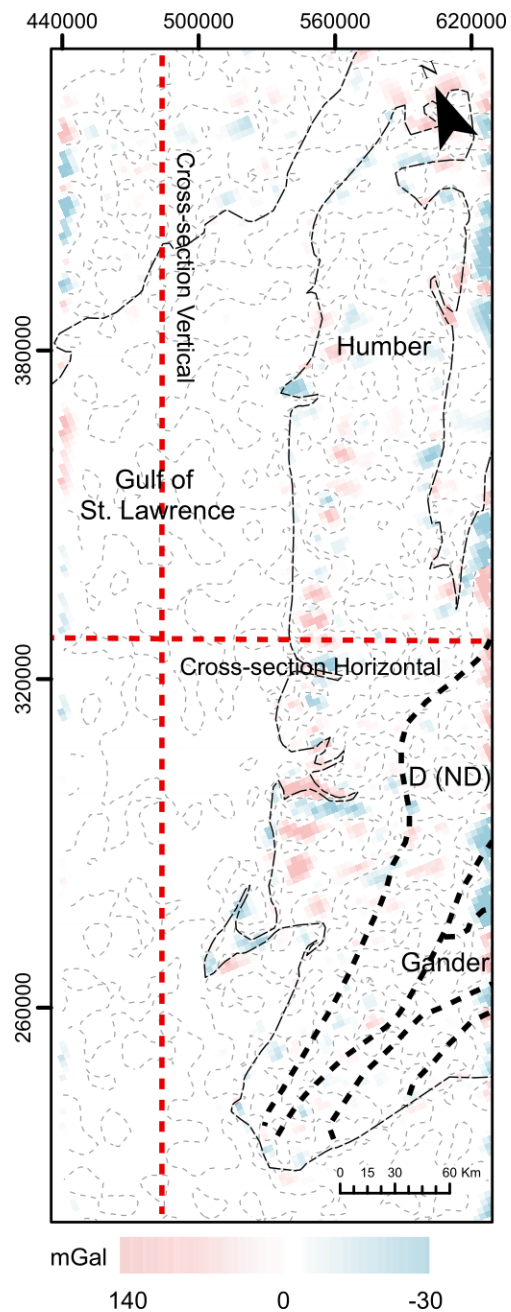


Figure 5. 2: Residual gravity field of the study area obtained by subtracting the calculated gravity effect of the 3D model from the observed gravity field, with sections in later figures shown by red dashed lines.

Inversions twelve and thirteen (Fig. 5.6 and 5.5d) use the previous parameters but the reference density model bounds for the sediments and crust are slightly modified (See Table 5.2)

Figures 5.3, 5.4, 5.5, and 5.6 show the same section through all of the 3D gravity inversions, changing different parameters for each inversion. Figures 5.3 and 5.4 seem not to vary

significantly. However, the biggest density contrast, which is thought to be the Moho discontinuity, gets shallower as the E-W and N-S directions are smoothed.

From Figures 5.3 and 5.6, the inversion results seem not to vary when the reference model is added. For Figure 5.4d, adding the reference model does not significantly improve the results. When adding a depth weighting function (Fig. 5.5c), the resolution of the inversion results decrease, and they are therefore unclear in comparison with the previous inversion results

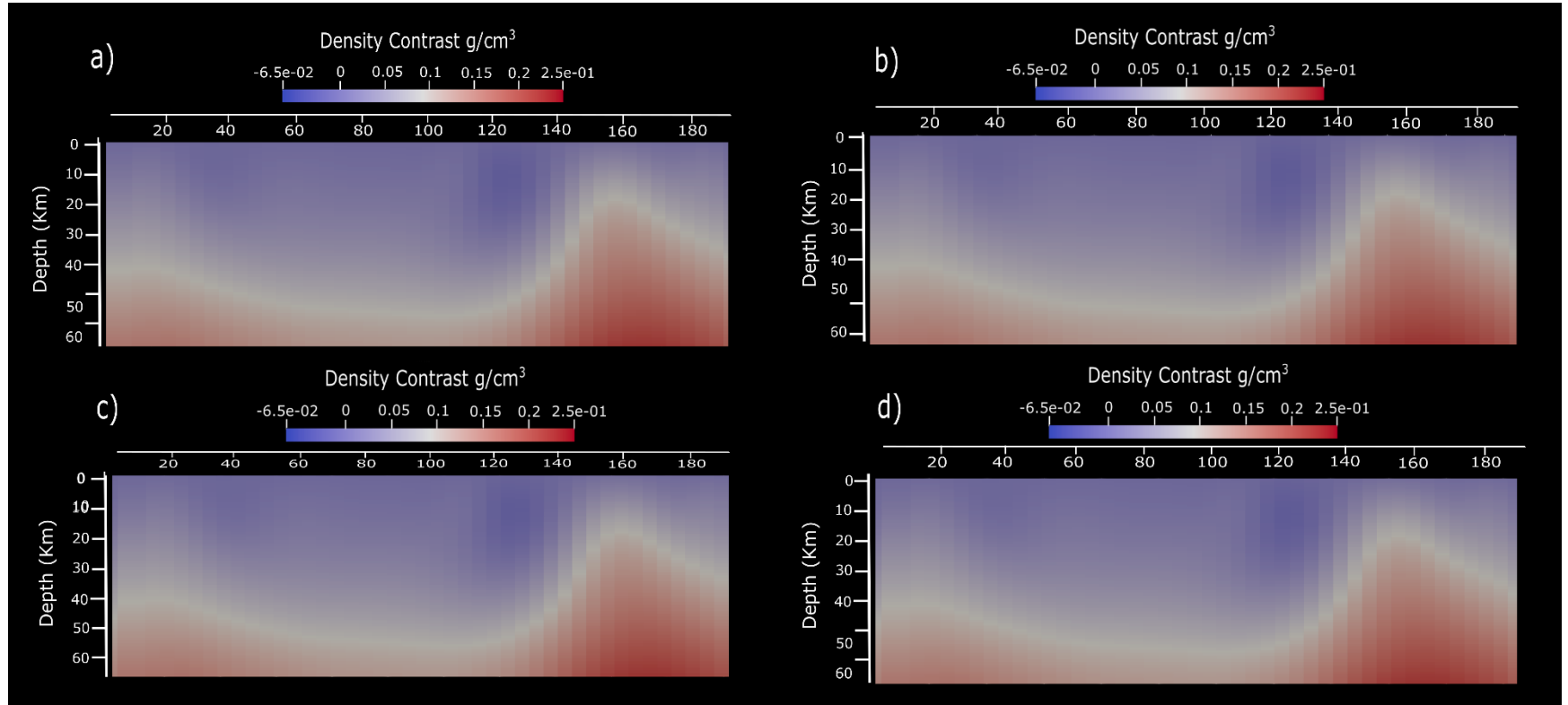


Figure 5. 3: Evolution of 2D W-E sections for the different gravity inversion setups. a) First result with proper mesh and default parameters, b) second inversion results with bathymetry of the study area added, c) third inversion results with previous parameters and a depth weighting function, d) fourth inversion results with previous parameters and density contrast bounds. See Figure 5.2 for location.

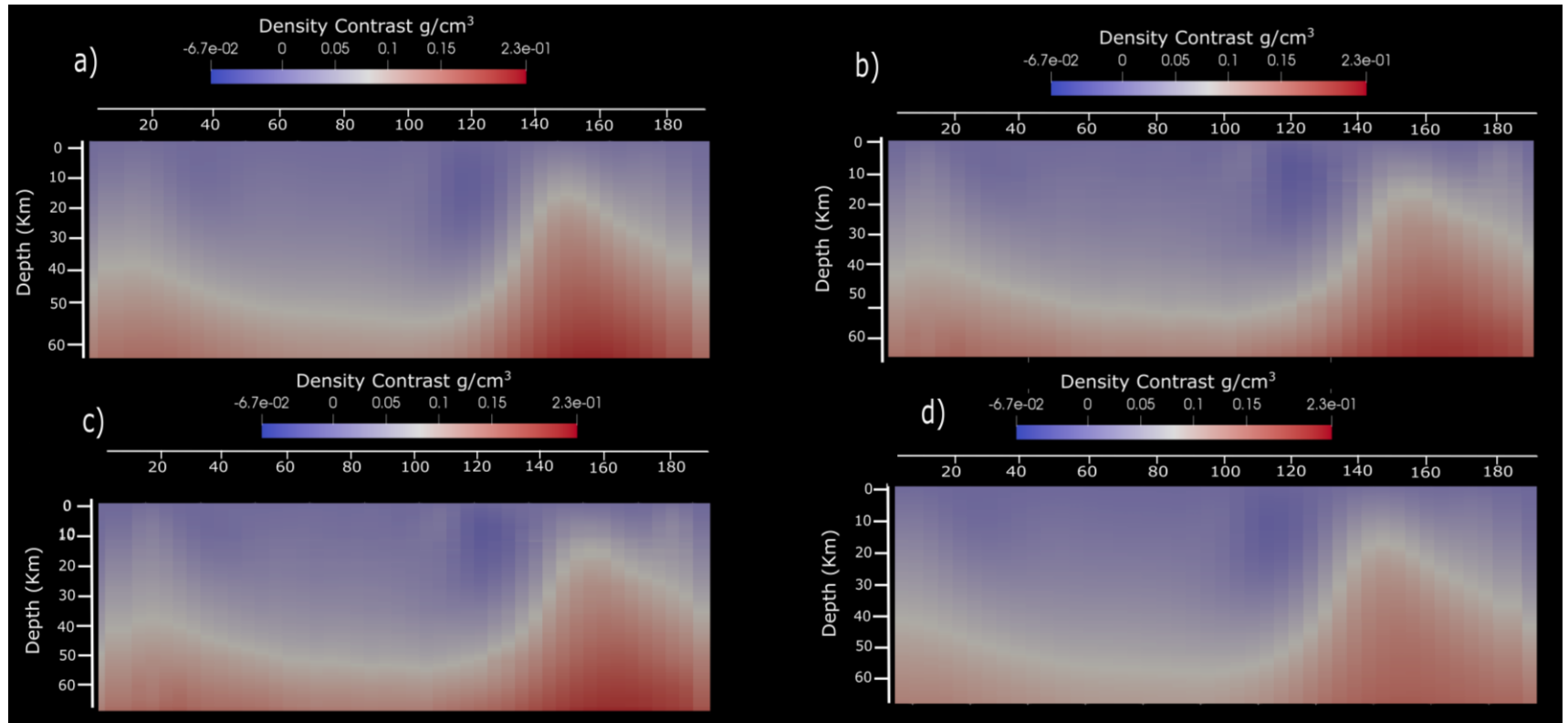


Figure 5. 4: Evolution of 2D E-W sections for the gravity inversion setups. a) inversion results with modified x length scale, b) inversion results with modified y length scale, c) inversion results with modified x and y length scales, d) inversion results with default parameters and forward model. See Figure 5.2 for location.

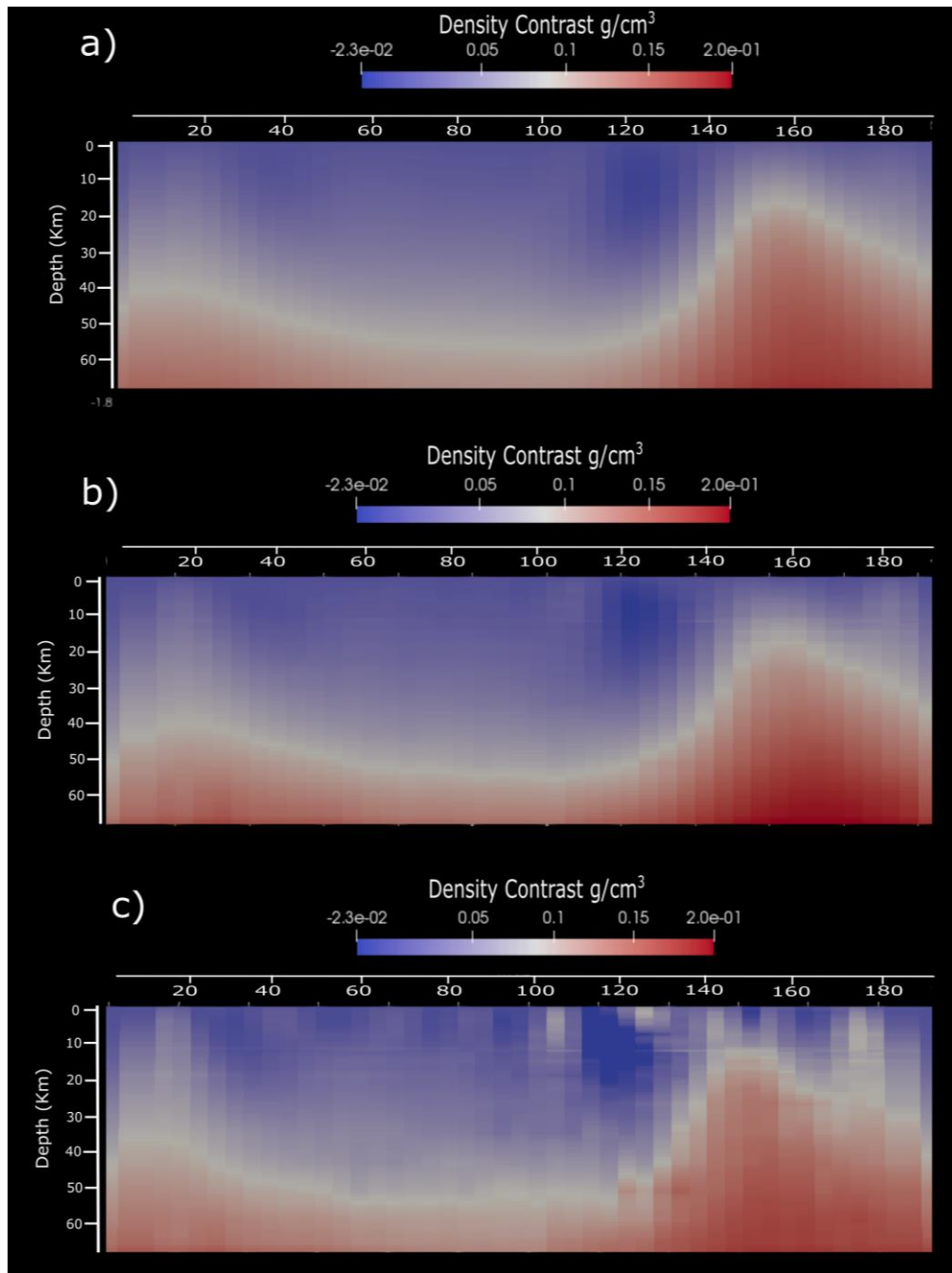


Figure 5. 5: Evolution of 2D W-E-sections for the gravity inversion setups. a) Ninth inversion results with reference model and bathymetry, b) tenth inversion results with depth weighting function and modified y-length scale, c) eleventh inversion results with the depth weighting function's exponent changed. See Figure 5.2 for location.

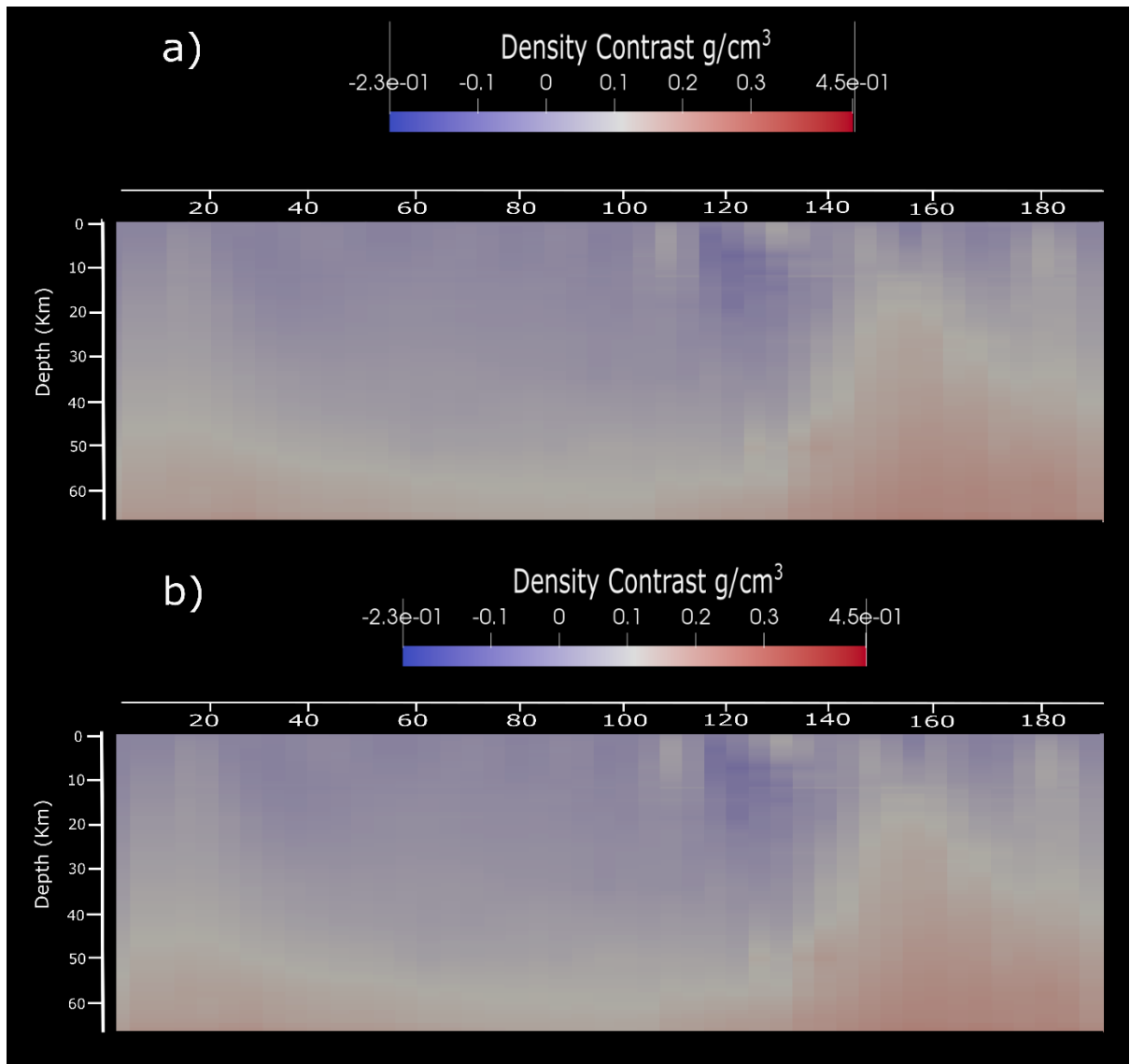


Figure 5. 6: Evolution of 2D W-E sections for the different gravity inversion setups. a) Twelfth inversion results with a change in the reference sediment density, b) thirteenth inversion results with a change in the reference sediment and crustal densities. See Figure 5.2 for location.

Figure 5.7 shows a comparison between the best inversion results with and without the reference model and the final forward gravity model discussed in section IV (Table 5.1). The inversion results without the reference model (Fig. 5.7b) are smoother than the one constrained by the reference model (Fig. 5.7c). However, both inversion results are similar and agree with the geometry of the possible Moho discontinuity. The Moho depths for the forward model are around 40 km while the Moho depths are slightly deeper for both

inversion results. To the south of the study area, the Moho depths from the inversions increase while they remain the same for the gravity forward model

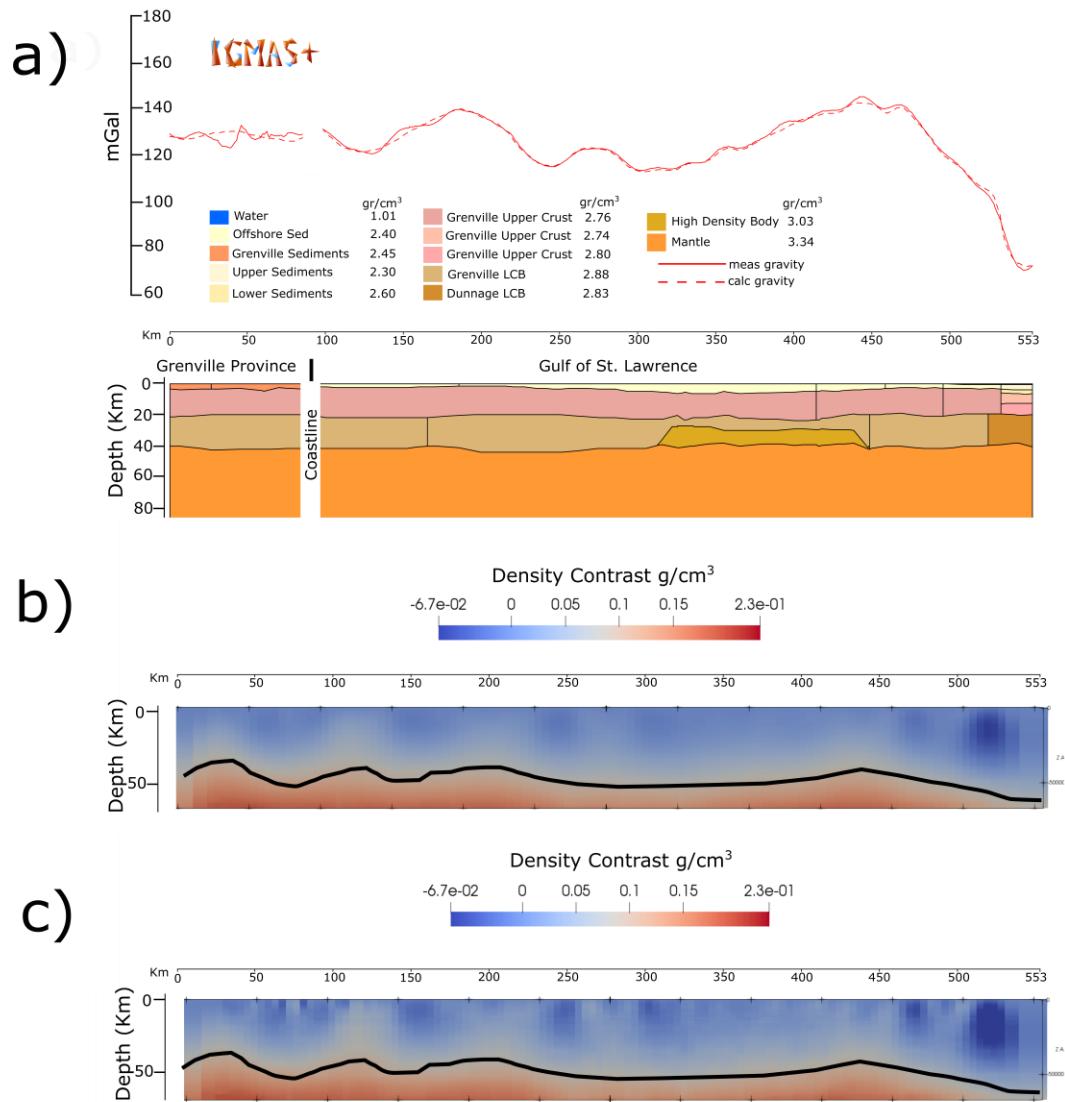


Figure 5. 7: Comparison of a) the N-S gravity forward model section with b) the seventh inversion results and c) the eleventh inversion results. Interpreted Moho identified by black thick lines. Location of these sections is found in Figure 5.2.

A negative density contrast is apparent in the inversion results in the south of the study area. The forward gravity model does not capture such anomalies. This southern area is characterized by thick sediments, which correspond to a strong negative anomaly in the

gravity map (Fig. 3.2, Chapter III). For the forward model, the upper crust in the southern area is divided into both an upper crust and a lower crust that have different density values from those in the north. This crustal density contrast, thought to be due to previously discussed tectonic domains, may have contributed to this strong negative anomaly, while the inversion compensated for this anomaly by altering the Moho depth.

Unfortunately, the inversion results do not show the presence of the high density lower crustal body as it was modelled in the forward model, although the non-uniqueness of the inversion does not preclude its existence.

In order to test the inversion results obtained through GRAV3D, numeric values were compared with a newly developed 3D gravity inversion algorithm, based on the probabilistic method discussed by Geng et al. (2017). For this inversion, only the depth to basement constraint obtained from the 3D gravity forward model is used. As shown in Figure 5.8, the new inversion results (i.e., the fourteenth inversion results) produced a smoother model than the previous inversions. Additionally, inversion fourteen seems to support the presence of a high density contrast towards the middle of the section shown in Figure 5.8c. This anomaly correlates spatially with the high density lower crustal body modelled in the forward model.

Figure 5.9 shows a comparison between the N-S section discussed in chapter IV and the inversion results with the probabilistic method obtained for the same section. As shown in this figure, the inversion results show a strong density contrast and a similar configuration to one where the high density lower crustal body is modelled in the forward model. To the south, there is also a strong density contrast which correlates with the division of the upper crust in the forward model. North of this anomaly, the density contrast is less and apparently corresponds to a typical continental crust with no large density modifications.

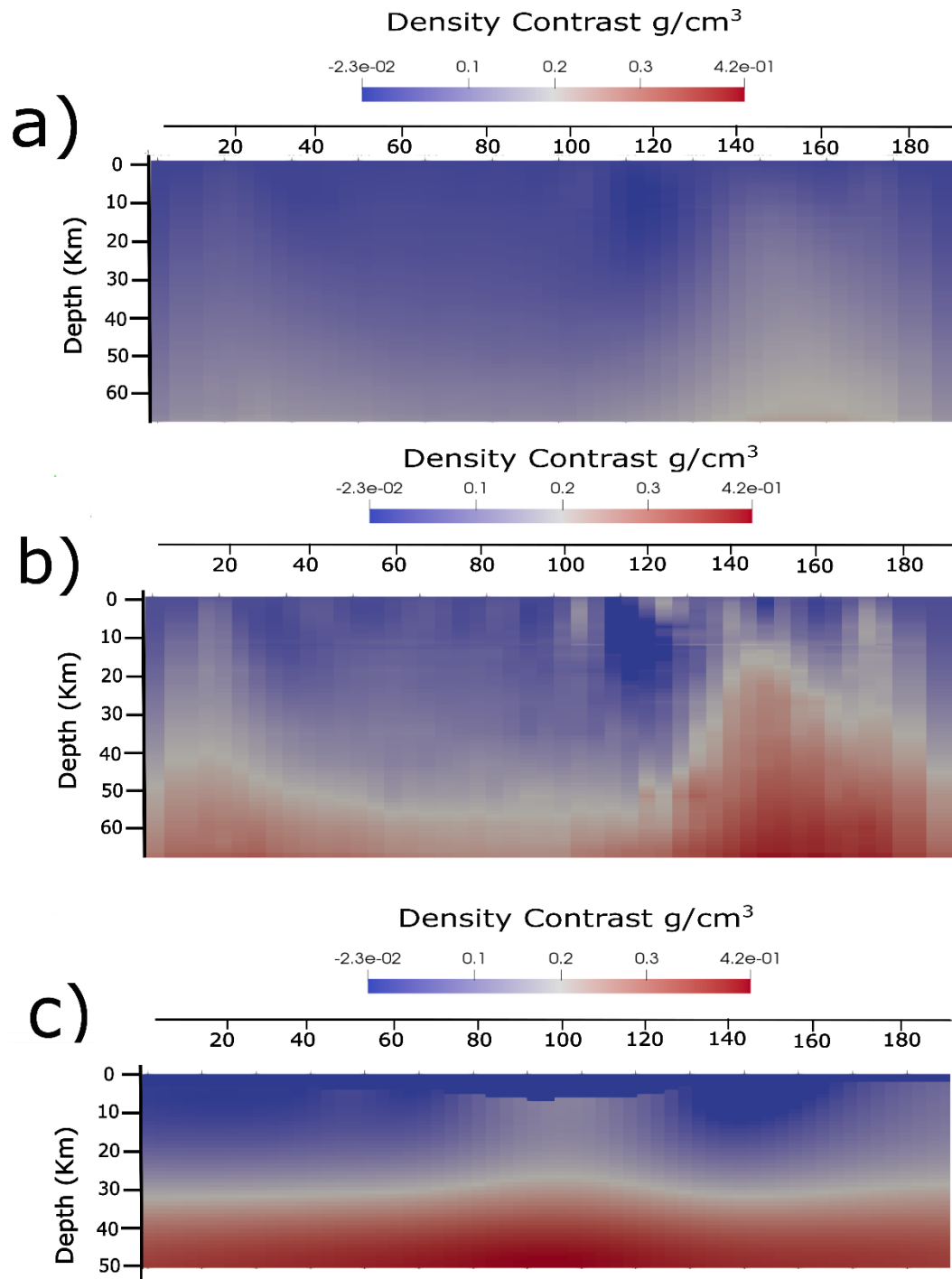


Figure 5. 8: Evolution of 2D W-E sections for the gravity inversion setups. a) Seventh inversion results with modified x and y length scales, b) thirteenth inversion results with a change in the reference sediment and crustal densities, c) fourteenth inversion results from the probabilistic inversion method using only the depth to basement constraints. See Figure 5.2 for location.

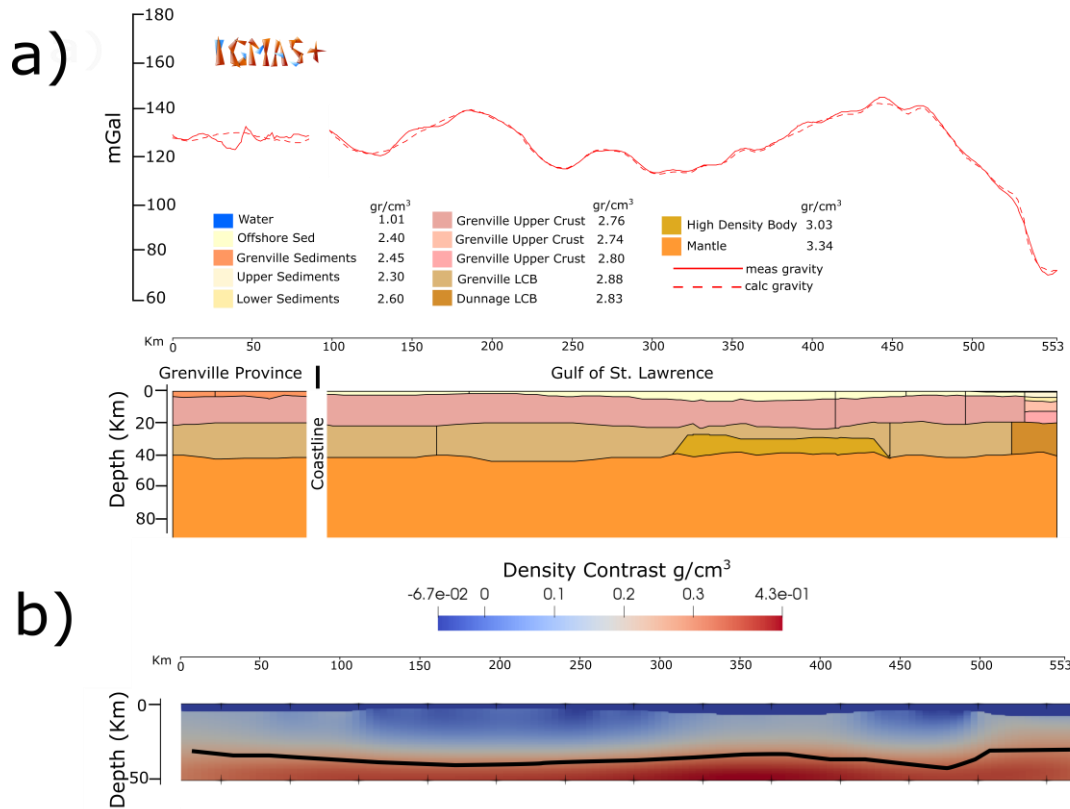


Figure 5. 9: Comparison of a) the N-S gravity forward model section with b) the fourteenth inversion results. Interpreted Moho identified by black thick line. Location of these sections is found in Figure 5.2.

The Moho depths from inversion models seven, thirteen, fourteen, and Moho depths obtained from the gravity forward modelling are plotted in Figure 5.10. The Moho depths obtained from inversions seven and thirteen are very similar. Despite adding a reference model, inversion thirteen did not produce any significant changes. Moho depths from the probabilistic method are smoother than those obtained from GRAV3D.

The Moho depths from the probabilistic method (Fig. 5.10d) show a shallow Moho towards the center of the study area. This pattern may be due to the presence of the high density lower crustal body which masks the true Moho depths. If so, the apparent shallow Moho actually corresponds to the position and the top of the anomalous lower crustal body (> 25 km), in agreement with the seismic refraction profile 88/3 and the final forward model.

For this area, the Moho depths from the gravity forward model and the probabilistic method are deeper than 35 km indicating both results seem to agree with one another. To the south of the study area, the Moho depths are shallower while, for the Grenville Province, the Moho depths do not vary. The major variations in the Moho are found in the Gulf of St. Lawrence adjacent to the Humber Arm, where the Moho reaches its maximum depth. The Moho depths vary between ~35-45 km, with 25 and 45 km below the Dunnage zone and the Humber zone, respectively.

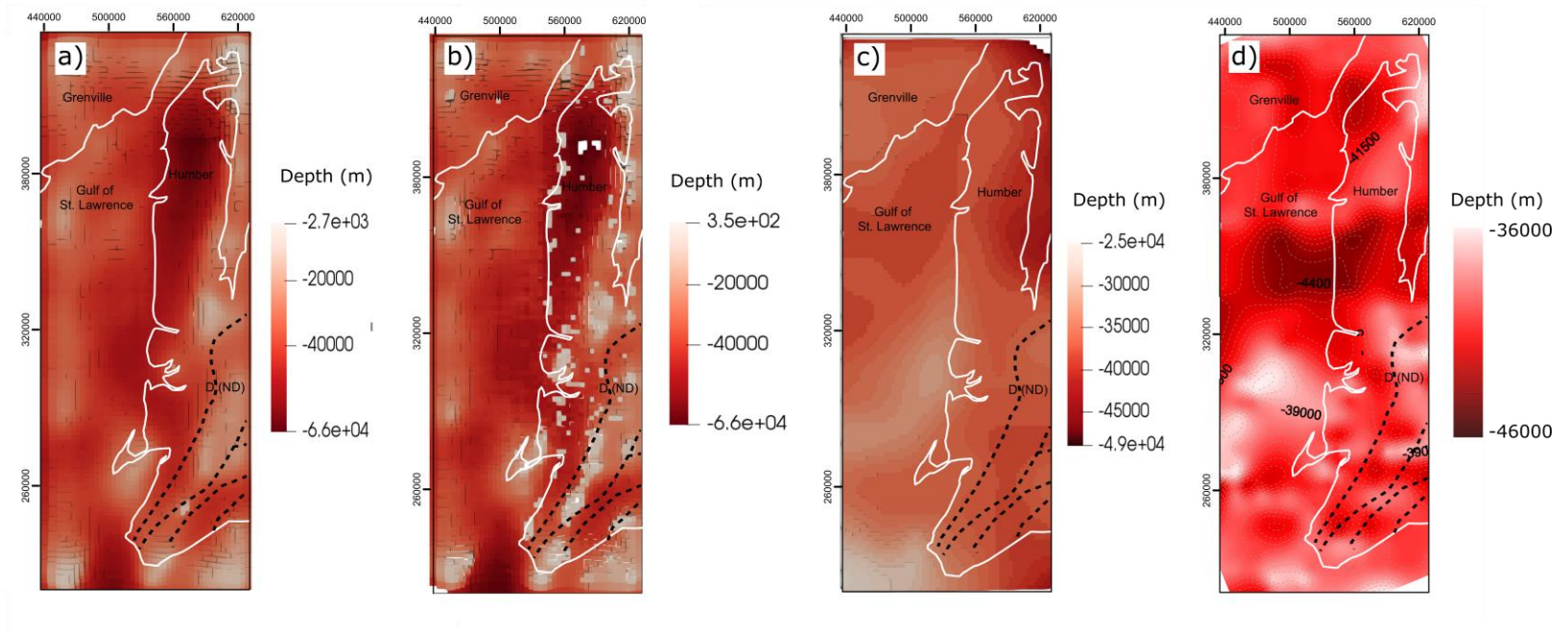


Figure 5. 10: Comparison of Moho depths for Western Newfoundland: a) Seventh inversion results, b) thirteenth inversion results, c) fourteenth inversion results and d) final gravity forward model

5.2 Summary

This chapter introduced the 3D gravity inversion results. First, the results obtained from the GRAV3D software were described. These results were shown as evolving sections with new constraints added each time the inversion was run. The best results from this method were compared to those obtained from the final forward model. Another methodology based on the probabilistic inversion method was also used to test the results obtained previously. The results obtained from this new inversion code developed in the Department of Earth Sciences at Memorial University by Dr. Meixia Geng, resulted in a smoother model which better corresponded to the forward modelling results. The high density lower crustal body is imaged using the new probabilistic method by only adding the bathymetry and depth to the basement as constraints while it was not shown in the GRAV3D results despite adding a reference model. The Moho depths from the inversion results vary from 35-50 km.

Chapter 6: Discussion

This chapter encompasses the discussion and integration of results. The discussion is divided into sub-topics according to scale, from crustal scale to local features. Hence, crustal thickness and crustal structure are first analyzed followed by sedimentary thickness. Ophiolites, faults and the Odd Twins anomaly are the last points to be discussed.

6.1 Crustal Thickness and Structure

Previous geophysical studies in Western Newfoundland have attempted to link the complex surface geology with the deep crustal structure in the area (Hall et al., 1998; Haworth, 1978; Jackson, 2002; Jackson et al., 1998; Marillier et al., 1989; Quinlan et al., 1992). Interpretations of seismic reflection data suggest that the crustal structure mimics the tectonic surface zones and carries lower crustal blocks (LCB) that may have (1), genetic relationships with the surface zones (Marillier et al., 1989) or (2), reflect fabric patterns that have overprinted older lower crust boundaries during the final collision of the terranes (Quinlan et al., 1992).

The 3D gravity forward model developed in this thesis follows the distribution of LCBs of Jackson et al. (1998) and Hall et al. (1998). Here, the lower crust is divided on the basis of densities derived from seismic refraction profiles. The Grenville LCB underlying the Grenville Province has a density of 2.88 g/cm^3 for all of the study area. Jackson et al. (1998) define the edge of the LCB as a transition from low to high Bouguer anomalies outboard of the coastline, and with a southward facing ramp that does not extend beneath the Humber and Dunnage surface terranes. By knitting together Free Air and Bouguer anomaly datasets, this transition could not be modelled. However, in all of the forward modelled 2D gravity sections, this transition is abrupt. Furthermore, the density of the LCB beneath the Humber zone region is also 2.88 g/cm^3 which suggests that Grenville Province rocks continue below the surface exposures of the Humber zone (Hall et al., 1998), making deep crustal boundaries even more difficult to detect. Additionally, the transition has also been linked

to the Appalachian front, as proposed by Haworth (1978). The new satellite Bouguer gravity data WGM2012 (Fig. 6.1) show that for the Humber zone, the low Bouguer gravity anomalies mask the position of this front, which suggests that the position of the Appalachian front may extend further into the Humber zone. In addition, recent upper crustal investigations in the Gulf of St. Lawrence suggest that the Appalachian structural front may be offset with respect to its mapped location (Kuponiyi et al., 2017).

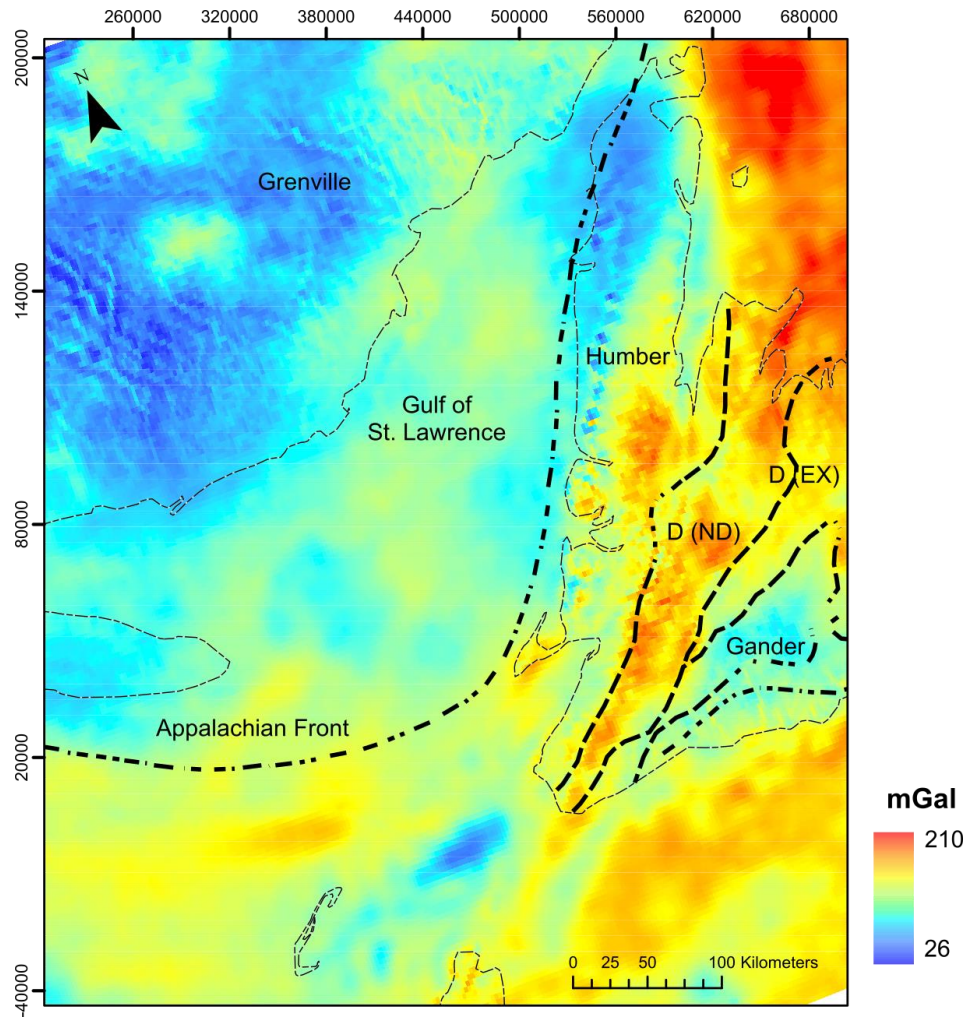


Figure 6. 1: Western Newfoundland Bouguer anomaly map. Map shows surface geological zones of the Appalachian Orogen in Newfoundland (Williams, 1995). Abbreviations: D (Ex), Exploits subzone of the Dunnage zone; D (ND), Notre Dame subzone of the Dunnage zone.

The Laurentia margin crust is a zone of complex structure affected by late Paleozoic strike-slip faulting. Faults mapped at surface in the Humber and Dunnage zones are interpreted as deep-seated, basement faults (Hall et al., 1998; Jackson et al., 1998). The LCB beneath the Humber zone has a density of 2.88 g/cm^3 and the Dunnage LCB varies from 2.83 to 2.88 g/cm^3 in this gravity forward model. Hall et al. (1998) state that the crust below the Humber zone includes high-velocity reflective material that indicates mafic intrusions. This denser body (3.03 g/cm^3) indeed intrudes the lower crust beneath the Humber zone but might also be modelled within the Grenville LCB. Hence, the results here presented suggest that the high density lower crustal body is found beneath both the Grenville and Humber (Laurentia) zones.

In the southern part of the study area (Fig. 4.12), lower crust of the Laurentian margin has a density of 2.88 g/cm^3 . The upper crust is divided into two layers with densities of 2.74 and 2.80 g/cm^3 . This configuration supports seismic refraction profile 91/4 (Hall et al., 1998), in which the crust transitions from 6.0 to 6.9 km/s . In the southern part of onshore Western Newfoundland, the Laurentian margin crust is modelled with a density of 2.80 g/cm^3 for the upper crustal layer and 2.83 g/cm^3 for the lower crust. This lower crust contrasts with the 2.88 g/cm^3 Grenville LCB. Even though there is a density difference for this southern onshore area, the transition between the Grenville LCB and the Laurentian Complex zone is not clear from this 3D density model. On the other hand, the Laurentian margin upper crust in this area (mainly Dunnage zone at surface) has a high density value for the entire layer (2.80 g/cm^3), which agrees with the widespread outcrops of mafic igneous rocks (Hall et al., 1998) and the strong positive Bouguer anomalies. Therefore, these mafic igneous rocks seem to extend into the upper crustal layer. The upper crust in the Grenville zone has a density of 2.76 g/cm^3 which agrees with the exposed metamorphic rocks of intermediate to high grade (Hall et al., 1998).

The crustal thickness varies between 33 and 43 km (Figure 6.2b). However, this variation is systematic across the study area, such that the crustal thickness for the Gulf of St. Lawrence is around 39 km and it thins (34 km) where the high density lower crustal

body is located and a thick accumulation of sediments is also found (Figure 6.2b). Although the thick low density sediments compensate for the high density lower crustal block, removing the high density lower crustal block would require thinner sediments for the same gravity response. Due to the non-uniqueness, the gravity data cannot differentiate between these two models.

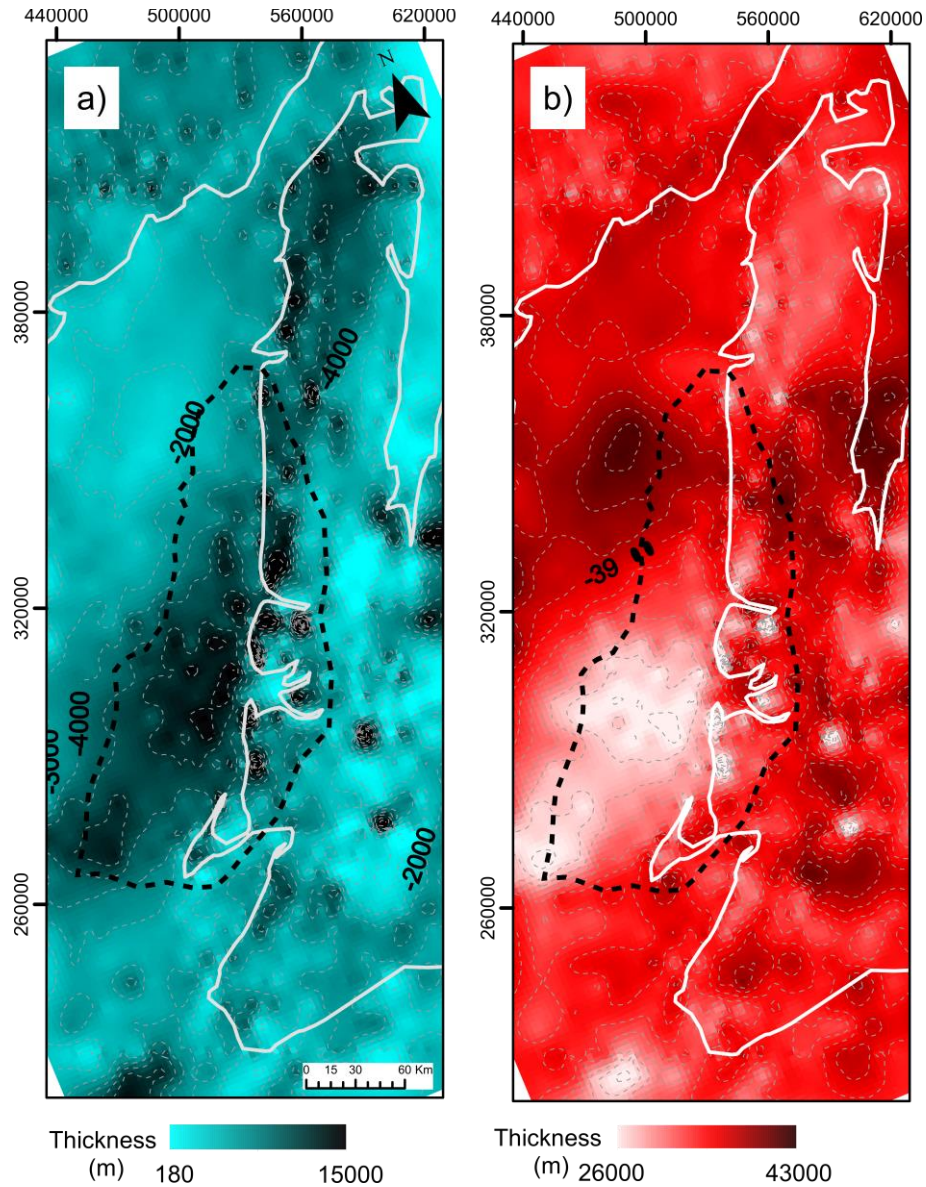


Figure 6. 2: a) Sediment thickness and b) crustal thickness map for Western Newfoundland. Dashed black lines represent the modelled position of the high density lower crustal body.

In the southern Labrador area, the crustal thickness is ~ 39 km (Figure 6.2b) which is expected for a stable continental crust (Baranov and Morelli, 2014). Towards the Long Range Massif, the crustal thickness increases which agrees with the outcrops of Laurentia basement in Western Newfoundland (Waldron, 1994). There are some localized low crustal thickness values in Western Newfoundland (Figure 6.2b), which are artefacts caused by the density selection and the broad regional constraints, and they should not be interpreted.

In the southern part of the study area, the crustal thickness values range between 36-38 km (Figure 6b). Hall et al. (1998), based on seismic profile 91/4, state that the crustal thickness for this area is 39 ± 2 km and that this estimate is similar to that obtained in the Avalon zone (40 km). However, the crustal thickness values presented here characterize the general 3D structure and not only a 2D profile. In that sense, these values seem to agree with the general structure of Western Newfoundland but cannot be used to deduce thickness in the Avalon zone.

6.2 High density lower crustal body

A lower crustal body with a velocity of 7.2 km/s is inferred below the Humber zone from seismic refraction lines 88/3 and 88/4 (Hall et al., 1998; Jackson et al., 1998; Marillier et al., 1991; Michel et al., 1992). The geometry of the body and the density of 3.03 g/cm^3 were derived for those seismic refraction lines (Marillier et al., 1991) and introduced in the 3D gravity forward modelling. The final results show that the high density body is indeed necessary since it has a significant effect on the gravity signal in the area. If the lower crust was uniform and the high density body did not exist, the modelling results would not agree with the seismic findings and the misfit between the observed and calculated gravity data would increase by ~ 9%. The high density assigned to the lower crustal body indicates rock of a mafic or ultramafic composition. In addition, the model is supportive of a feature that runs parallel to the coast of Western Newfoundland. It extends for almost 200 km from north to south, and it is apparently less thick and wider in the south compared to thicker and less wide to the north. Hence, this non-unique 3D gravity model does support the

presence of this body and provides additional geometry information about it. Additionally, the probabilistic method 3D gravity inversion results, only constrained by bathymetry and depth to the basement, also show the presence of a high density contrast that could mean either a shallower mantle or the presence of a lower crustal high density block.

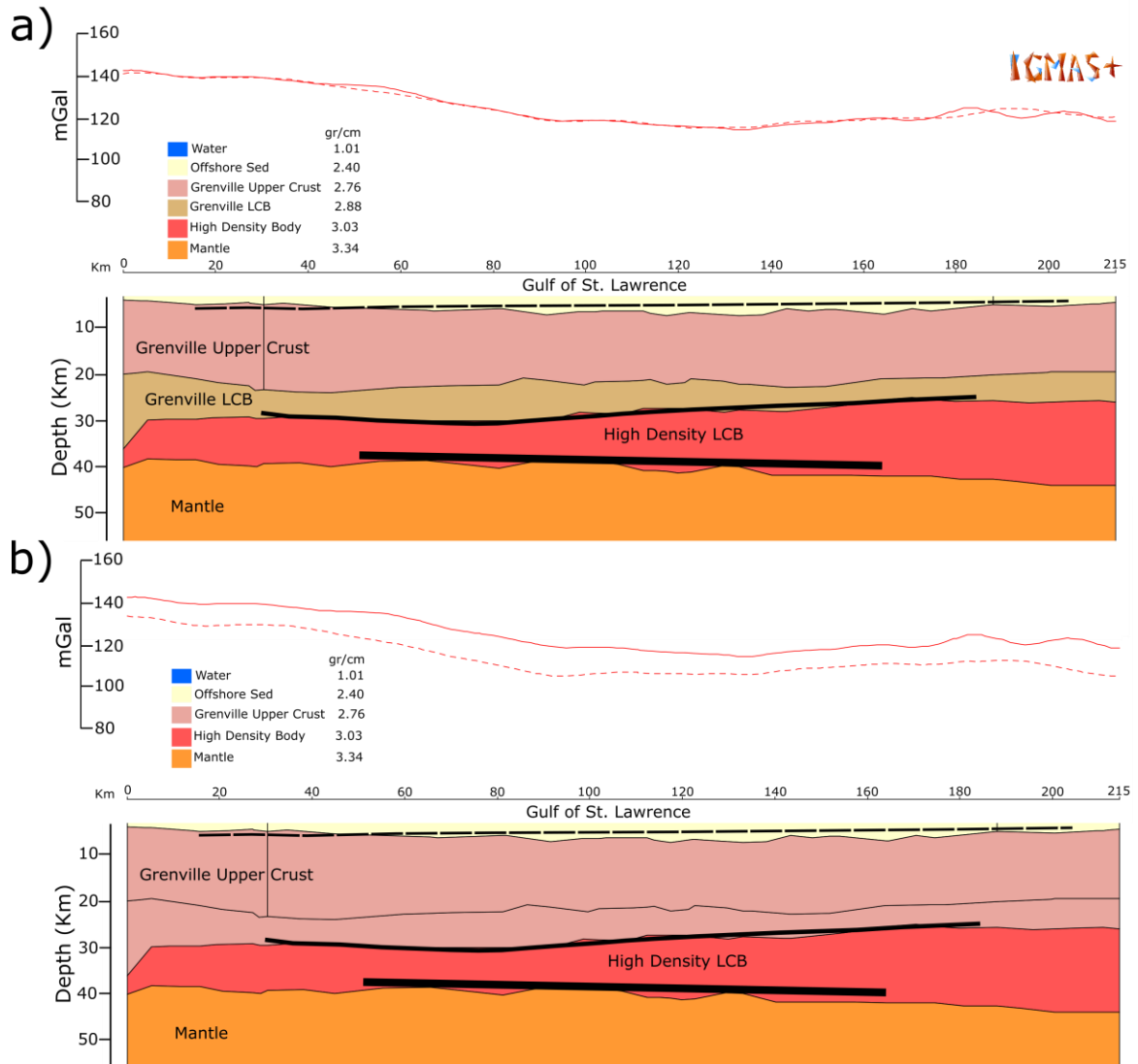


Figure 6. 3: Section 88-4, parallel to the coast line. Solid black lines are reflectors. Base of the crust (Moho) identified by the thick black lines. The dashed black lines are model boundaries. a) Grenville lower crust above the high density lower crustal body and b) Grenville upper crust over the high density body.

The high density body is interpreted as a partial intrusion into the lower crust in this study (Fig. 6.3a) (Marillier et al., 1991). In other crustal-scale seismic studies in Western

Newfoundland, this body was either modelled as intruding through the entire lower crust or as a completely different lower crustal body (Fig. 6.3b) (Hall et al., 1998; Jackson et al., 1998). If the body actually did take up the entire lower crust and the seismically-derived densities in the model remain the same without accounting for the higher density material throughout the lower crust, the calculated anomaly would decrease relative to the observed gravity (Figure 6.3b). In order to correct this misfit, the upper and lower crust would need a density increase of $\sim 0.15 \text{ g/cm}^3$. These increased densities do not agree with the seismic refraction velocities and hence, the high density body may only partially intrude into the lower crust and may not be considered a distinct lower crustal body.

Marillier et al. (1991) suggest that a high density lower crustal body of mafic or ultramafic composition, underplated the crust either during late Precambrian to Early Cambrian rifting of the Iapetus Ocean or during Late Paleozoic strike-slip movement that led to the formation of pull-apart basins in the Canadian Appalachians. Michel et al. (1992) proposed that the high velocity lower crust may correspond to a zone of either mafic intrusions formed by decompressional melting during delamination of the crust from the mantle which would be consistent with the lithospheric delamination model of Stockmal et al. (1987) or mafic intrusions formed during progressive Iapetean rifting of the original Grenville crust. Hall et al. (1998) conclude that the high density body has to be from an intrusive source, which may have a post-Grenvillian age. Hall et al. (1998) support the Michel et al. (1992) hypothesis. Jackson et al. (1998) do not elaborate on any other theory about the genesis of the denser lower crust. However, Funck et al. (2001) studied the Grenville crust in southeastern Labrador through seismic refraction and gravity data and found similar high velocity lower crust in that area. Funck et al. (2001) proposed that both high velocity bodies may actually be connected and concluded that this denser lower crust was formed during Iapetean rifting in the late Neoproterozoic.

The sedimentary layer in the Gulf of St. Lawrence thickens where the high density lower crustal body is located (Figure 6.2), which may agree with genesis during the rifting of the Iapetus Ocean. However, the sediments in the area are largely passive margin and

also orogen derived, and do not correspond to a rifting event. Therefore, this possibility is dismissed. Similarly, a post-collision extension origin may agree with this thickness of sediments (> 4 km) and may also explain the genesis of the high density body as postulated for the Carboniferous Magdalen Basin (Marillier et al., 1989). However, the sediments in the Magdalen Basin are greater than 12 km thick (Marillier et al., 1989), which is a considerably larger amount of sediment in comparison to Western Newfoundland. This difference in sediment thickness between the two areas made Michel et al. (1992) dismiss this possibility.

The magnetic residual map of Western Newfoundland shows circular magnetic anomalies in the Grenville Province and its offshore continuation in the Gulf of St. Lawrence that could be caused by dykes. Funck et al. (2001) noticed that the distribution of 615 Ma Long Range dykes in the easternmost Grenville province seems to be underlain by the presence of the high density lower crustal body. Consequently, the high density lower crustal body may extend further N-S and could be related to the denser body found in southeast Labrador. However, modelling the high density body up to this area is beyond the scope of this thesis.

6.3 Sedimentary basin thickness and Humber Arm Allochthon

Figure 6.2a shows the sedimentary thickness for the study area. From this map, a large accumulation of sediments (~3-6 km thick) exists in the Gulf of St. Lawrence. Similarly, a N-S trend of ~4 km sediment thickness is found over the Humber Arm, which correlates with the platform succession and parts of the Humber zone Allochthon.

The geometry of the Humber Arm Allochthon was modelled based on seismic reflection lines. Because the HAA was emplaced over shallow-water, time-correlative sediments, a density contrast is not expected and so not modelled between them. The similarity between the computed density (2.4 g/cm^3) for the HAA structure and the

surrounding sedimentary layers does not allow for definitive conclusions about its lateral extent.

Marillier et al. (1989), through gravity inversion, reported an increase in sediment thickness from 2 km to 10 km in the southern part of the study area. The increase towards the south is also indicated in Figure 6.2b. However, the sediment thickness values of Marillier et al. (1989) are higher. The highest sediment thickness in the southern area for this research project is ~ 7 km whereas Marillier et al. (1989) reported ~ 12 km for the same location.

The gravity Free Air and Bouguer anomaly map shows that the St. George Sub-basin has a low Bouguer anomaly to the north, whereas it increases to the south. This could imply that the sedimentary cover is thicker in the north than in the south for this basin. The modelled sedimentary thickness shows that the sediments are indeed thicker in the north (> 4 km), as also concluded by Miller et al. (1990), with 4 km of sediments in the onshore St. George Sub-basin. Additionally, the shape of the depocenter follows the Bouguer gravity anomaly and the sediments are thinner where the gravity value is higher. From the gravity modelling, it is possible to conclude that the St. George Sub-basin has a northeast-southwest elongated shape, with its margin defined by the Cabot Fault. Nearby offshore, the sediments do not thicken, and remain approximately ~4 km thick which disagrees with Miller et al. (1990) who found a 6 km thick depocenter offshore. Seismic interpretation of the CAH91-20 and GE-83-504A seismic lines indicates that the basement offshore is ~ 4 km deep.

6.4 Ophiolites and Odd Twins Anomaly

The magnetic anomalies of the study area show high positive anomalies related to ophiolite complexes onshore. The shapes of these anomalies are highlighted by the curvature analysis (Figs. 3.14 and 3.16, section 4, chapter III). The 3D magnetic modelling for these local bodies was not performed since the focus of this thesis was at the crustal-

scale. However, the spectral analysis for each of the high resolution magnetic surveys indicates that some of these bodies may have a deeper root. The power spectrum of the magnetic anomalies in the Corner Brook area suggest that these Humber Arm Allochthon ophiolite complexes may extend to a depth of 6 km and may flexurally weigh down the crust. This result can be supported by the observed and calculated gravity misfit obtained in those areas (>10 mGal) since these local bodies may require a higher density and a better definition of their depth extent. Local 3D magnetic inversions may be helpful for better characterizing these shallow and magnetisable bodies.

Offshore, the Odd Twins Anomaly is shown as two strong magnetic markers. The curvature analysis resolved these anomalies well. They extend ~ 98 km N-S immediately offshore of Western Newfoundland and vanish close to the Port-au-Port Peninsula. This finding corroborates that the magnetic anomalies found on the Port-au-Port Peninsula by Waldron et al., (2002) are connected to the Odd Twins Anomaly. The source for this anomaly may come from the erosion of the surrounding ophiolite complexes since both features are close to each other, as shown in the curvature analysis (Fig. 3.14, section 4, chapter III). The ophiolite complexes were obducted during the Taconian Orogen. Hence, the Odd Twins Anomaly may date from the Late Ordovician.

6.5 Faults

Western Newfoundland is a complex area characterized by a basement-involved structural style (Cooper et al., 2001; Jackson et al., 1998). If those listric faults exist, they do not involve large modifications of the crustal structure since the 3D forward model did not require structural modifications at that scale to satisfy the gravity observations. The residual magnetic anomalies of the study area show two WNW-ESE linear anomalies in the Gulf of St. Lawrence. The Euler deconvolution points indicate that the depths to the cluster points around these anomalies could extend to ~ 7.9 km. Since the top of basement is at 4 km depth, the source of this anomaly may be in the shallow upper crust. The gravity

anomaly map does not show similar behaviour in the same location, either from the gravity forward modelling or from the gravity inversion.

The Laurentian margin in Western Newfoundland acted as an eastward-facing passive continental margin during the opening of the Iapetus ocean (Waldron et al., 2012). These perpendicular to the coast strong magnetic anomalies in the Grenville area could be explained by the presence of basement involved transfer faults which formed perpendicular to extensional faults and ancient ridge axis segments during the opening of this ocean. However, this explanation is only supported by the magnetic data.

6.6 Summary

This chapter included the discussion of the main results obtained from this research. Additionally, it tied together the different geophysical methods used and previous studies in the study area. The discussion focused on the crustal structure of Western Newfoundland, the structure and genesis of the lower crustal high density body, sedimentary basins, the ophiolites and the Odd Twins Anomaly, and the possible faults found in the study area. In the following chapter, chapter VII, the conclusions from this study are presented.

Chapter 7: Conclusions and Future work

Western Newfoundland is characterized as a geologically complex region, for which the general surface geology is relatively well known (Knight, 1983; Lavoie, 2008; Waldron et al., 2012; Williams, 1995). However, no comprehensive attempt has been made to incorporate gravity and magnetic data from Western Newfoundland into tectonic models. To this end, a 3D lithospheric model of Western Newfoundland using a multi-method geophysical approach was constructed to better understand the Appalachian structures in the region.

The Free Air and Bouguer gravity anomalies used in this study showed a good correspondence between the potential field anomalies and the surface geology. New satellite derived Bouguer gravity data WGM2012 show that for the Humber zone, low Bouguer gravity anomalies mask the position of the Appalachian front; the position of this boundary may still be unknown in this area. In addition, recent upper crustal investigations in the Gulf of St. Lawrence suggest that the Appalachian structural front may be offset with respect to its current mapped location (Kuponyi et al., 2017).

The residual high resolution magnetic anomaly maps, produced by the federal and provincial governments, show large positive anomalies on land that are related to ophiolite complexes. Spectral analysis for each of the high resolution magnetic surveys indicates that some of these igneous bodies may extend to 6 km depth.

The high resolution magnetic maps, the curvature analysis and the derivative-based filters highlighted strong magnetic markers offshore, known as the Odd Twins Anomaly. The analysis of the results led to the conclusion that this feature extends ~ 98 km N-S immediately offshore of Western Newfoundland and seems to vanish close to the Port-au-Port Peninsula. It is proposed that the magnetic source for this anomaly may be the surrounding ophiolite complexes, and that this anomaly may date from the Late Ordovician.

Two WNW-ESE linear magnetic anomalies in the Gulf of St. Lawrence and perpendicular to the Newfoundland coast could be explained by the presence of ancient inherited transfer faults that resulted from offset ancient ridge axis segments during the opening of the Iapetus Ocean.

The 3D gravity forward model developed in this thesis followed the distribution of LCBs of Jackson et al. (1998) and Hall et al. (1998). Following those earlier studies, the lower crust was divided into LCBs whose densities were derived from the available seismic refraction profiles. The Grenville LCB underlies the Grenville Province and had a density of 2.88 g/cm^3 for all of the study area. The density of the LCB beneath the Humber Arm is also 2.88 g/cm^3 which suggests that the Grenville province rocks may well continue below the surface Humber zone in the crust (Hall et al., 1998).

The crustal thickness varies between 33 and 43 km across Western Newfoundland. However, the crustal thickness varies systematically across the study area, such that the crustal thickness for the Gulf of St. Lawrence is around 39 km and it thins (34 km) where the high density lower crustal body is located and a thick accumulation of sediments is also found. In the Labrador area, the crustal thickness is ~ 39 km which is expected for a stable continental crust (Baranov and Morelli, 2014).

The 3D gravity forward model supports that the 3.03 g/cm^3 high density lower crustal body is indeed necessary since it has a significant effect on the gravity signal in the area whereas an uniform lower crust, in which the high density body does not exist, does not agree with the seismic findings and increases the misfit between the observed and calculated gravity data. Regarding the density of this body, the composition may be mafic or ultramafic. The model indicated that the body runs parallel to the coast of Western Newfoundland, extending for almost 200 km from north to south, and that it is less thick and wider in the south compared to thicker and less wide to the north. It is possible that the high density lower crustal body may extend further N-S and could be related to the denser body found in southeast Labrador (Funck et al., 2001).

A large accumulation of sediments (~3-6 km thick) is modelled in the Gulf of St. Lawrence. Similarly, a N-S trend of ~4 km sediment thickness is found over the Humber Arm. The highest sediment thickness in the southern area for this research project is ~ 7 km. The St. George Sub-basin has a northeast-southwest elongated shape, with its margin defined by the Cabot Fault.

Future work across Western Newfoundland should include 3D magnetic inversions of the high resolution magnetic anomalies and 3D gravity tensor inversions for the areas containing ophiolite complexes; these two techniques may be helpful for enhancing characteristics of shallow and magnetisable bodies and to find their roots.

New seismic refraction data acquisition in Western Newfoundland and surrounding areas would greatly improve confidence limits surrounding the extent and genesis of a high density lower crustal body and possibly the existence of other lower crust bodies in the Canadian Appalachians.

References

- Alsadi, H., Baban, E., 2014. Introduction to gravity exploration method, University. ed. Paiwand press, Kurdistan Region.
- Ante, C., Eakins, B.W., 2009. ETOPO1 1 Arc-Minute Global Relief Model: Procedures, Data Sources and Analysis NOAA Techn. doi:10.7289/V5C8276M
- Arisoy, M.Ö., Dikmen, U., 2013. Edge Detection of Magnetic Sources Using Enhanced Total Horizontal Derivative of the Tilt Angle. Bull. Earth Sci. Appl. Res. Cent. Hacettepe Univ. 34, 73–82.
- Baker, D., Knight, I., 1993. The Catoche dolomite project, Anticosti Basin, eastern Canada. St. John's, Nfld.
- Baranov, A., Morelli, A., 2014. The global Moho depth map for continental crust. Geophys. Res. Abstr. 16.
- Baranov, V., 1957. A NEW METHOD FOR INTERPRETATION OF AEROMAGNETIC MAPS: PSEUDO-GRAVIMETRIC ANOMALIES. GEOPHYSICS 22, 359–382. doi:10.1190/1.1438369
- Barnett, C.T., 1976. THEORETICAL MODELING OF THE MAGNETIC AND GRAVITATIONAL FIELDS OF AN ARBITRARILY SHAPED THREE-DIMENSIONAL BODY. GEOPHYSICS 41, 1353–1364. doi:10.1190/1.1440685
- Blakely, R.J., 1995. Potential Theory in Gravity and Magnetic Applications. Cambridge University Press, Cambridge. doi:10.1017/CBO9780511549816
- Bonvalot, S., Balmino, G., Briais, A., Kuhn, M., Peyrefitte, A., Vales, N., Biancale, R., Gabalda, G., Reinquin, F., Sarrailh, M., 2012. World Gravity Map. Bureau Gravimetrique International (BGI), Paris.
- Burden, E., Burden, D., Parsons, G., 2014. Finding the Parts : a searchable database and report of petroleum geology and geophysics literature for Paleozoic Basins of Newfoundland and Labrador. Canada.
- Burden, E.T., Quinn, L., Nowlan, G.S., Bailey-Nill, L.A., 2002. Palynology and Micropaleontology of the Clam Bank Formation (Lower Devonian) of Western Newfoundland, Canada. Palynology 26, 185–215.
- Burden, E.T., Williams, H., 1995. Biostratigraphy and thermal maturity of strata in Hunt-PanCanadian Port au Port well #1.
- Burger, H.R., Sheehan, A.F., Jones, C.H., Burger, H.R., 2006. Introduction to applied geophysics : exploring the shallow subsurface. W.W. Norton, New York.
- Cawood, P.A., 1993. Acadian Orogeny in west Newfoundland: Definition, character, and significance. Geol. Soc. Am. Spec. Pap. 275, 135–152. doi:10.1130/SPE275

- Cawood, P.A., Dunning, G.R., Lux, D., Van Gool, J.A.M., 1994. Timing of peak metamorphism and deformation along the Appalachian margin of Laurentia in Newfoundland: Silurian, not Ordovician. *Geology* 22, 399–402. doi:10.1130/0091-7613(1994)022<0399:TOPMAD>2.3.CO;2
- Cawood, P.A., Williams, H., 1988. Acadian basement thrusting, crustal delamination, and structural styles in and around the Humber Arm allochthon, western Newfoundland. *Geology* 16, 370–373. doi:10.1130/0091-7613(1988)016<0370:ABTCDA>2.3.CO;2
- Colman-Sadd, S.P., Hayes, J.P., Knight, I., 2000. Geology of the Island of Newfoundland (digital version of Map 90-01 with minor revisions).
- Cooper, M., Weissenberger, J., Knight, I., Hostad, D., Gillespie, D., Williams, H., Burden, E., Porter-Chaudhry, J., Rae, D., Clark, E., 2001. Basin evolution in western Newfoundland: New insights from hydrocarbon exploration. *Am. Assoc. Pet. Geol. Bull.* 3, 393–418.
- Denker, H., Tziavos, I.N., 1999. Investigation of the Molodensky series terms for terrain reduced gravity field data. *Boll. DI Geofis. Teor. ED Appl.* 40, 195–203.
- Dian, Y.L., Wang, J.X.M., 2013. Reduction to the Pole at the Geomagnetic Equator. *Chinese J. Geophys.* 53, 1082–1089. doi:10.1002/cjg2.1578
- Dimitriadis, K., Tselentis, G.-A., Thanassoulas, K., 1987. A BASIC program for 2-D spectral analysis of gravity data and source-depth estimation. *Comput. Geosci.* 13, 549–560. doi:10.1016/0098-3004(87)90056-2
- Dumont, R., Jones, A., 2013. Aeromagnetic Survey of Western Newfoundland, Newfoundland and Labrador.
- Enachescu, M., 2012. Geophysical Interpretation Report: Exploration Licence 1120 Anticosti Basin (Western Newfoundland Offshore).
- Fairhead, J.D., Salem, A., Williams, S.E., 2008. Tilt-Depth : A Simple Depth-Estimation Method Using First Order Magnetic Derivatives, in: AAPG International Conference and Exhibition. Cape Town, South Africa, October 26-29.
- Fowler, M.G., Hamblin, A.P., Hawkins, D., Stasiuk, L.D., Knight, I., 1995. Petroleum geochemistry and hydrocarbon potential of Cambrian and Ordovician rocks of western Newfoundland. *Bull. Can. Pet. Geol.* 43, 187–213.
- Funck, T., Loudon, K.E., Reid, I.D., 2001. Crustal structure of the Grenville Province in southeastern Labrador from refraction seismic data: evidence for a high-velocity lower crustal wedge. *Can. J. Earth Sci.* 38, 1463–1478. doi:10.1139/cjes-38-10-1463
- Geng, M., Welford, J.K., Farquharson, C.G., 2017. 3D gravity inversion using the constrained stochastic method: Applications to crustal-scale models of rifted margins, in: 79th EAGE Conference and Exhibition 2017.
- Geng, M., Welford, J.K., Farquharson, C.G., Hu, X., n.d. 3-D gravity inversion using the

- constrained probabilistic method: applications to crustal-scale models of rifted continental margins. *Geophysics*.
- Gubbins, D., 2004. *Time Series Analysis and Inverse Theory for Geophysicists*. Cambridge University Press, Cambridge. doi:10.1017/CBO9780511840302
- Hadidi, R., Gucunski, N., 2009. Probabilistic Inversion: A New Approach to Inversion Problems in Pavement and Geomechanical Engineering, in: Gopalakrishnan, K., Ceylan, H., Attoh-Okine, N.O. (Eds.), *Intelligent and Soft Computing in Infrastructure Systems Engineering: Recent Advances*. Springer Berlin Heidelberg, Berlin, Heidelberg, pp. 21–45. doi:10.1007/978-3-642-04586-8_2
- Hall, J., Marillier, F., Dehler, S., 1998. Geophysical studies of the structure of the Appalachian Orogen in the Atlantic borderlands of Canada. *Can. J. Earth Sci.* 35, 1205–1221. doi:10.1139/e98-075
- Hall, J., Roberts, B., Hawkins, D., Fagan, A., Knight, I., Kilfoil, G., 1992. Reflection seismic imaging of the Carboniferous Bay St. George Subbasin, onshore western Newfoundland: a reappraisal of Paleozoic stratigraphic thickness. *Bull. Can. Pet. Geol.* 40, 321–334.
- Haworth, R.T., 1978. Interpretation of geophysical data in the northern Gulf of St. Lawrence and its relevance to lower Paleozoic geology. *Bull. Geol. Soc. Am.* 89, 1091–1110. doi:10.1130/0016-7606(1978)89<1091:IOGDIT>2.0.CO;2
- Hayward, N., Dehler, S.A., Oakey, G.N., 2001. The structure of the northeastern Gulf of St. Lawrence, Canada: new insight from geophysical data analysis 1. *Can. J. Earth Sci.* 38, 1495–1516. doi:10.1139/cjes-38-11-1495
- Heaman, L.M., Erdmer, P., Owen, J. V., 2002. U–Pb geochronologic constraints on the crustal evolution of the Long Range Inlier, Newfoundland. *Can. J. Earth Sci.* 39, 845–865. doi:10.1139/e02-015
- Heiskanen, W.A., Moritz, H., 1967. Physical geodesy. *Bull. Géodésique* 86, 491–492. doi:10.1007/BF02525647
- Hinchey, A.M., Knight, I., Kilfoil, G., Hicks, L., 2015. Geological Overview and Hydrocarbon Potential of Cambrian-Ordovician strata of the outer Humber Zone, Western Newfoundland, Current Research-Report 15-1. St. John's, Nfld.
- Hughes, S., Hall, J., Luetgert, J.H., Survey, U.S.G., Park, M., 1994. The seismic velocity structure of the Newfoundland Appalachian orogen. *J. Geophys. Res.* 99, 13633–13653.
- Jackson, H.R., 2002. Seismic refraction profiles in the Gulf of Saint Lawrence and implications for extent of continuous Grenville lower crust. *Can. J. Earth Sci.* 39, 1–17. doi:10.1139/e01-054
- Jackson, H.R., Marillier, F., Hall, J., 1998. Seismic refraction data in the Gulf of Saint Lawrence: implications for the lower-crustal blocks. *Can. J. Earth Sci.* 35, 1222–

1237. doi:10.1139/e98-043

- Jacobi, R.D., 1981. Peripheral bulge—a causal mechanism for the Lower/Middle Ordovician unconformity along the western margin of the Northern Appalachians. *Earth Planet. Sci. Lett.* 56, 245–251. doi:10.1016/0012-821X(81)90131-X
- James, N.P., Stevens, R.K., 1986. Stratigraphy and correlation of the Cambro-Ordovician Cow Head Group, western Newfoundland. Geological Survey of Canada.
- James, N.P., Stevens, R.K., Barnes, C.R., Knight, I., 1989. Evolution of a Lower Paleozoic continental-margin carbonate platform, northern Canadian Appalachians, in: Crevello, P., Wilson, J.L., Sarg, J.F., Read, J.F. (Eds.), *Controls on Carbonate Platform and Basin Development*. Society of Economic Paleontologists and Mineralogists, pp. 123–146.
- Jenner, G. a., Dunning, G.R., Malpas, J., Brown, M., Brace, T., 1991. Bay of Islands and Little Port complexes, revisited: age, geochemical and isotopic evidence confirm suprasubduction-zone origin. *Can. J. Earth Sci.* 28, 1635–1652. doi:10.1139/e91-146
- Kearey, P., Brooks, M., Hill, I., 2002. *An Introduction to Geophysical Exploration*, Third edit. ed. Blackwell Publishing, Oxford.
- Kilfoil, G., 2009. Geophysical Data From Recent Airborne Surveys , Newfoundland and Labrador 305–314.
- Kilfoil, G.J., Cook, L.A., 2009. Residual Magnetic Field.
- Klappa, C.F., Opalinski, P.R., James, N.P., 1980. Middle Ordovician Table Head Group of western Newfoundland: a revised stratigraphy. *Can. J. Earth Sci.* 17, 1007–1019. doi:10.1139/e80-101
- Knight, I., 1983. Geology of the Carboniferous Bay St. George subbasin, Western Newfoundland. Mineral Development Division, Government of Newfoundland and Labrador, St. John's, Nfld.
- Knight, I., Cawood, P.A., 1991. Paleozoic geology of western Newfoundland: an exploration of a deformed Cambro-Ordovician passive margin and foreland basin, and Carboniferous successor basin. Centre for Earth Resources, St. John's, Newfoundland.
- Knight, I., James, N.P., Lane, T.E., 1991. The Ordovician St. George unconformity, northern Appalachians: the relationship of plate convergence at the St. Lawrence promontory to the Sauk/Tippecanoe sequence boundary. *Geol. Soc. Am. Bull.* 103, 1200–1225. doi:10.1130/0016-7606(1991)103<1200:TOSGUN>2.3.CO;2
- Kuponiyi, A.P., Kao, H., van Staal, C.R., Dosso, S.E., Cassidy, J.F., Spence, G.D., 2017. Upper crustal investigation of the Gulf of Saint Lawrence region, eastern Canada using ambient noise tomography. *J. Geophys. Res. Solid Earth* 122, 5208–5227. doi:10.1002/2016JB013865

- Lavoie, D., 2008. Appalachian Foreland Basin of Canada, in: Miall, A.D. (Ed.), *Sedimentary Basins of the World*, Vol 5. Elsevier, The Netherlands, pp. 65–103.
- Lavoie, D., Burden, E., Lebel, D., 2003. Stratigraphic framework for the Cambrian–Ordovician rift and passive margin successions from southern Quebec to western Newfoundland. *Can. J. Earth Sci.* 40, 177–205. doi:10.1139/e02-078
- Lavoie, D., Pinet, N., Dietrich, J., Hannigan, P., Castonguay, S., Hamblin, A.P., Giles, P., 2009. Petroleum Resource Assessment, Paleozoic successions of the St. Lawrence Platform and Appalachians of eastern Canada, Geological Survey of Canada.
- Li, X., 2015. Curvature of a geometric surface and curvature of gravity and magnetic anomalies. *GEOPHYSICS* 80, G15–G26. doi:10.1190/geo2014-0108.1
- Li, X., Götze, H.J., 2001. Tutorial Ellipsoid , geoid , gravity , geodesy , and geophysics. *Geophysics* 66, 1660–1668.
- Lowrie, W., 2007. *Fundamentals of geophysics*. Cambridge University Press.
- Madeline, L., William, M., George, L., Jeff, H., 2013. Curvature analysis to differentiate magnetic sources for geologic mapping. *Geophys. Prospect.* 61, 572–585. doi:10.1111/j.1365-2478.2012.01111.x
- Marillier, F., Dentith, M., Michel, K., Reid, I., Hall, J., Roberts, B., Wright, J., Loudon, K., Morel-à-l’Huissier, P., Spencer, C., 1991. Coincident seismic-wave velocity and reflectivity properties of the lower crust beneath the Appalachian Front, west of Newfoundland. *Can. J. Earth Sci.* 28, 94–101.
- Marillier, F., Hall, J., Hughes, S., Loudon, K., Reid, I., Roberts, B., Clowes, R., Coté, T., Fowler, J., Guest, S., Lu, H., Luetgert, J., Quinlan, G., Spencer, C., Wright, J., 1994. LITHOPROBE East onshore-offshore seismic refraction survey -constraints on interpretation of reflection data in the Newfoundland Appalachians. *Tectonophysics* 232, 43–58. doi:10.1016/0040-1951(94)90075-2
- Marillier, F., Keen, C.E., Stockmal, G.S., Quinlan, G., Williams, H., Colman-Sadd, S.P., O’Brien, S.J., 1989. Crustal structure and surface zonation of the Canadian Appalachians: implications of deep seismic reflection data. *Can. J. Earth Sci.* 26, 305–321.
- Meju, M.A., 1994. *Geophysical data analysis : understanding inverse problem theory and practice*. Society Exploration Geophysicists, Tulsa, OK.
- Michel, H.K., Loudon, K.E., Marillier, F., Reid, I., 1992. The seismic velocity structure of northern Appalachian crust around western Newfoundland. *Can. J. Earth Sci.* 29, 462–478.
- Miles, W., Oneschuk, D., 2016. *Magnetic anomaly map, Canada*.
- Miller, H.G., 1990. A synthesis of the geophysical characteristics of terranes in eastern Canada. *Tectonics* 177, 171–191.

- Miller, H.G., Kilfoil, G.J., Peavy, S.T., 1990. An integrated geophysical interpretation of the Carboniferous Bay St. George Subbasin, western Newfoundland. *Bull. Can. Pet. Geol.* 38, 320–331.
- Miller, H.G., Singh, V., 1994. Potential field tilt a new concept for location of potential field sources. *J. Appl. Geophys.* 32, 213–217.
- Molodetsky, M.S., Eremeev, V.F., Yurkina, M.I., 1962. Methods for study of the external gravitational field and figure of the Earth. Jerusalem, Isr. Progr. Sci. Transl.
- Nabighian, M., Grauch, V., Hansen, R., LaFehr, T., Li, Y., Peirce, J., Phillips, J., Ruder, M., 2005. The historical development of the magnetic method in exploration. *GEOPHYSICS* 70, 33ND–61ND. doi:10.1190/1.2133784
- Nabighian, M.N., 1984. Toward the three-dimensional automatic interpretation of potential field data via generalized Hilbert transforms. *Fundam. relations Geophys.* 53, 957–966.
- Nabighian, M.N., 1972. The analytic signal of two-dimensional magnetic bodies with polygonal cross-section: its properties and use for automated anomaly interpretation. *Geophysics* 37, 507–517.
- Nagy, D., 1966. THE GRAVITATIONAL ATTRACTION OF A RIGHT RECTANGULAR PRISM. *GEOPHYSICS* 31, 362–371. doi:10.1190/1.1439779
- Newfoundland and Labrador Geological Survey, 2013. Detailed Bedrock Geology [WWW Document]. Newfoundland. Labrador Geosci. Atlas OnLine.
- Okabe, M., 1979. Analytical expressions for gravity anomalies due to homogeneous polyhedral bodies and translations into magnetic anomalies. *GEOPHYSICS* 44, 730–741. doi:10.1190/1.1440973
- Pavlis, N.K., Holmes, S. a., Kenyon, S.C., Factor, J.K., 2008. An earth gravitational model to degree 2160: EGM2008. Present. 2008 Gen. Assem. Eur. Geosci. Union, Vienna, Austria, April 13-18 84, 2–4.
- Peavy, S.T., 1985. A gravity and magnetic interpretation of the bay St. George Carboniferous Subbasin in Western Newfoundland. Memorial University of Newfoundland.
- Quinlan, G., Hall, J., Williams, H., Wright, J., Colman-Sadd, S.P., O'Brien, S.J., Stockmal, G.S., Marillier, F., 1992. Lithoprobe onshore seismic reflection transects across the Newfoundland Appalachians. *Can. J. Earth Sci.* 29, 1865–1877.
- Quinn, L., 1992. Foreland and trench slope basin sandstones of the Goose Tickle Group and Lower Head Formation, western Newfoundland. Memorial University.
- Quinn, L., Harper, D.A.T., Williams, S.H., Clarkson, E.N.K., 1999. Late Ordovician foreland basin fill: Long Point Group of onshore western Newfoundland. *Bull. Can. Pet. Geol.* 47, 63–80.

- Ravat, D., 2007. Reduction to Pole, in: Gubbins, D., Herrero-Bervera, E. (Eds.), *Encyclopedia of Geomagnetism and Paleomagnetism*. Springer Netherlands, Dordrecht, pp. 856–858. doi:10.1007/978-1-4020-4423-6_275
- Reid, A.B., Ebbing, J., Webb, S.J., 2014. Avoidable Euler Errors - the use and abuse of Euler deconvolution applied to potential fields. *Geophys. Prospect.* 62, 1162–1168. doi:10.1111/1365-2478.12119
- Roberts, A., 2001. Curvature attributes and their application to 3D interpreted horizons. *First Break* 19, 85–100. doi:10.1046/j.0263-5046.2001.00142.x
- Ruffman, A., Woodside, J., 1970. The Odd-twins magnetic anomaly and its possible relationship to the Humber Arm Klippe of Western Newfoundland, Canada. *Can. J. Earth Sci.* 7, 326–337.
- Salem, A., Williams, S., Fairhead, D., Smith, R., Ravat, D., 2007. Interpretation of magnetic data using tilt-angle derivatives. *GEOPHYSICS* 73, L1–L10. doi:10.1190/1.2799992
- Schmidt, S., Götze, H.J., 2003. Pre-interpretation of potential fields by aid of curvature attributes. A poster Present. *Eur. Geophys. Soc. Annu. Meet.*
- Snieder, R., Trampert, J., 1999. Inverse Problems in Geophysics, in: Wirgin, A. (Ed.), *Wavefield Inversion*. Springer Vienna, Vienna, pp. 119–190.
- Spector, A., Grant, F.S., 1970. STATISTICAL MODELS FOR INTERPRETING AEROMAGNETIC DATA. *GEOPHYSICS* 35, 293–302. doi:10.1190/1.1440092
- Stacey, F.O., 1977. *Physics of the Earth*. John Wiley & Sons, Ltd, New York.
- Stenzel, S.R., Knight, I., James, N.P., 1990. Carbonate platform to foreland basin: revised stratigraphy of the Table Head Group (Middle Ordovician), western Newfoundland. *Can. J. Earth Sci.* 27, 14–26. doi:10.1139/e90-002
- Stockmal, G.S., Colman-Sadd, S.P., Keen, C.E., O'Brien, S.J., Quinlan, G., 1987. Collision along an irregular margin: a regional plate tectonic interpretation of the Canadian Appalachians. *Can. J. Earth Sci.* 24, 1098–1107. doi:10.1139/e87-107
- Stockmal, G.S., Slingsby, A., Waldron, J.W.F., 2004. Basement-involved inversion at the Appalachian structural front, western Newfoundland: An interpretation of seismic reflection data with implications for petroleum prospectivity. *Bull. Can. Pet. Geol.* 52, 215–233.
- Stockmal, G.S., Slingsby, A., Waldron, J.W.F., 1998. Deformation styles at the Appalachian structural front, western Newfoundland: implications of new industry seismic reflection data. *Can. J. Earth Sci.* 35, 1288–1306.
- Stockmal, G.S., Waldron, J.W.F., 1990. Structure of the Appalachian deformation front in western Newfoundland: Implications of multichannel seismic reflection data. *Geology* 18, 765–768.

- Talwani, M., Ewing, M., 1960. RAPID COMPUTATION OF GRAVITATIONAL ATTRACTION OF THREE-DIMENSIONAL BODIES OF ARBITRARY SHAPE. *GEOPHYSICS* 25, 203–225. doi:10.1190/1.1438687
- Tarantola, A., 2005. *Inverse Problem Theory and Methods for Model Parameter Estimation*. Society for Industrial and Applied Mathematics. doi:10.1137/1.9780898717921
- Tassara, A., Götze, H.J., Schmidt, S., Hackney, R., 2006. Three-dimensional density model of the Nazca plate and the Andean continental margin. *J. Geophys. Res. Solid Earth* 111, 1–26. doi:10.1029/2005JB003976
- van der Velden, A.J., van Staal, C.R., Cook, F.A., 2004. Crustal structure, fossil subduction, and the tectonic evolution of the Newfoundland Appalachians: Evidence from a reprocessed seismic reflection survey. *Bull. Geol. Soc. Am.* 116, 1485–1498. doi:10.1130/B25518.1
- van Staal, C.R., Barr, S.M., 2012. Lithospheric architecture and tectonic evolution of the Canadian Appalachians and associated Atlantic margin, in: Percival, J.A., Cook, F.A., Clowes, R.M. (Eds.), *Tectonic Styles in Canada: The Lithoprobe Perspective*. Geological Association of Canada, pp. 41–95.
- Verduzco, B., Fairhead, J., Green, C., MacKenzie, C., 2004. New insights into magnetic derivatives for structural mapping. *Lead. Edge* 23, 116–119. doi:10.1190/1.1651454
- Waldron, J.W., Anderson, S.D., Cawood, P. a, Goodwin, L.B., Hall, J., Jamieson, R. a, Palmer, S.E., Stockmal, G.S., Williams, P.F., 1998. Evolution of the Appalachian Laurentian margin: Lithoprobe results in western Newfoundland. *Can. J. Earth Sci.* 35, 1271–1287. doi:10.1139/e98-053
- Waldron, J.W., DeWolfe, J., Courtney, R., Fox, D., 2002. Origin of the Odd-twins anomaly: magnetic effect of a unique stratigraphic marker in the Appalachian foreland basin, Gulf of St. Lawrence. *Can. J. Earth Sci.* 39, 1675–1687. doi:10.1139/e02-071
- Waldron, J.W.F., 1994. Structural and tectonic evolution of the Humber Zone, western Newfoundland 2. A regional model for Acadian thrust tectonics. *Tectonics* 13, 1498–1513.
- Waldron, J.W.F., Barr, S.M., Park, A.F., White, C.E., Hibbard, J., 2015. Late Paleozoic strike-slip faults in Maritime Canada and their role in the reconfiguration of the northern Appalachian orogen. *Tectonics* 34, 1661–1684. doi:10.1002/2015TC003882
- Waldron, J.W.F., Hicks, L., White, S.E., 2012. Stratigraphy, tectonics and petroleum potential of the deformed Laurentia margin and foreland basins in western Newfoundland, Field Trip. ed. Geological Association of Canada-Mineralogical Association of Canada Joint Annual Meeting, Canada.

- Waldron, J.W.F., Stockmal, G.S., Corney, R.E., Stenzel, S.R., 1993. Basin development and inversion at the Appalachian structural front, Port au Port Peninsula, western Newfoundland Appalachians. *Can. J. Earth Sci.* 30, 1759–1772. doi:10.1139/e93-156
- Waldron, J.W.F., van Staal, C.R., 2001. Taconian orogeny and the accretion of the Dashwoods block: A peri-Laurentian microcontinent in the Iapetus Ocean. *Geology* 29, 811–814. doi:10.1130/0091-7613(2001)029<0811:TOATAO>2.0.CO;2
- Welford, J.K., Peace, A.L., Geng, M., Dehler, S.A., Dickie, K., 2018. Crustal structure of Baffin Bay from constrained 3-D gravity inversion and deformable plate tectonic models. *Geophys. J. Int.* 1–49. doi:10.1093/gji/ggy193
- White, S.E., Waldron, J.W.F., 2018. Inversion of Taconian extensional structures during Paleozoic orogenesis in western Newfoundland. *Geol. Soc. London, Spec. Publ.* 470.
- Williams, H., 1995. *Geology of the Appalachian-Caledonian orogen in Canada and Greenland*. Geological Survey of Canada, Canada.
- Williams, H., 1979. Appalachian Orogen in Canada. *Can. J. Earth Sci.* 16, 792–807.
- Williams, H., Colman-Sadd, S.P., Swinden, H.S., 1988. Tectonic-stratigraphic subdivisions of central Newfoundland, in: *Current Research, Part B*. Geological Survey of Canada, Canada, pp. 91–98.

Appendix A: Elements of GRAV3D 2.0 Program Library

The GRAV3D 2.0 program consists of three modules:

- GZFOR3D: performs the forward modelling.
- GZSEN3D: calculates sensitivity and the depth weighting function.
- GZINV3D: performs the 3D gravity inversion.

Each of the above programs requires input files and certain specific parameters to run properly. Figure 8.1 shows the graphic interface of GRAV3D and also shows the input parameters.

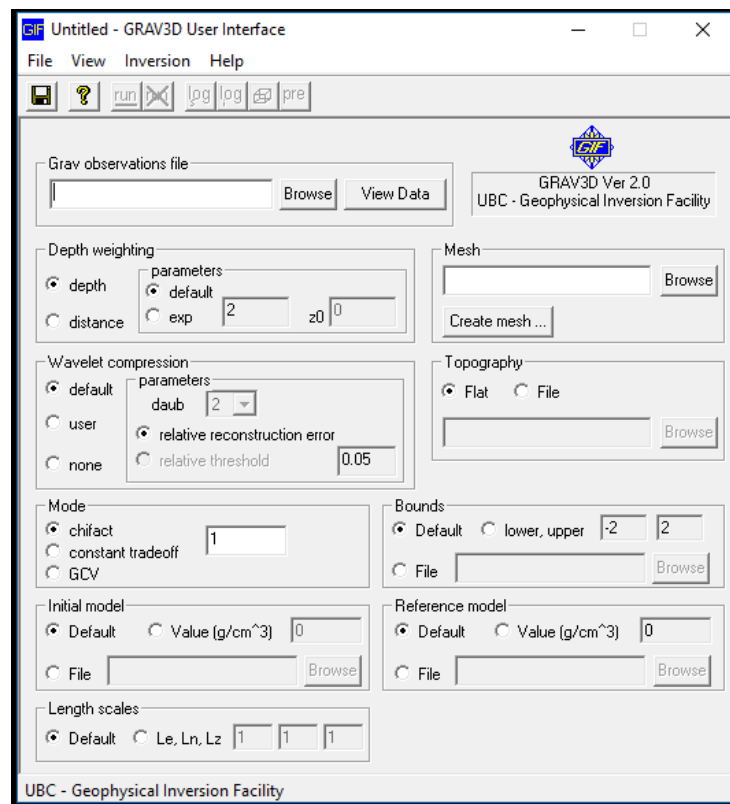


Figure 8.1: GRAV3D User Interface

The gravity observation file is of the extension “name.grv”. In this file, the observed gravity, data values, their locations and their estimated standard deviations are defined. Figure 8.2 shows an example of the structure of the gravity observation file.

In Figure 8.2, n_{dat} refers to the number of observations. $E_{n_{\text{dat}}}$, $N_{n_{\text{dat}}}$, $Elev_{n_{\text{dat}}}$ are the easting, northing and elevation of each observation, measured in meters. $Grav_{n_{\text{dat}}}$ is the gravity anomaly value in mGal and $Err_{n_{\text{dat}}}$ is the absolute standard deviation of $Grav_{n_{\text{dat}}}$.

```

! comments ...
!
ndat
E1      N1      Elev1    Grav1    Err1
E2      N2      Elev2    Grav2    Err2
:
Endat    Nndat    Elevndat Gravndat    Errndat

```

Figure 8.2: Structure of the gravity observation file “name.grv”

The Mesh file defines the model region. This input file must be designed in accordance with the area of interest and desired resolution. Figure 8.3 shows the example structure of the mesh file. NE, NN and NV are the number of cells in the East, North and vertical directions, respectively. E_0 , N_0 and V_0 are the coordinates, in meters, of the southwest top corner. ΔE_n , ΔN_n and ΔV_n are the cell widths and depths in the different directions.

```

NE NN NV
E0 N0 V0
ΔE1 ΔE2 ... ΔENE
ΔN1 ΔN2 ... ΔNNN
ΔV1 ΔV2 ... ΔVNV

```

Figure 8.3: Structure of the mesh file.

The topography file, “name.dat”, is used to define the topography/bathymetry of the 3D model. The file follows the structure shown in Figure 8.4. npt represents the number of

points and E_{npt} , N_{npt} and $elev_{npt}$ are the Easting, Northing and elevation values defining the top of the model.

```
! comment
!  
npt  
E1      N1      elev1  
E2      N2      elev2  
:  
Enpt    Nnpt    elevnpt
```

Figure 8.4: Structure of the topography file “name.dat”.

The user interface, Figure 8.1, also allows the user to choose and change the depth weighting function. The user can choose between a distance or a depth weighting function based on knowledge of the geology of the study area.

Due to the large amount of memory required for the solution of inverse problems, GZSEN3D generates a sparse representation of the sensitivity matrix G using a wavelet transform based on supported and orthonormal wavelets. The program allows the user to choose between a default setting or a different relative error or relative threshold level. These parameters are related to the reconstruction of the sensitivity matrix.